HIGHLIGHTING CICECO SCIENCE

Associate Laboratories´ Review, 2010

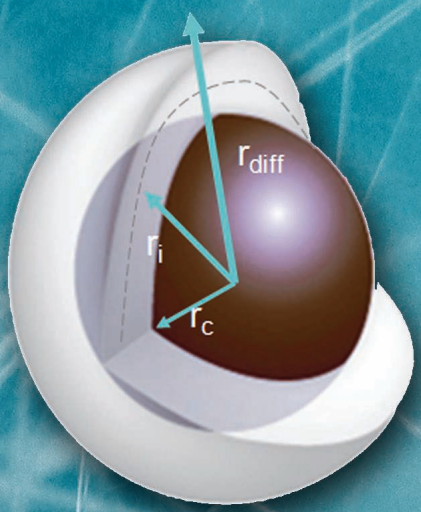

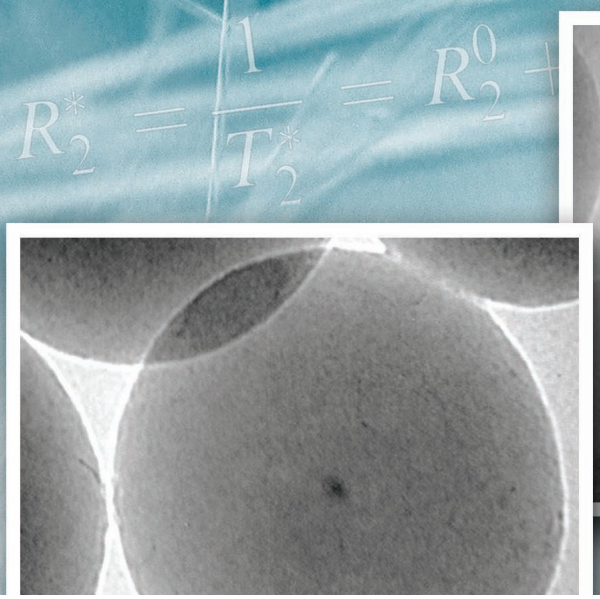

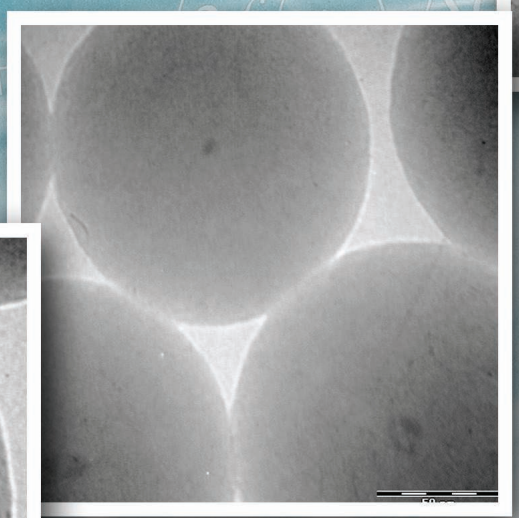

HIGHLIGHTING CICECO SCIENCE

The Associate Laboratory Review 2010

free edition

A WORD FROM THE DIRECTORS

Almost nine years have passed since the associate laboratory CICECO was created in March 2002 at the University of Aveiro, Portugal, with the mission of developing the scientific and technological knowledge necessary for the innovative production and transformation of ceramics and composite materials. In 2010 we are a mature institute with a European status.

CICECO is the largest Portuguese institute in the field of materials science and engineering, comprising (Dec. 2009) 49 academic staff, 35 full-time researchers, 47 post-doctoral associates, 87 PhD students, and some 120 other students, working in the Departments of Chemistry, Physics, and Ceramics and Glass Engineering. Our main areas of expertise are advanced micro- and nano-structured materials for communications technologies; advanced materials for industrial applications; and biorefineries and biomaterials.

These research highlights present some of the excellent work our researchers have performed in the last three years or so. As Directors, we are proud and honored to have had the privilege of helping make CICECO what it is today.

Aveiro, 5 December 2010.

João Rocha, Joaquim Vieira, Luís Dias Carlos

INDEX

Nanomaterials and Nanostructures

Energy, Lighting and Photonics

Dielectrics and Ferroics

Catalysis and Separation

Biorefineries and Materias from Renewable Sources

Nanomaterials and Nanostructures

THE KEY ROLE OF THE SURFACE MEMBRANE IN WHY GASTROPOD NACRE GROWS IN TOWERS

Checa AG[1], Cartwright JHE[2], Willinger MG[3]

Nacre is by far the most intensively studied non-human organo–mineral biocomposite. Its superior biomechanical properties and possible biomedical uses make nacre the subject of many biomimetic studies. An ultimate aim of such work is to mimic nacre in the laboratory, following the biological principles used by molluscs to produce such a biomaterial. Intriguingly, the nacre of gastropod molluscs is stacked in towers. It is covered by a surface membrane, which protects the growing nacre surface from damage when the animal withdraws into its shell. The surface membrane is supplied by vesicles that adhere to it on its mantle side and secretes interlamellar membranes from the nacre side. Nacre tablets rapidly grow in height and later expand sideways; the part of the tablet formed during this initial growth phase is defined by an organic rich core.

In a recently established collaboration between CICECO and the University of Granada, Spain, the role of the surface membrane in the formation of the nacre towers was investigated. Transmission electron microscopic studies performed at the University of Aveiro (using the facilities of the RMNE, funded by FCT) revealed continuous lattice fringes in the region of the core and hence, that the towers of nacre tablets are continuous along the central axis (Fig.1)[1]. Based on these observations, a growth model for gastropod nacre was derived, according to which the core formation precedes that of the interlamellar membrane. Once the core is complete, a new interlamellar membrane detaches from the surface membrane. In this way, the tower-like growth of gastropod nacre becomes understandable.

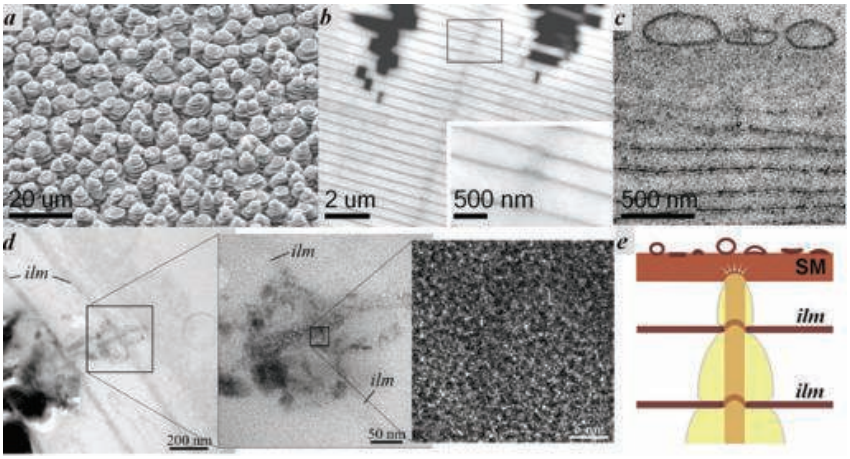

Figure 1. (a) Oblique view of the towered nacre of the gastropod Perotrochus caledonicust. (b) SEM image of a polished section through the axis of a nacre tower (BSE mode). (c) TEM section of decalcified nacre with vesicles adhering to the mantle side of the surface membrane (SM). (d) TEM study of the axial zones of nacre tablets of M.labio, showing that the contact between the last two tablets is fully crystalline and consists of a single crystal domain. ilm: interlamellar membrane. (e) schematical sketch showing the tower formation.

[1] Departamento de Estratigrafía y Paleontología, Facultad de Ciencias, Universidad de Granada, (Spain), [2] Instituto Andaluz de Ciencias de la Tierra, Consejo Superior de Investigaciones Cientificas–Universidad de Granada (Spain), [3] Department of Chemistry, CICECO, University of Aveiro, 3810-193 Aveiro, Portugal

Reference paper

[1] Checa AC, Cartwright JHE, Willinger MG. "The key role of the surface membrane in why gastropod nacre grows in towers", Proceedings of the National Academy of Sciences of the United State of America 2009, 106, 38-43.

A LUMINESCENT MOLECULAR THERMOMETER FOR LONG-TERM ABSOLUTE TEMPERATURE MEASUREMENTS AT THE NANOSCALE

Brites CDS[1], Lima PP[1], Silva NJO[1], Millán A[2], Amaral V[1], Palacio F[2], Carlos LD[1]

Temperature is a fundamental thermodynamic variable, the measurement of which is crucial in countless scientific investigations and technological developments, accounting at present for 75%–80% of the sensor market throughout the world. The traditional liquid-filled and bimetallic thermometers, the thermocouples, the pyrometers and the thermistors are generally not suitable for temperature measurements at scales below 10 mm. This intrinsic limitation has encouraged the development of new non-contact accurate thermometers with micrometric and nanometric precision, a challenging research topic increasingly hankered for. At CICECO and ICMA we have addressed this issue during the last 4 years and recently we have patented[1] and reported[2] a unique Eu^{3+}/Tb^{3+} luminescent self-referencing nanothermometer allowing absolute measurements in the 10-350 K temperature range and submicrometer spatial resolution. The developed thermometer

has up to 4.9%·K^{-1} temperature sensitivity (1.5 times larger than the highest value reported previously) and it exhibits high photostability for long-term use. The variation of the Eu^{3+}/Tb^{3+} ratio affords tunability to the temperature working range. Alternatively, tunability is also accomplished by changing the host matrix, thus modifying the interaction between the Ln^{3+} and the host matrix energy levels. The nanothermometer is a versatile material which can be processed in different forms adapted to the desired application. So far we have processed this nanothermometer in two different forms; i) a thin film coating an integrated circuit trough which we obtain an high resolution 2-dimensional temperature mapping and ii) nanobeads composed of magnetic nanoparticles (γ-Fe_2O_3) used as a magnetic-actuated heat sources covered by a matrix containing Eu^{3+}/Tb^{3+} chelates (Fig.1). The resolution of these thermometers is constrained by the spatial resolution of the optical detector and not by the material itself. The ultimate resolution limit of the thermometer is expected to be of a few nanometers and can be achieved in the future by using better sensing/mapping devices. We anticipate that the synergetic outcomes arising by combining temperature sensing/mapping and superparamagnetism opens the way for new exciting applications, especially in the biomedical field. In particular, such association will provide a unique instrument to map, in a non-invasive way, temperature distributions in biological tissues (e.g., in tumors) during heat release, due to the application of an ac field to magnetic nanoparticles (magnetic hyperthermia), this being a powerful tool for the study of biochemical microprocesses occurring within a cell.

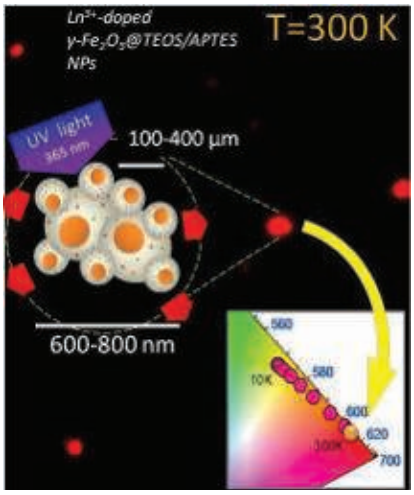

Figure 1. Red spots on a black background corresponding to the temperature-dependent emission of the nanothermometer observed at 300 K under an optical microscope. Inset shows a scheme of the nanothermometer composed of maghemite (γ-Fe203) nanoparticles recovered by a lanthanide-doped TEOS/APTES matrix and the dependence of the emission color on the temperature between 10 and 300 K.

This work was highlighted in the HOT TOPICS section of Wiley, MRS news of MRS, Chemical & Engineering News of ACS and Materials Today.

[1] Department of Physics, CICECO, University of Aveiro, 3810-193 Aveiro, Portugal

[2] Departamento de Fisica de la Materia Condensada, Facultad de Ciencias and Instituto de Ciencia de Materiales de Aragón, CSIC–Universidad de Zaragoza

Reference paper

[1] Palacio F, Millán A, Silva NJ, Carlos LD, Amaral V, Lima PP, Brites CDS, Spain Patent P200930367, 2009.

[2] Brites CDS, Lima PP, Silva NJO, Millán A, Amaral V, Palacio F, Carlos LD. "A luminescent molecular thermometer for long-term absolute temperature measurements at the nanoscale", Adv. Mater, 2010, 22, 4499.

TUNNING THE PROPERTIES OF γ-Fe_2O_3@SiO_2 NANOPARTICLES AS MRI CONTRAST AGENTS BY ADJUSTING THE SILICA COATING THICKNESS

Rocha J[1], Carlos LD[1], Pinho SLC[1,2], Geraldes CFGC[3], Pereira GA[1,3], Voisin P[4], Kassem J[4], Bouchaud V[4], Etienne L[2], Peters JA[5], Mornet S[2], Delville M-H[2]

Nanoparticles (NPs) made of inorganic or organic materials exhibit many novel properties compared with the bulk materials. Magnetic NPs have unique properties such as superparamagnetism, high coercivity, low Curie temperature and high magnetic susceptibility. We are particularly interested in the applications of magnetic NPs as contrast agents in Magnetic Resonance Imaging. In collaboration with colleagues from Université de Bordeaux, Universidade de Coimbra and Delft University of Technology, we reported in 2010 the fine tuning of the relaxometry of γ-Fe_2O_3 core-shell nanoparticles by adjusting the width of the coated silica layer (Fig.1). The coating thickness of γ-Fe_2O_3@SiO_2 nanoparticles has a significant impact on the r_1 (at lower fields), r_2 and r_2* relaxivities of their aqueous suspensions. The silica layer was shown to have regions which are porous to water and other regions which are not. The viability and mitochondrial dehydrogenase expression of the microglial cells are not sensitive to the vesicular load with these core-shell nanoparticles. A nice compromise on the silica shell thickness may be found to allow both, a high enough response as contrast agent, and a grafting of targeted biomolecules.

Understanding the relationship between the coating properties and the changes in relaxivity is vital for designing magnetic nanoparticle probes for MRI. This is important for medical applications, as a higher contrast leads to a higher sensitivity and reduces the amount of contrast agent required for imaging. Our choice of a silica coating was motivated by the increased stability of the resulting nanoparticle suspensions and the ensuing ease of conjugation of targeting molecules to the surface of the contrast agents for sensing and imaging. We have shown that in γ-Fe_2O_3@SiO_2 core-shell NPs, the coating thickness has a significant impact on their r_2 and r_2* relaxivities at medium and high fields and on r_1 relaxivities at medium fields, as a result of decreased outer-sphere

relaxation effects (Fig.2). Comparing the r_2 and r_2* values for the different sizes of particles we were able to divide the silica coating in two regions, one impermeable close to the γ-Fe_2O_3 core and one permeable to water and at the interface with the bulk water. We have shown that by controlling this coating we are able to tune the size of these two regions. The impermeable one seems to increase up to a maximum value of 40 nm, while the permeable region goes on increasing with the coating thickness. The diffusion of the water molecules in the permeable silica region is relatively slow resulting in zero contribution to r_2. The effect of silica coating of increasing thickness on the r_2/r_1 ratio is different from that reported for nanocrystalline superparamagnetic iron oxide NPs (MIONs) coated with a polyethylene glycol (PEG)-modified, phospholipid micelle coating with increasing molecular weights which increase the particle diameter, where this increase causes a r_2 decrease and a r_1 increase.

Therefore, our results provide clues for the design of contrast agents based on magnetic nanoparticle and their optimisation for specific applications in medical diagnosis. NMR is up to now the only technique to provide clear evidence that a silica layer used as a coating in a core-shell system exhibits regions that are porous to water and regions that are not. Careful studies of all the factors that influence the relaxation properties of such contrast agents are under scrutiny. The knowledge of theses systems may be extended to other systems and applications. Additionally, preliminary cytotoxicity studies confirmed that these contrast agents do not appear detrimental to microglial cells. However, as the naked nanoparticles have the highest relaxivities, and the coating thickness does not play a role in their cytotoxicity, a preliminary conclusion is that overall optimal particles should have a minimal coating thickness to provide solution stability and a basis for surface conjugation without compromising their relaxivities.

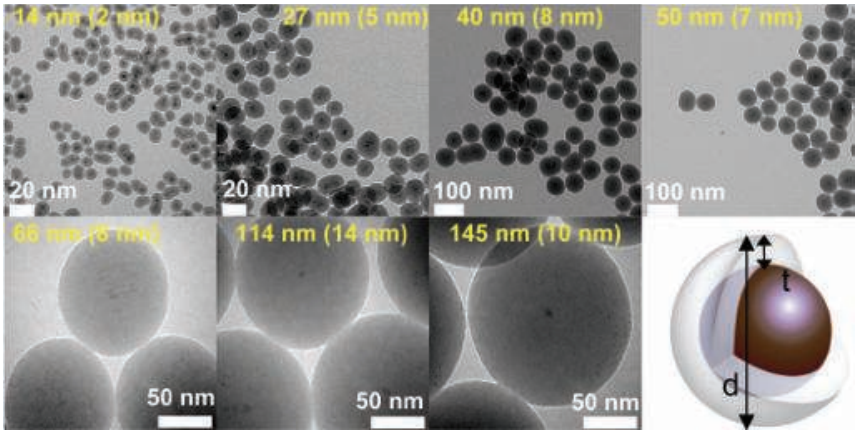

Figure 1. **(top)** TEM images showing the average size (diameter d) of different maghemite core-shell (γ-Fe_2O_3@SiO_2) nanoparticles and of their silica shell thickness (t).

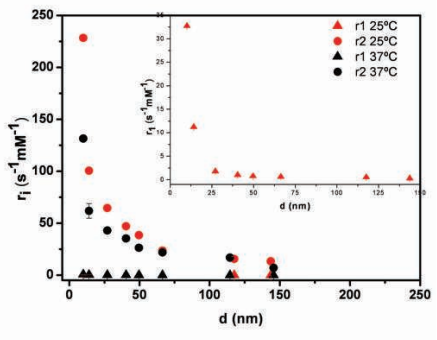

Figure 2. **(left)** Dependence of water relaxivities of aqueous suspensions of the γ-Fe_2O_3@SiO_2 nanoparticles on their diameter, as a result of increased silica layer thickness: **a)** inset: r_1 at 20 MHz (25 ºC); **b)** main plot: r_i (i =1, 2) at 500 MHz (25 ºC and 37 ºC). r_2 relaxivities were measured at τ_{CP} = 1.6 ms.

[1] Departments of Chemistry and Physics, CICECO, University of Aveiro, 3810-193 Aveiro, Portugal

[2] CNRS, Université de Bordeaux, ICMCB, 87 avenue du Dr. A. Schweitzer, Pessac, F-33608, France

[3] Department of Life Sciences, Faculty of Science and Technology, and Centre of Neurosciences and Cell Biology, University of Coimbra, 3001-401 Coimbra, Portugal

[4] Centre de Résonance Magnétique des Systèmes Biologiques, UMR 5536 CNRS, UMR 5536 CNRS, 146 rue Victor Segalen, F-33076 Bordeaux cedex, France.

[5] Laboratory of Biocatalysis and Organic Chemistry, Department of Biotechnology, Delft University of Technology, Julianalaan 136, 2628 BL Delft, The Netherlands

Funding

We thank FCT and NoE FAME.

Reference paper

[1] Pinho SLC, Pereira, GA, Voisin P, Kassem J, Bouchaud V, Etienne L, Peters JA, Carlos L, Geraldes CFGC, Rocha J, Delville M-H. "Fine Tuning of the Relaxometry of g-Fe_2O_3@SiO_2 Nanoparticles by Tweaking the Silica Coating Thickness", ACS Nano, 2010, 4, 5339-5349.

GRAFTING POLY(METH)ACRYLATES FROM CARBON NANOSTRUCTURED MATERIALS VIA ATRP

Barros-Timmons A[1]

Polymerizations from surfaces, also known as SIP (surface initiated polymerization), have been widely used in the preparation of nanocomposites. Amongst these strategies living/controlled radical polymerization mechanisms, such as atom transfer radical polymerization (ATRP), offer the possibility of preparing multifunctional materials with good control over the polymer molecular weight, polydispersity index and end group functionality. Furthermore, the living and controlled characteristics of this mechanism also provide a way to grow block copolymers of well defined composition and length. For these reasons the ATRP mechanism has been explored to graft polymer brushes from the surface of nanostructured reinforcing materials to prepare hybrids wich in turn can be easily dispersed in solvents and / or in dense polymer matrices yielding tougher composites. Furthermore, judicious tuning of the length and composition of the blocks of the copolymers grafted

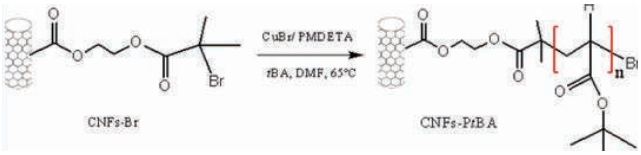

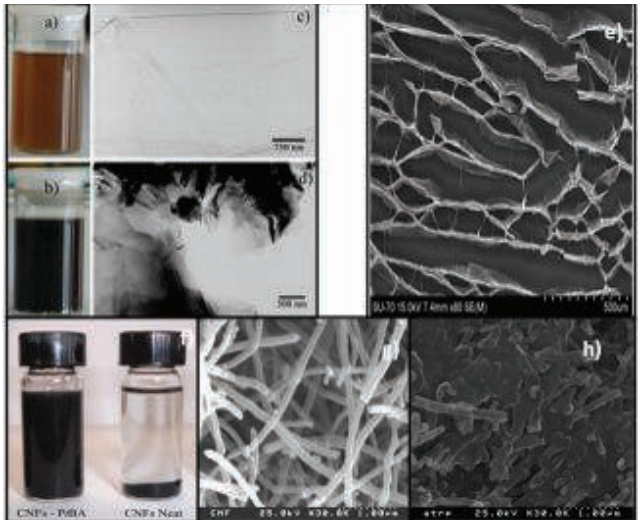

Figure 1. Synthetic path followed to graft poly(*t*-butyl acrylate) from the surface of CNFs via ATRP ; Photographs of (a) GO dispersed in water and (b) G-PMMA dispersed in chloroform; TEM micrographs of (c) GO nanosheets, (d) G-PMMA nanosheets; (e) SEM micrograph of VACNT-PMMA; (f) photographs of CNF-*Pt*BA and CNF in toluene, (g) and (f) SEM micrographs of pristine CNFs and CNF-*Pt*BA respectively.

from the surface of the fillers provides extra possibilities to improve the stress transfer from matrix to fillers.

In our laboratory, ATRP has been successfully explored to grow poly(methyl methacrylate) and poly(*t*-butyl acrylate) chains from the surface of graphene oxide (GO) and carbon nanofibers (CNFs). Figure 1 illustrates the synthetic path used to grow poly(*t*-butyl acrylate) chains from the surface of CNFs via ATRP and photographs proving the presence of the polymer grown from different carbon nanostructured materials. The resulting graphene oxide/PMMA or CNF/*Pt*-BA have been blended with PMMA and poliamide12 dense matrices, respectively. The nanocomposites prepared using loads as low as 1% (w/w) of carbon reinforcing materials are tougher than those prepared using unmodified fillers proving that this strategy promotes stronger interfacial interactions with the polymer matrices. These studies have been done in collaboration with researchers from TEMA and from the Technical University of Hamburg, respectively[1-3]. As regards the work on graphene oxide/PMMA nanocomposites, which was carried out in close collaboration with TEMA, AFM studies in friction mode provided important information regarding adhesion forces and the distribution of the fillers at the surface which correlate well with the results obtained from nanoindentation and uniaxial tensile tests.

Whilst the surface modification of carbon nanostructured materials with acids is very efficient to generate oxygen reactive sites that can be used for grafting the ARTP initiator, such treatments may cause significant damage to the surfaces. Therefore, plasma surface treatment is now being used. This method is particularly useful for grafting polymer brushes from the surface of vertically aligned carbon nanotubes (VACNTs). In fact, this approach is presently being exploited to grow PMMA chains from the surface of VACNTs in collaboration with members of CICECO. Furthermore, the effect of the length and composition of blocks of the copolymers grafted from the surface of the fillers is under current investigation to assess the mechanism of stress transfer from matrix to the carbon nanostructured fillers.

[1] Department of Chemistry, CICECO, University of Aveiro, 3810-193 Aveiro, Portugal

Reference paper

[1] Ghislandi MG, Prado LASA, Oyerviedes AV, Wittich H, Schulte K, Barros-Timmons A. J. Polym. Sci.: Part A: Polymer Chemistry. **2008**. 46, 3326–3335.

[2] Gonçalves G, Marques PAAP, Barros-Timmons A, Bdkin I, Singh MK, Emami N, Grácio J. J. Mater. Chem., in press. DOI: 10.1039/c0jm01674h.

[3] Ghislandi MG. **2007**. M.Sc. Thesis/ Technische Universität Hamburg.

SYNTHESIS, CHARACTERIZATION AND GAS SENSING PROPERTIES OF Mo_x/CNT HETEROSTRUCTURES OBTAINED VIA A NOVEL NON-AQUEOUS ROUTE TO ATOMIC LAYER DEPOSITION

Marichy C[1], Willinger M-G[1], Pinna N[1,2]

Carbon nanotubes offer a high surface area, good thermal and electric conductivity and mechanical as well as chemical stability. As such, they are ideally suited as support for a second material that can be deposited onto their surface either as particles or as a thin film. Such heterostructures find applications in catalysis, energy storage or gas sensing, where it is essential to expose the active phase on a large surface area. Due to the small dimensions, interactions between the deposited material and the tubes at the interface can significantly alter the properties of the composite. This is specifically the case for semiconducting materials when the dimensions are in the range of the Debye length. Studying such synergetic phenomena and size dependent properties in a systematic way relies on a method that allows a precise control of the particle or film growth during the deposition.

Atomic layer deposition (ALD) is specifically suited for the production of such heterostructures. It is based on subsequent gas-surface reactions and therefore, allows the coating of flat surfaces as well as complex and high surface ar-

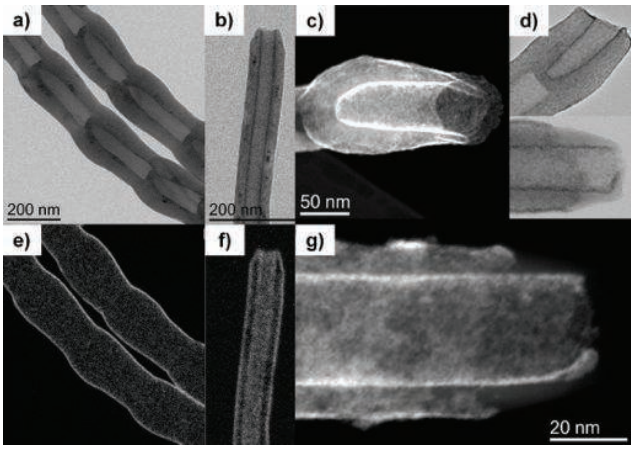

Figure 1. TEM images recorded from CNTs coated with V204 (a, b) and corresponding energy filtered images showing the distribution of vanadium on the surface of the tubes (e,f). High angle annular dark-field STEM images of CNTs coated with Sn02 and corresponding TEM images are shown in c), g) and d), respectively.

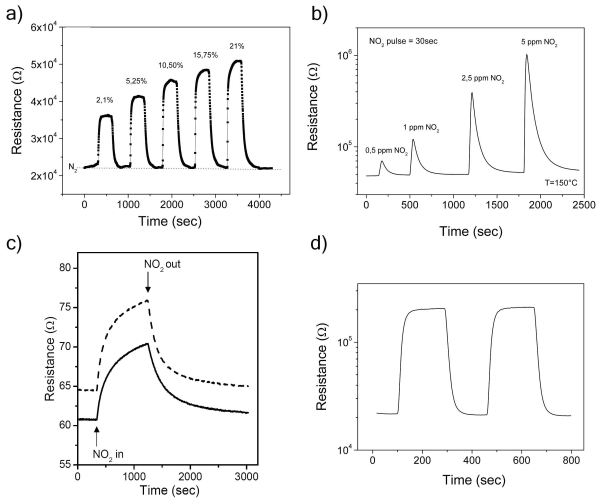

Figure 2. Transient response of the sensor made of 3 nm SnO_2 coated CNTs exposed to different concentrations of (a) O_2 at 200 °C and (b) NO_2 at 150 °C. (c) Transient response of CNTs coated with a 4.5 nm (solid line) and 2 nm (dotted line) thick vanadium oxide film. (d) Transient response of 3.0 nm SnO_2 coated CNTs sensor to 5 ppm of NO_2 at 200 °C.

ea nanostructures in a conformal and homogeneous manner with a precise control of the thickness of the deposited film in the range of a few angstroms. Recently we have introduced a non-aqueous sol-gel approach for the deposition of metal oxide thin films via ALD using metal alkoxides and carboxylic acids as precursors [1].

The reaction takes place in two steps: the formation of surface carboxylate species (eq.1) and subsequently, the formation of the metal-oxide bond through an aprotic condensation (eq. 2).

≡M-OR' + RCOOH → ≡M-OOCR + R'OH (eq. 1)

≡M-OOCR + M-OR' → ≡M-O-M≡ + RCO-OR' (eq. 2)

Beside other substrates, this process was successfully applied for the conformal and homogeneous coating of the inner and outer surface of carbon nanotubes with thin films of hafnium-, titanium-, vanadium-, and tin-oxide, even at deposition temperatures as low as 50°C[1]. The obtained heterostructures were characterized by analytical electron microscopy using high resolution imaging, electron energy-loss- and energy dispersive X-ray spectroscopy as well as elemental mapping (Fig.1). ALD-coated tubes with thin layers of V_2O_4 and SnO_2, respectively, were investigated as active component in gas-sensing devices [2, 3]. Response to O_2 and NO_2 at different concentrations and sensor temperature were investigated. Due to the formation of a p-n heterojunction between the p-type conductive CNTs and the n-type thin film, an enhancement of the gas-sensing response was observed (Fig.2). This synergetic effect, caused by the interaction of film and support, enables the detection of sub-ppm concentrations of NO_2 at low temperature (150°C) and in just few seconds. The proportion to which this effect determines the sensing properties highly depends on the film thickness. Therefore, the highest sensitivity and sensor response is expected for a film whose thickness is in the range of the respective Debye length.

[1] Department of Chemistry, CICECO, University of Aveiro, 3810-193 Aveiro, Portugal

[2] World Class University (WCU) program of Chemical Convergence for Energy & Environment (C2E2), School of Chemical and Biological Engineering, College of Engineering, Seoul National University (SNU), Seoul 151-744, Korea.

Reference paper

[1] Rauwel E, Clavel G., Willinger M-G, Rauwel P, Pinna N. Angew. Chem., Int. Ed. 2008, 47, 3592–3595

[2] Willinger M-G., Neri G, Rauwel E, Bonavita A, Micali G, Pinna N. Nano Lett. 2008, 8, 4201-4204.

[3] Marichy C, Donato N, Willinger MG, Latino M, Karpinsky D, Neri G, Pinna N. accepted for publication in Adv. Funct. Mater.

LDH-NANOCONTAINERS FOR SELF-HEALING ANTICORROSION COATINGS

Zheludkevich ML[1], Tedim J[1], Poznyak SK[1], Salak AN[1], Ferreira MGS[1]

Anticorrosion pigments are normally added to polymer coatings in order to provide an additional active corrosion protection and to hinder the corrosion activity on the metal surface in defect sites. However the normal inhibiting pigments are prone to uncontrollable leaching of an active component leading to fast exhausting of self-healing potential and to osmotic blistering of polymer films. Due to very high carcinogenic potential of chromates, the most efficient inhibiting pigments, is banned since 2007. Thus development of new active corrosion protection

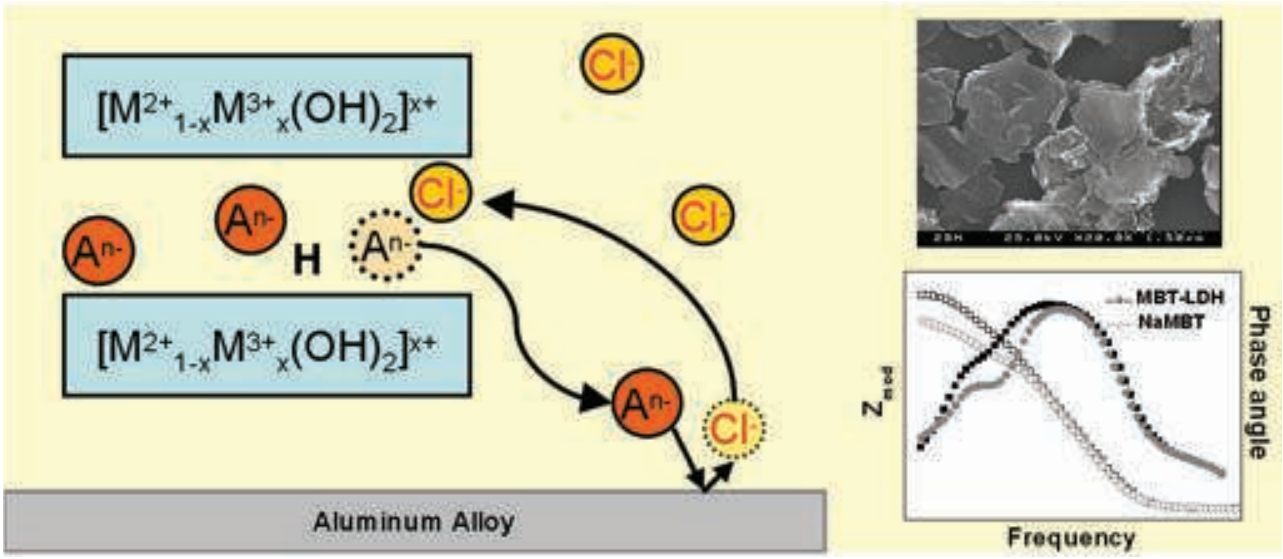

Figure 1. Principal schema of triggered release of corrosion inhibitors from LDH nanocontainers.

systems with self-healing ability becomes now a very important challenging issue for many industries. A very interesting alternative which allows a controllable leaching triggered by a corrosion related stimuli is the use of ion-exchange clays as reservoirs of corrosion inhibitors. The release of inhibitor anions can be provoked in this case by exchange with aggressive corrosive chloride ions. The anion exchange pigment can play a double role absorbing the harmful chlorides and releasing the inhibiting ions in response (Fig.1). Absorption of chlorides from an aggressive electrolyte in a vicinity of a defect decreases the aggressiveness of the corrosive medium, and thereby reduces the rate of the corrosion processes.

Novel LDH-based nanocontainers of corrosion inhibitor were developed in our group. The reservoirs are composed by nanostructured layered double Mg/Al and Zn/Al hydroxides with corrosion inhibitors (divanadate anions, phosphates, molybdates, quinaldate and mercaptobenzothiazole) located in the interlayer regions[1-4]. The anion-exchange reaction of nitrate-loaded LDH precursors was used to create the containers of the inhibitors. The compounds obtained are nanocrystalline with a plate-like morphology (Fig. 2)[2, 3]. Corrosion protection effect of the LDH powders directly added to corrosive electrolyte or to commercial coatings used for aeronautical application has been studied by electrochemical impedance spectroscopy and standard accelerated corrosion tests. Aluminum alloy 2024 was used here as substrate. The anticorrosion capabilities of LDHs loaded with organic inhibitors towards the AA2024 aluminum alloy were analyzed by electrochemical impedance spectroscopy (EIS). Significant reduction of the corrosion rate is observed when the LDH nanopigments are present in the corrosive media. The mechanism by which the inhibiting anions can be released from the LDHs underlines the versatility of these environmentally friendly structures and their potential application as nanocontainers in self-healing coatings. The coatings doped with Zn/Al LDH nanocontainers provide well defined self-healing effect and confer corrosion protection properties superior than currently used environmentally unfriendly chromate-based systems. The combination of several types of nanocontainers in the same or in different functional coating layers is a versatile route for designing active corrosion protection systems with superior performance[4].

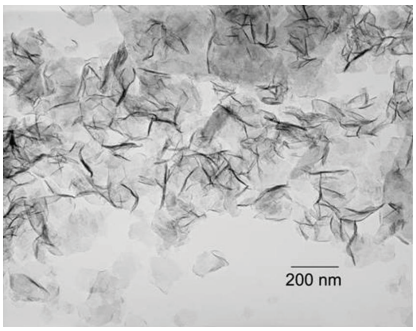

Figure 2. TEM image of Zn-Al LDH nanocontainers with vanadate contr-ion as corrosion inhibitor.

[1] Department of Ceramics and Glass Engineering, CICECO, University of Aveiro, 3810-193 Aveiro, Portugal

Reference paper

[1] Zheludkevich ML, Poznyak SK, Rodrigues LM, Raps D, Hack T, Dick LF, Nunes T, Ferreira MGS. *Corrosion Science*. **2010**, 52, 602-611

[2] Salak AN, Tedim J, Kuznetsova AI, Zheludkevich ML, Ferreira MGS. *Chemical Physics Letters.* **2010,** 495, 73-76

[3] Poznyak SK, Tedim J, Rodrigues LM, Salak AN, Zheludkevich ML, Dick LFP, Ferreira MGS. *ACS Appl. Mater. Interfaces*. **2009,** 1, 2353-2362

[4] Tedim J, Poznyak SK, Kuznetsova A, Raps D, Hack T, Zheludkevich ML, Ferreira MGS. *ACS Appl. Mater. Interfaces*. **2010**, 2, 1528-1535

Aknowledgement

This work has been funded by FCT Portugal (PTDC/CTM/65632/2006), by EU FP6 project "Multiprotect" NMP3-CT-2005-011783 and EU FP7 project "MUST" NMP3- CP-IP 214261-2

UNFOLDING THE MAGNETISM OF ANTIFERROMAGNETIC NANOPARTICLES

Silva NJO[1], Carlos LD[1], Amaral V[1], Martins M[2], Trindade T[2]

In the last years and in the frame of different international collaborations we have revealed and understood different interesting aspects of antiferromagnetic nanoparticles (AFNPs). Despite their low magnetic moment, they have high anisotropy which is a crucial requisite in the use of increasingly smaller NPs in recording media, increasing the data storage density. Using neutron diffraction techniques, we were able to determine the average "crystalline" size and the average "magnetic" size of CoO AFNPs[1]. The latter is smaller, revealing thus the existence of a surface layer (of about 2 nm thick) where the atoms are ordered but the spins are disordered. This picture is further supported by high-resolution microscopy studies (Fig.1a). The uncompensated spins are responsible for a remanent moment, which has typical characteristics of a surface moment. In the last decade, the antiferromagnetic susceptibility of AFNPs was supposed to decrease with temperature below the Néel temperature and no definite explanation to this behavior was given. Recently, we have shown that in ferritin this only occurs at low fields, where the uncompensated moment of the NPs is not saturated, and that at sufficiently high fields (~30 T) the antiferromagnetic susceptibility increases with temperature as expected from the mean-field and superantiferromagnetism descriptions (Fig. 1b)[2]. The relation between structural and magnetic physical quantities in AFNPs is not straightforward as in the case of ferromagnetic NPs. To unfold these relations we have developed a method based on the analysis of the statistical distribution of the quantities with a power relation with unknown parameters. We have applied this method to ferrihydrite nanoparticles and found that the anisotropy energy barrier is proportional to the square root of the volume thus indicating a random distribution of energy barriers[3].

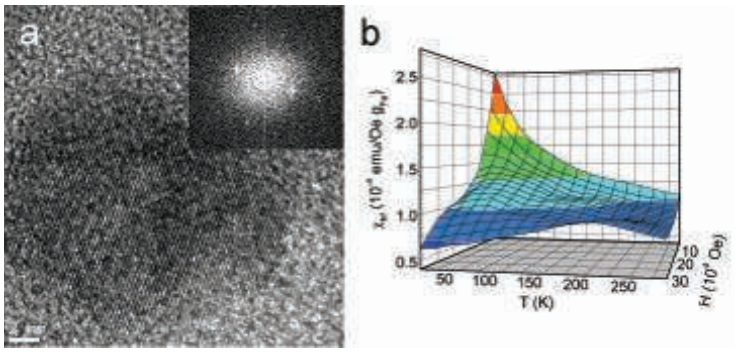

Figure 1. a) High resolution transmission electron microscopy image of a CoO AFNP with inset showing the Fourier transform of the image; b) temperature and field dependence of the antiferromagnetic susceptibility in ferritin.

[1] Department of Physics, CICECO, University of Aveiro, 3810-193 Aveiro, Portugal

[2] Department of Chemistry, CICECO, University of Aveiro, 3810-193 Aveiro, Portugal

Aknowledgment

This work was performed in collaboration with researchers from Universidade de Trás-os-Montes e Alto Douro (Vila Real, Portugal), Instituto de Ciencia de Materiales de Aragón (Zaragoza, Spain), Institut Laue-Langevin (Grenoble, France), Institute for Rock Magnetism (Minnesota, USA), Universidad de Vigo (Vigo, Spain), High Field Magnet Laboratory (Nijmegen, The Netherlands) and LNCMP (Toulouse, France).

Reference paper

[1] Silva NJO, Millán A, Palacio F, Martins M, Trindade T, Puente-Orench I, Campo J. "Remanent magnetization in CoO antiferromagnetic nanoparticles", *Phys. Rev. B*. **2010**. 82 094433

[2] Silva NJO, Millán A, Palacio F, Kampert E, Zeitler U, Amaral VS. "Temperature dependence of antiferromagnetic susceptibility in ferritin", *Phys. Rev. B*. **2009**. 79, 104405

[3] Silva NJO, Amaral VS, Carlos LD, Rodríguez-González B, Liz-Marzán LM, Berquó TS, Banerjee SK, de Zea Bermúdez V, Millán A, Palacio F. "Evidence of random magnetic anisotropy in ferrihydrite nanoparticles based on analysis of statistical distributions" *Phys. Rev. B*. **2008**. *77*, 134426.

UNDERSTANDING THE RESPONSE OF INDIVIDUAL NANOSTRUCTURES TO AN EXTERNAL STIMULUS

Costa PMFJ[1], Gautam UK[2], Cachim PB[3], Wang MS[2], Wagner JB[4], Hansen TW[4], Dunin-Borkowski RE[4], Bando Y[2], Golberg D[2]

For the last two decades there has been an exceptional amount of new nanoscaled materials reported. Spanning from quantum dots to extended atomic layers, these nanostructures show a myriad of useful properties and an elevated potential for next-generation technological applications. In spite of the progress on the synthesis front, the comprehensive characterization of nanoscaled materials, particularly at the single-nanostructure level, is still rare. For the most part, analytical studies are carried out in bulk quantities and provide only limited information on the average structure, chemical composition and, eventually, on a specific functional property (optical, magnetic, ...). Yet, the integration of any substance onto a technological application - may that be a sensor or an electronic circuit - requires a much broader knowledge of the material. Furthermore, when using the so-called "bottom-up" approach, single-nanostructure studies become imperative to distinguish the exact characteristics of a nanoscaled material as opposed to its bulk-level collective responses (generally influenced by factors such as purity, structure orientation and sample homogeneity).

Carbon nanotubes (CNTs) filled with inorganic substances is a class of nanoscaled composite materials which provides added functionalities to one-dimensional structures. Since 2008, an international collaboration involving the University of Aveiro (Portugal), the National Institute for Materials Science (Japan) and the Technical University of Denmark (Denmark) has been actively changing the *status quo*

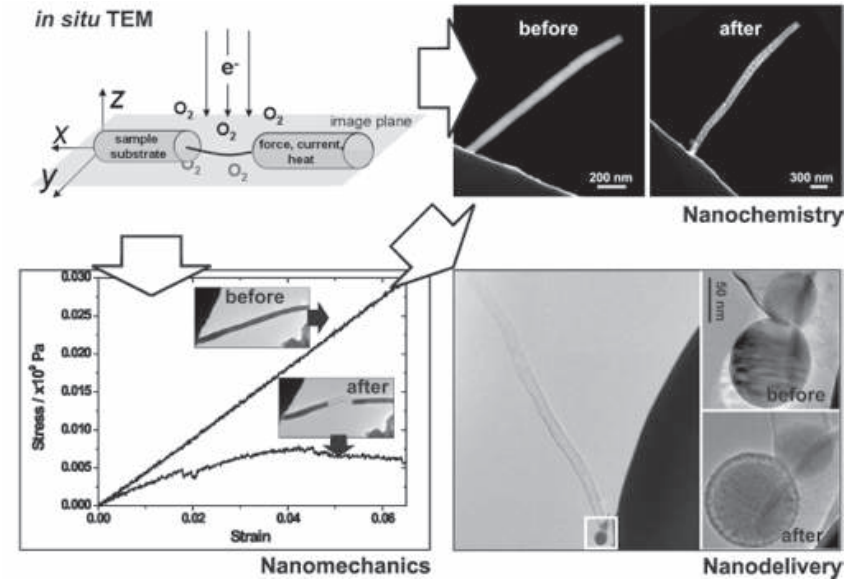

Figure 1. in situ TEM: using the microscope as a laboratory it becomes possible to carry out single-nanostructure testing and controlled manipulation.

for these poorly characterised materials. Using turbostratic carbon nanotubes filled with a II-VI semiconductor material (a.k.a. $Zn_{0.92}Ga_{0.08}S$@CNT) as a model-system[1], an exhaustive study was designed to evaluate the responses of individual nanostructures to a variety of externally applied stimuli. These included exposing the core-shell materials to compressive loads, harsh chemical environments, high current densities and high energy particle beams (Fig.1). The experiments performed required the use of sophisticated transmission electron microscopes (TEM) and dedicated sample holders.

Initially, the thermal and chemical stabilities were investigated by subjecting the nanostructures to temperatures in excess of 500ºC both in vacuum and under a reactive atmosphere (oxygen gas)[2]. For the first time, it was possible to live-image the Kirkendall effect via which the initial core-shell structure was transformed into a polycrystalline oxide tube. In addition to this, we found that the structural stability of isolated $Zn_{0.92}Ga_{0.08}S$@CNTs bombarded with high energy particles is strongly dependent on temperature. Next, the electrical and mechanical behaviour were examined. Two-terminal probing confirmed the metal-like conductivity of the system, opening up the way to use high current densities as a means to engineer the $Zn_{0.92}Ga_{0.08}S$@CNTs. By partially removing the optically-active content, the stiffness of the composite could be tailored with an unprecedented control[3,4]. In fact, the core influence in the nanomechanics of filled CNTs had been theoretically predicted for more than a decade but up until the present work it had not been experimentally investigated. Finally, we performed nanodelivery of the II-VI semiconductor and analysed the comparative stability of encapsulated and expelled nanoparticles when exposed to air[5]. This experiment substantiated the widely-believed-but-not-demonstrated concept of CNTs acting as protective shells for sensitive inorganic materials.

Together with the structural, chemical and optical data previously gathered for the $Zn_{0.92}Ga_{0.08}S$@CNT system, the set of experiments described here constitute a unique body-of-work for single-nanostructure studies. This exceptional insight into how one-dimensional materials react to different stimuli, and to which extent it is possible to engineer them, may motivate new approaches for the manufacture of nanoscaled devices and associated reliability tests.

[1] Department of Ceramics and Glass Engineering, CICECO, University of Aveiro, 3810-193 Aveiro, Portugal

[2] MANA, National Institute for Materials Science (NIMS), 305-0044 Ibaraki, Japan

[3] Department of Civil Engineering, University of Aveiro, 3810-193 Aveiro, Portugal

[4] CEN, Technical University of Denmark (DTU), DK-2800 Kgs Lyngby, Denmark

Aknowledgment

This work was supported by the Ciencia2007 programme, the Royal Society of Chemistry, NIMS and CICECO.

Reference paper

[1] Gautam UK, Bando Y, Zhan JH, Costa PMFJ, Fang XS, Golberg D, "Ga-doped ZnS nanowires as precursors for ZnO/$ZnGa_2O_4$ nanotubes", Advanced Materials **2008**, 20, 810-814

[2] Costa PMFJ, Hansen TW, Wagner JB, Dunin-Borkowski RE, "Imaging the oxidation of ZnS encapsulated in carbon nanotubes", Chemistry – A European Journal **2010**, 16, 11809-11812

[3] Costa PMFJ, Gautam UK, Wang MS, Bando Y, Golberg D, "Effect of crystalline filling on the mechanical response of carbon nanotubes", Carbon **2009**, 47, 541-544

[4] Costa PMFJ, Cachim PB, Gautam UK, Bando Y, Golber D, "The mechanical response of turbostratic carbon nanotubes filled with Ga-doped ZnS: II. Slenderness ratio and crystalline filling effects", Nanotechnology **2009**, 20, art. 405707

[5] Costa PMFJ, Gautam UK, Bando Y, Golberg D, "Comparitive study of the stability of sulphide materials encapsulated in and expelled from multi-walled carbon nanotubes capsules", Carbon. doi: 10.1016/j.carbon.2010.08.058

DESIGN AND CHARACTERIZATION OF MOLECULAR MAGNETS FOR QUANTUM INFORMATION AT ROOM TEMPERATURE

Brandão P[1], Moreira dos Santos A[2], Reis M[3]

Since the early years of quantum mechanics, entanglement has attracted much attention due to its fascinating features, such as nonlocality, as exemplified in the Einstein, Podolsky, and Rosen parado[1]. Recently, it has been discovered that entangled states constitute a valuable resource for quantum information processing and it has raised a great number of studies about entanglement in many different quantum systems. Over the past few years, much effort has been done

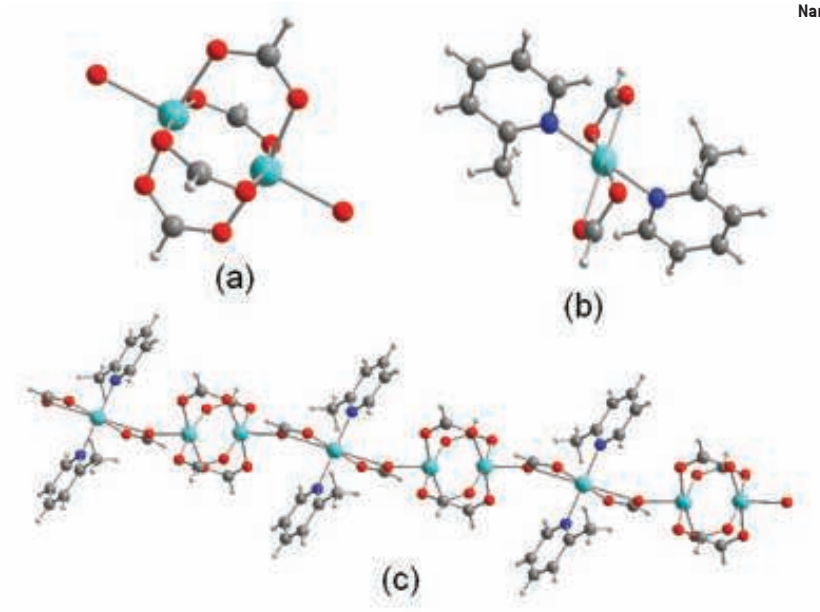

Figure 1. Detailed view of the structural motifs of (a) Dicopper tetracarboxylate dimer unit, (b) copper dimethylpyridine monomeric unit, and (c) view of the chain formed by alternating dimers and monomers.

in developing methods to detect and quantify entanglement. Surprisingly, it was theoretically demonstrated that entangled states can exist in solids at finite temperature and this kind of entanglement is referred in literature as "thermal entanglement"[2].

Since the publication of several theoretical works, a few experimental evidences have been reported, confirming the presence of entanglement in solids state systems[3,4]. The study of entanglement in solid state physics is of great relevance to the area of quantum information and quantum computation since many proposals of quantum chips are solid state based. Furthermore, the demonstration that entanglement can change the thermodynamical properties of solids, such as magnetic susceptibility, shows that entanglement can be related to significant macroscopic effects. Hence, this subject establishes an interesting connection between quantum information theory and condensed matter physics.

For this purpose we have studied a family of magnetic materials that can support entanglement at very high temperatures, namely, metal carboxylates with syn-syn conformation. For the compound $\{Cu_2(O_2CH_4)\}\{Cu(O_2CH)_2(2\text{-methylpyridine})_2\}$[5], we determined that the critical temperature for bipartite entanglement is $Te \sim 630$ K. Furthermore, we could also conclude that the system remains maximally entangled up to ~100 K and the Bell's inequality can be violated up to close room temperature (~290 K), which is an interesting feature of this material since Bell's inequalities are of great importance to quantum information science. This metal carboxylate contains copper dimers and copper monomers. The dimer is formed by opposing square pyramidal CuO_5. The base oxygen atoms on the adjoining pyramids are part of the four-connecting carboxylate groups in a syn-syn conformation which leads to a strong magnetic interaction between the dimer's atoms (Fig.1a). The Cu-Cu distance in this ensemble is 2.63 Å. This square pyramid is slightly distorted from the tetrahedral shape, with an average Oap-Cu-Oeq angle of about 95°. The apical oxygen of the pyramid is connected, via another carboxylate group, to the Cu(2-methylpyridine) in a syn-anti configuration. This copper, the monomer (Fig.1b), is in a pseudo-octahedral coordination with four oxygen atoms; two from each carboxylate group along the chain and two opposing nitrogen ions from the methylpyridine group. These alternating dimers and monomers extend in one direction forming a chain (Fig.1c) of alternating dimers and monomers (or a syn-syn-anti progression) where the magnetic interaction between the dimer's atoms is strong, and weak between the dimer and the monomer, as may be deduced from the structural characterization.

We believe that the study of such class of materials can open the doors for new research toward the realization of solid-state quantum devices since molecular magnets have been studied for some time by the solid-state community.

[1] Department of Chemistry, CICECO, University of Aveiro, 3810-193 Aveiro, Portugal

[2] NSSD, Oak Ridge National Laboratory, Oak Ridge, Tennessee 37831-6475, USA

[3] Instituto de Física, Universidade Federal Fluminense, 24210-340, Rio de Janeiro, Brasil

Reference paper

[1] Einstein A, Podolsky B, Rosen N, *Phys. Rev.* **1935**. *47*, *777*.

[2] Arnesen MC, Bose S, Vedral V, *Phys. Rev. Lett.* **2001**. *87*, 017901.

[3] Osterloh A, Amico L, Falci G, *Fazio R. Nature (London)*. **2002**. 416, 608.

[4] Rappoport TG, Ghivelder L, Fernandes JC, Guimarães RB, Continentino MA. *Phys. Rev. B.* **2007**. *75*, 054422, 2007.

[5] Souza AM, Soares-Pinto DO, Sarthour RS, Oliveira IS, Reis MS, Brandão P, dos Santos AM, *Phys. Rev. B.* **2009**. *79*, 054408.

NO EXPONENTIAL IS FOREVER . . . BUT WE CAN DELAY "FOREVER" - THE CONTRIBUTION OF ADDITIVE - ASSISTED AQUEOUS SYNTHESIS OF $BaTiO_3$ NANOPOWDERS

Maxim F[1], Ferreira P[1], Vilarinho PM[1], Aimable A[2], Bowen P[2]

In 1965 Gordon Moore predicted an exponential increase of the number of devices per silicon chip and this prediction became known as Moore´s law. Indeed the density has been increasing at an exponential rate (doubling every 18 months) for an amazing length of time (more than 30 years) (Fig.1). However with the approach of the minimum feature length size allowed by lithographic processes alternative approaches are required to keep device scalling. Bottom up approaches are now being considered in the so-called 'nanoscale' technology era. Switchable polarization, piezoelectricity, pyroelectricity, high non-linear optical activity and non-linear dielectric behaviour important for microelectronics are intrinsic characteristics of ferroelectrics. In addition the understanding of the relationship between structure and properties is fundamental to answer to this "scalling down" microelectronic industry demands and sough of new device architecture. Morphology control and fabrication of anysometric ferroelectric nanoparticles is then of critical importance. In the frame of the COST 539 Action – ELENA, a collaboration between CICECO and Powder Technology Laboratory of the École Polytechnique Fédérale de Lausanne addressed this topic and insights on the understanding on how the addition of different molecules can affect the growth of barium titanate in aqueous medium achieved. Poly(acrylic acid), poly(vinyl pyrrolidone), sodium dodecylsulfate, D-fructose and hydroxypropylmethylcellulose (HPMC) were used as additives to control the growth of $BaTiO_3$ particles in aqueous synthesis (Fig.2). The structural and chemical nature of each additive governs the interaction behaviour with the $BaTiO_3$ particles. At low concentrations the additives did not affect the crystallization of $BaTiO_3$. For high concentration of PAA, the additive is specifically adsorbed on the $BaTiO_3$ crystallographic planes, decreasing the energy of these faces and promotes the oriented attachment of the particles. PVP seems not to adsorb on $BaTiO_3$ surfaces but it acts as a dispersive agent and as growth inhibitor when increasing the additive concentration by modifying the solution viscosity. SDS in high concentration forms micelles, and consequently acts as growth inhibitor due to the limitation of mass transport of barium and titanium species. The inverse solubility of HPMC with increasing the additive concentration and synthesis temperature is the reason for $BaTiO_3$ growth inhibition. Finally D-fructose in high content changes the energy barrier of $BaTiO_3$ nucleation presenting a threshold concentration for the nucleation. The present study gives useful insights on how additives control barium titanate growth from aqueous solutions and above all demonstrates that the morphological control of complex oxides by chemical methods is complex. It is suggested that in order to control the morphology of $BaTiO_3$ particles by aqueous synthesis a fast, and homogenous nucleation is required. In addition among the analyzed additives the most promising crystal habit modifiers is PAA.

The authors acknowledge FCT, FEDER, European Network of Excellence FAME and Cost Action 539.

[1] Department of Ceramics and Glass Engineering, CICECO, University of Aveiro, 3810-193 Aveiro, Portugal

[2] Powder Technology Laboratory, Materials Department, Swiss Federal Institute of Technology Lausanne (EPFL), Switzerland

Reference paper

Gordon EM, "Cramming more components onto integrated circuits", *Electronics*, **1965**, 38, 8, 19.

Maxim F, Ferreira P, Vilarinho PM, Aimable A, Bowen P, "Additive-assisted aqueous synthesis of $BaTiO_3$ nanopowders", *Crystal Growth & Design* **2010**, 10, 3996-4004.

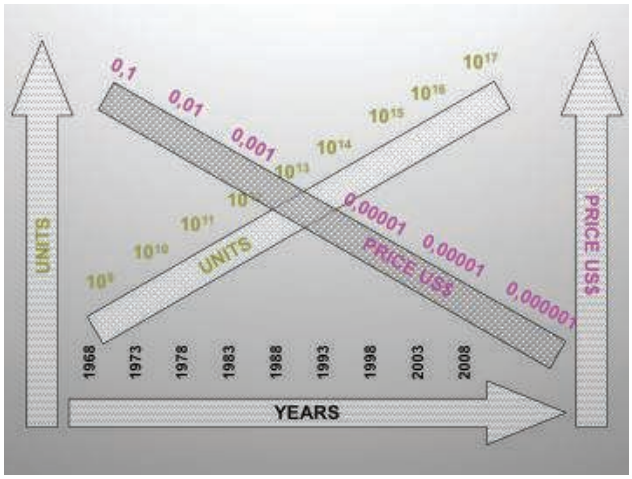

Figure 1. Scalling down tendency of microelectronics.

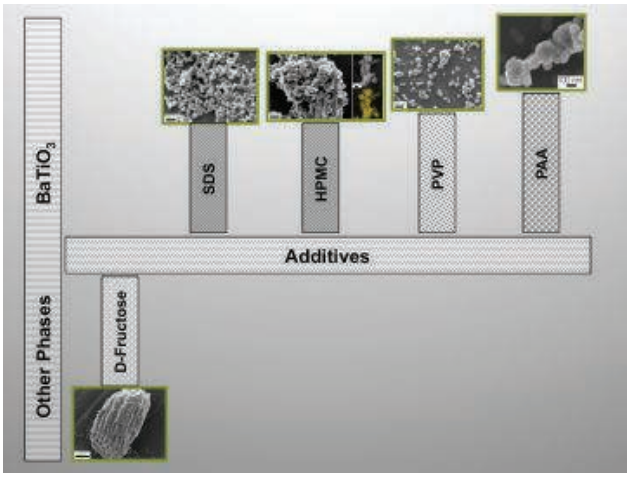

Figure 2. Effect of additives on the growth of $BaTiO_3$ nanoparticles in aqueous solution.

ECO-NANOMAGNETS FOR THE UPTAKE OF METAL IONS FROM WATER

Girginova PI[1], Daniel-da-Silva AL[1], Lopes CB[2], Figueira P[1], Otero M[2], Amaral VS[1], Pereira E[2], Trindade T[1]

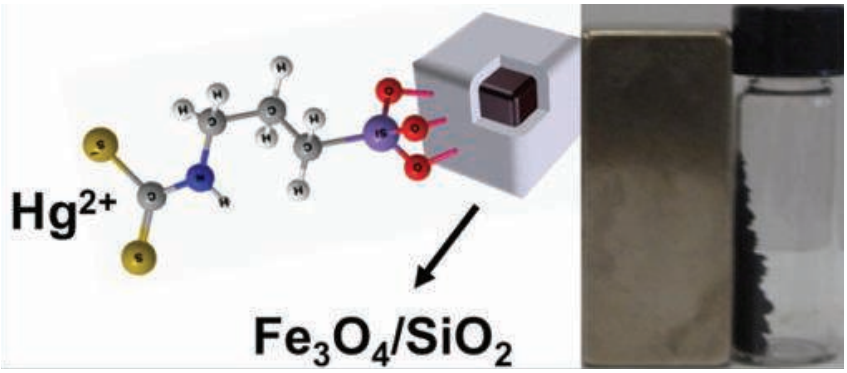

Figure 1. Core/shell Fe_3O_4/SiO_2 particles functionalized with terminal dithiocarbamate groups show strong affinity for aqueous Hg^{2+} and can be magnetically removed from water using a NdFeB magnet.

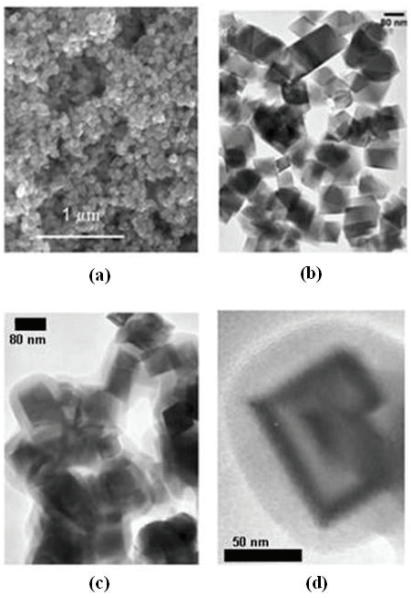

Figure 2. SEM image of cubic magnetite particles (a); TEM images of magnetite (b) and silica coated magnetite (c, d).[1]

Water pollution by trace heavy metals is well-known as a serious environmental and public problem. Among trace metals, there is a great concern about mercury pollution, which is due to its toxicity, persistent character in the environment and biota as well as bioamplification and bioaccumulation along the food chain. In order to provide long term high quality water or to enable water recycling, there has been research in alternative remediation processes involving diverse adsorbents and ion exchangers. However, because the determination of low mercury concentrations (<100 μg L^{-1}) poses several analytical limitations, most of the published work deals with relatively high and environmental unrealistic mercury concentrations (≥ 20 mg L^{-1}). Consequently, the development of efficient new materials and clean-up technologies for removing mercury from water is extremely urgent.

In the last few years, researchers from CICECO & CESAM have developed a new type of eco-nanomagnets composed of amorphous SiO_2 shells coating magnetite (Fe_3O_4) particles functionalized at the surface with dithiocarbamate (DTC) groups (Fig.1)[1]. The uncoated particles, used as starting material, showed higher values of magnetization saturation than the silica coated particles and both exhibit coercivity and remanent magnetization (M_R/M_S=0.15 and 0.18, respectively for uncoated and silica coated Fe_3O_4). The analysis of several electron microscopy images showed every single cubic particle coated with amorphous SiO_2 (Fig.2). Subsequent chemical surface modification procedures did not affect the morphology (confirmed from microscopy) or chemical composition (confirmed from Mössbauer measurements) of the magnetite cores. Water samples have been analyzed for the Hg^{2+} concentration after the magnetic separation of eco-nanomagnets that have been previously in contact with those solutions, over variable periods of time. It turns out that these materials showed an exceptional efficiency for Hg^{2+} uptake (as determined by ICP), even at trace levels found in natural waters and in strong saline conditions, as compared to common materials reported in the literature. This research indicated that the uptake efficiency for Hg^{2+} was the highest for the nanoparticles bearing DTC groups at the surface which might be related to the high stability of the chelates formed between the DTC groups and Hg^{2+} ions.

Finally we note that although these nanoenginneered particulates have been investigated here for water cleaning and analytical technologies, they can be surface modified to produce nanomaterials of interest in other research contexts such as in Nanomedicine. The understanding of the surface coordination chemistry in these nanomaterials seems crucial for example to optimize their performance and, eventually, to investigate systems containing other metal ions. As such, studies are in progress using radioactive Hg isotopes (CERN, Geneve) to probe the coordination environment of the surface metal sites.

1 Department of Chemistry, CICECO, University of Aveiro, 3810-193 Aveiro, Portugal

2 CESAM, University of Aveiro, 3810-193 Aveiro, Portugal

Reference paper

[1] Girginova PI, Daniel-da-Silva AL, Lopes CB, Figueira P, Otero M, Amaral VS, Pereira E, Trindade T, "Silica coated magnetite particles for magnetic removal of Hg^{2+} from water", *Journal of Colloid and Interface Science* **2010**, 345, 234–240.

NEW WC-STAINLESS STEEL COMPOSITES

Fernandes CM[1], Senos AMR[1], Vieira MT[2]

The best known hardmetal is a combination of a very hard and brittle tungsten carbide, WC, with small amounts of a soft and ductile metal of the iron group, usually cobalt. These composites find a wide range of applications, especially when combinations of high hardness and fracture toughness are required and ceramics or metals alone will not serve. The hardmetal Portuguese industry has worldwide recognition by its quality and innovation ability, being highly competitive within the international market. Actual research trends, directly linked to industrial interests, include new compositions and new processes to develop composites with better performance and enlarging application fields. Therefore, the research reported here was centered on the use of an alternative binder to Co, the stainless steel AISI 304 (SS) and the application of an innovative powder coating process, sputtering, to prepare WC-SS compositions. The effects on the microstructure and mechanical properties of the composites (2-15 wt.% SS) were evaluated.

The application of a sputtered coating on WC powder was highly successful in producing uniformly coated particles (Fig.1) and nanostructured coatings. Chemical, physical, structural and morphological modifications were achieved on the particle surfaces, markedly affecting the powder characteristics, such as rheology, oxidation resistance, and sintering behaviour, among others. Highly densified compacts could be obtained by vacuum sintering showing uniform microstructures without significant grain growth (Fig.1). The binder phase (Fe rich) spread as well on the WC as on the $(M,W)_6C$ surfaces with an excellent interpenetration between the grains, see TEM images in Fig.1. Very interesting mechanical properties, with an excellent compromise between hardness and toughness, were attained in these composites either using sputter-coated powders or conventional mixed ones, when compared with reported results of traditional WC-Co hardmetals (Fig.2). This mechanical behaviour is related to the SS binder characteristics, such as high ductility and wettability, final phase composition and microstructure. These features are improved when a sputter-coating process is used by the attainment of a higher uniformity in the binder phase distribution and a nanocrystalline structure, remaining from the coated powder.

Sputtering proved to be a very promising technique, alternative to the powder mixing, with benefits both in processing and in properties. In fact, composites with low amounts of SS binders prepared by sputtering are especially interesting for applications requiring a very high hardness. Furthermore, the relative high cost of the coated powders production can be balanced with the manufacturing cost reduction, coming from the elimination of milling and dewaxed steps, the decreasing of sintering temperatures, and the total densification of compacts by a conventional vacuum sintering.

[1] Department of Ceramics and Glass Engineering, CICECO, University of Aveiro, 3810-193 Aveiro, Portugal

[2] Mechanical Engineering Department, CEMUC, University of Coimbra, Rua Luís Reis Santos, Pinhal de Marrocos, 3030-788 Coimbra, Portugal

Funding

This work was financed by the FCT.

Reference paper

[1] Fernandes CM, Senos AMR, Vieira MT, Fernandes JV, "Composites from WC powders sputter-deposited with iron rich binders", *Ceramics International* **2009**, 35-4, 1617-1623.

[2] Chermant JL, Osterstock F, "Fracture toughness and fracture of WC-Co composites", *Journal of Materials Science* **1976**, 11, 1939-51.

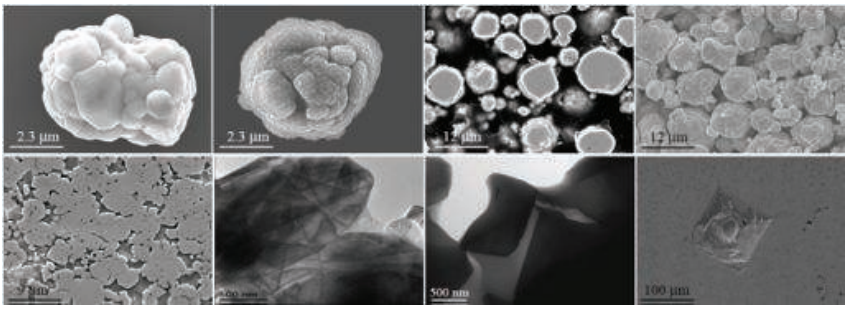

Figure 1. SEM microstructures of WC powder as-received (top, left) and coated with 10 wt.% SS (top) and SEM/TEM images of sintered WC-10 wt.% SS (down).

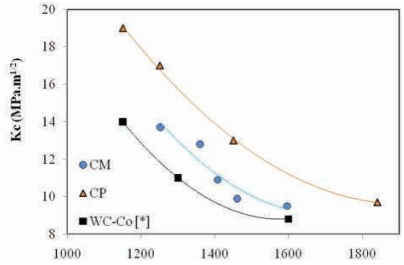

Figure 2. Toughness vs Vickers hardness for composites prepared with coated powders (CP) and conventional mixed (CM) compared with bibliographic results for WC-Co [2].

3D-2D-0D STEPWISE DECONSTRUCTION OF A WATER FRAMEWORK TEMPLATED BY A NANOPOROUS ORGANIC-INORGANIC HYBRID HOST

Rocha J[1], Shi F-N[1], Almeida Paz FA[1], Mafra L[1], Sardo M[1], Cunha-Silva L[1], Chisholm J[2], Ribeiro-Claro P[1], Trindade T[1]

Water, the basis of life, plays an important role in many biological and chemical systems and also in atmospheric chemistry. Remarkably, it may self-assemble into nanoclusters, which are discrete hydrogen-bonded assemblies of molecules of water, rather than as an isotropic collection. The study of these individual clusters in confined spaces has received increasing attention in recent years due to various widespread improved techniques for treating hydrogen-bonded systems. Indeed, the exploration of the structural and bind-

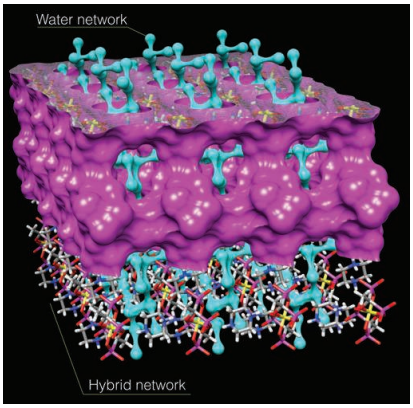

Figure 1. Representation of the interwoven nature of water (in blue) and hybrid (in purple) networks present in the present material.

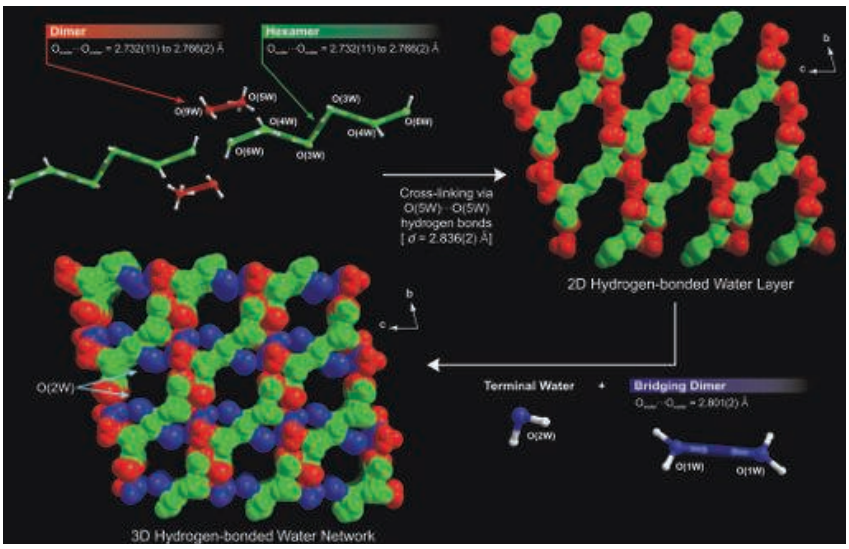

Figure 3. (top) Construction of the 3D hydrogen-bonded water network through the self-assembly of three distinct hydrogen-bonded units based on the strength of the interactions. For simplicity only one position of the disordered water molecules is represented.

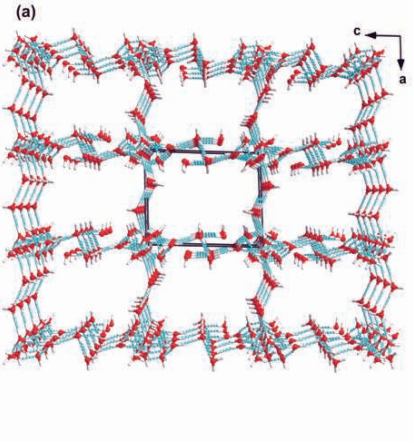

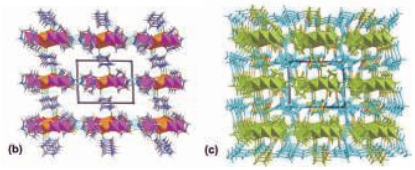

Figure 2. (left) Perspective views along the [010] direction of the unit cell of the 3D hydrogen-bonded interwoven frameworks: **(a)** water framework (hydrogen bonds represented as light-blue dashed lines); **(b)** hybrid framework (hydrogen bonds represented as green dashed lines) and **(c)** interpenetration of the frameworks (with the hydrogen bonds involving the two frameworks represented as orange dashed lines).

ing properties of small water clusters provides a key for understanding bulk water, either in its liquid or solid phase, and also provides insight into the solvation phenomena. Pores, channels, and cavities of microporous organic-inorganic hybrid materials are ideal containers for studying the nature and behaviour of water clusters.

We have recently reported a supramolecular salt, $(H_2pip)_3[Ge(hedp)_2]\cdot 14(H_2O)$ [H_2pip^{2+} = piperazine cation $C_4H_{12}N_2^{2+}$, $hedp^{5-}$ = deprotonated form of etidronic acid, $C_2H_3P_2O_7^{5-}$], consisting of an organic-inorganic hybrid hydrogen-bonded nanoporous framework, embedding a rare 3D assembly of hydrogen-bonded water molecules (Fig.1)[1]. The hybrid framework is assembled by a centrosymmetric $[Ge(hedp)_2]^{6-}$ anion and two crystallographically (and centrosymmetric) independent H_2pip^{2+} cations (Fig.2), which play distinct roles: while the anion has an entourage of oxygen atoms acting as acceptors in hydrogen-bonding networks, the cations are the donators. One type of H_2pip^{2+} cations encloses the anion, with all the strong and highly directional N^+–H···O^- bonds leading to the formation of a layer in the *bc* plane. The second kind of H_2pip^{2+} cation acts as pillars between the layers (along [100]) through a single N^+–H···O^- bond. The result is a porous framework with *ca.* 36% accessible volume which is occupied by structurally organised water molecules (Fig. 2 and 3), seven of which are crystallographically independent. While the internal surface of this hybrid framework is rich in hydrogen-bonding acceptors (O-atoms of the anions), the pillaring H_2pip^{2+} cation has one free N^+–H able to establish connections with water molecules. As a consequence, the distribution of the water molecules within the voids is not random. This 'ice' scaffold is constructed from three different water nanoclusters, with distinct hydrogen-bonding strengths, templated by the hybrid framework. Above *ca.* 0 ºC, the water molecules become increasingly mobile and disordered. Intriguingly, the 'ice' framework is stable up to *ca.* 22 ºC (TGA) and its deconstruction occurs in a stepwise fashion from 3D to 2D and discrete water aggregates (0D) (Fig.3). In the process, however, the long-range order of the hybrid host is preserved.

In summary, this material is very unusual because: few nanoporous materials exhibit a well-organised 3D framework of water molecules; it provides a unique opportunity to follow experimentally and to rationalise the deconstruction of a 3D water framework; despite the fact that the hybrid framework is a supramolecular salt, after dehydration the structure does not collapse and the final material is crystalline.

[1] Department of Chemistry, CICECO, University of Aveiro, 3810-193 Aveiro, Portugal

[2] Cambridge Crystallographic Data Centre, 12 Union Road, Cambridge, CB2 1EZ, UK

Funding

This research was financed by FCT under the R&D project PTDC/QUI/65805/2006.

Reference papers

[1] Rocha J, Shi F-N, Almeida Paz FA, Mafra L, Sardo M, Cunha-Silva L, Chisholm J, Ribeiro-Claro P, Trindade T, "3D-2D-0D Stepwise Deconstruction of a Water Framework Templated by a Nanoporous Organic-Inorganic Hybrid Host", *Chemistry - A European Journal* **2010**, 16, 7741-7749.

Energy, Lighting and Photonics

INTERCONVERTABLE MODULAR FRAMEWORK AND LAYERED LANTHANIDE(III)-ETIDRONIC ACID COORDINATION POLYMERS

Shi F-N[2], Cunha-Silva L[1], Sá Ferreira RA[2], Mafra L[1], Trindade T[1], Carlos LD[2], Paz FAA[1], Rocha J[1]

Metal-Organic Framework (MOF) materials are of considerable scientific interest. Indeed, while the combination of inorganic and organic components (*i.e.*, primary building units) can produce an endless number of new crystal architectures, this self-assembly process can also allow the rational design of solids with specific functions or properties, some of which may lead to industrial applications. Interesting applications include gas storage and separation, catalysis, guest-exchange and sensors based on optical and magnetic properties. Remarkably, only about 10% of MOFs are effectively microporous and exhibit zeolite-type behaviour such as reversible solvent sorption, ion-exchange capacity and thermal stability.

By using as primary building units lanthanide centers and etidronic acid (H_5hedp), we discovered a series of novel[5] modular multi-dimensional coordination polymers: framework-type (*i.e.*, 3D) $Na_2[Y(hedp)(H_2O)_{0.67}]$ and $Na_4[Ln_2(hedp)_2(H_2O)_2]\cdot nH_2O$ [Ln^{3+} = La^{3+}, Ce^{3+}, Nd^{3+}, Eu^{3+}, Gd^{3+}, Tb^{3+} and Er^{3+}], layered (*i.e.*, 2D) orthorhombic $[Eu(H_2hedp)(H_2O)_2]\cdot H_2O$ and $Na_{0.9}[Nd_{0.9}Ge_{0.10}(Hhedp)(H_2O)_2]$, and layered monoclinic $[M(H_2hedp)(H_2O)]\cdot 3H_2O$ (M^{3+} = Y^{3+} or Tb^{3+}). Each one of these compounds could be directly isolated from hydrothermal synthesis as depicted in Figure 1 simply using appropriate reaction conditions (which were optimised for each material).

This large family of structures exhibits an unusual combination of rare structural features. Firstly, 3D materials combine zeolite-type behavior (reversible adsorption-desorption of water molecules residing in the channels) with photoluminescence properties (improved by removing the water molecule coordinated to the lanthanide centre). This latter feature was studied in detail for the Eu^{3+}-containing material. Secondly, framework and layered materials are, to a certain extent, interconvertable at the hydrothermal synthetic stage *via* the addition of acid (HCl) or sodium chloride (Fig.2): on the one hand, the acid (HCl) treatment of $Na_4[Tb_2(hedp)_2(H_2O)_2]\cdot nH_2O$, under hydrothermal conditions affords $[Tb(H_2hedp)(H_2O)]\cdot 3H_2O$; on the other, $[Tb(H_2hedp)(H_2O)_2]\cdot H_2O$ can react with sodium chloride (hydrothermally) yielding $Na_4[Tb_2(hedp)_2(H_2O)_2]\cdot nH_2O$. This peculiar interconversion can be rationalised by solely taking into consideration topological aspects of the networks: the 3D material is a 10-connected uninodal framework which can be "sliced" into 8- and 5-connected 2D plane nets topologically identical to the orthorhombic and monoclinic materials, respectively.

[1] Department of Chemistry, CICECO ,University of Aveiro, 3810-193 Aveiro, Portugal.

[2] Department of Physics, CICECO ,University of Aveiro, 3810-193 Aveiro, Portugal.

Funding

Fundação para a Ciência e a Tecnologia: R&D project POCI/QUI/58377/2004.

Reference paper

Shi F-N, Cunha-Silva L, Sá Ferreira RA, Mafra L, Trindate T, Carlos LD, Almeida Paz FA, Rocha J, "Interconvertable Modular Framework and Layered Lanthanide(III)-Etidronic Acid Coordination Polymers", *Journal of the American Chemical Society* **2008**, 130, 150-167.

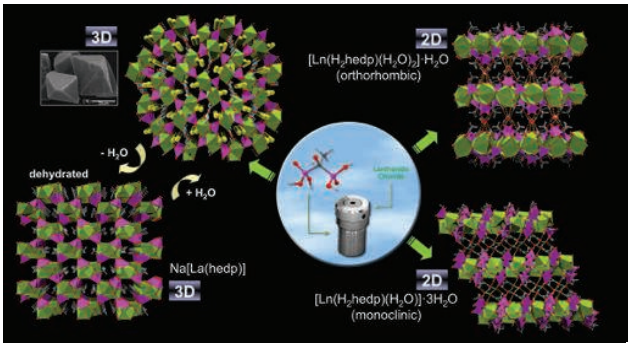

Figure 1. Framework-type (3D) $Na_2[Y(hedp)(H_2O)_{0.67}]$ and $Na_4[Ln_2(hedp)_2(H_2O)_2]\cdot nH_2O$ [Ln^{3+} = La^{3+}, Ce^{3+}, Nd^{3+}, Eu^{3+}, Gd^{3+}, Tb^{3+} and Er^{3+}], and layered (2D) orthorhombic $[Eu(H_2hedp)(H_2O)_2]\cdot H_2O$ and $Na_{0.9}[Nd_{0.9}Ge_{0.10}(Hhedp)(H_2O)_2]$, or monoclinic $[M(H_2hedp)(H_2O)]\cdot 3H_2O$ (M = Y^{3+} or Tb^{3+}) materials isolated directly from hydrothermal synthesis. Framework materials can be de- and rehydrated in a reversible fashion.

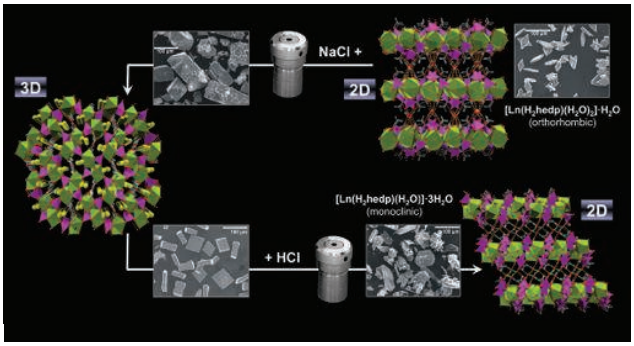

Figure 2. Interconversion between layered (2D) and framework (3D) architectures by treating the materials with either NaCl or HCl under hydrothermal conditions.

A MINIATURIZED LINEAR PH SENSOR BASED ON A HIGHLY PHOTOLUMINESCENT SELF-ASSEMBLED EUROPIUM(III) METAL–ORGANIC FRAMEWORK

Harbuzaru BV[1], Corma A[1], Rey F[1], Jordá JL[1], Ananias D[2], Carlos LD[2], Rocha J[2]

Local acidity plays a central role in many chemical and physiological processes. Molecular-scale tools that can sense or alter the pH of their environment are, therefore, eagerly sought. In the frame of the European Network of Excellence, FAME, collaboration between CICECO and the Instituto de Tecnologia Química in Valencia resulted in a miniaturized pH sensor operative in the physiologically relevant pH 5 to 7.5 range[1]. The sensor is based on a metal-organic framework solid that contains strongly photoluminescent (emission quantum yield of 0.58) trivalent europium ions in two distinct coordination environments (Fig. 1). This material was combined with commercial optical fibres in a prototype design. Because only one of the two ion sites is sensitive to pH, the sensor is self-calibrating.

We focused our attention on 1,10-phenanthroline-2,9-dicarboxylic acid as a suitable organic ligand because this is a well known sensitising agent for Eu^{3+} and is able to coordinate the metal centres through the oxygen atoms of the carboxylate groups and the phenanthroline nitrogen (Fig. 1). The hydrothermal synthetic route was used and the crystal structure of the material was solved from single crystal X-ray diffraction data collected at the ESRF synchrotron, beamline BM16.

Preliminary results of the use of the material as a pH sensor were very encouraging. The intensity of the $^5D_0 \rightarrow {}^7F_0$ transition for Eu2 varies linearly and is fully reversible within the pH range in which the material is stable. Interestingly, this is the pH range required for working with biological fluids, such as blood and cell-culture media. No calibration is required because the Eu1 intensity is not affected by pH, and may be used as an internal standard. The pH of a solution may be determined with high accuracy from the linear relationship between the relative $^5D_0 \rightarrow {}^7F_0$ Eu2/Eu1 emission intensities (I_r). Thus, by taking advantage of the main properties of the material (high emission quantum efficiency, insolubility in aqueous media, stability in a relatively wide range of pH, and pH-sensing capability) it was possible to design a miniaturised pH sensor prototype, with a good accuracy and a rapid response.

[1] Instituto de Tecnologia Química, (UPV-CSIC), Valência (Spain)
[2] Departments of Chemistry and Physics, CICECO, University of Aveiro, 3810-193 Aveiro, Portugal

Aknowledgment
This work was highlighted in *Science* ('Editors Choice', 21 August 2009) and *Highlights 2009*, European Synchrotron Radiation Facility, p. 50. We thank FCT and EC NoE FAME for financial support.

Reference paper

[1] Harbuzaru BV, Corma A, Rey F, Jordá JL, Ananias D, Carlos LD, Rocha J, "A Miniaturized Linear pH Sensor Based on a Highly Photoluminescent Self-Assembled Europium(III) Metal–Organic Framework", *Angewandte Chemie International Edition* **2009**, *48*, 6476-6479.

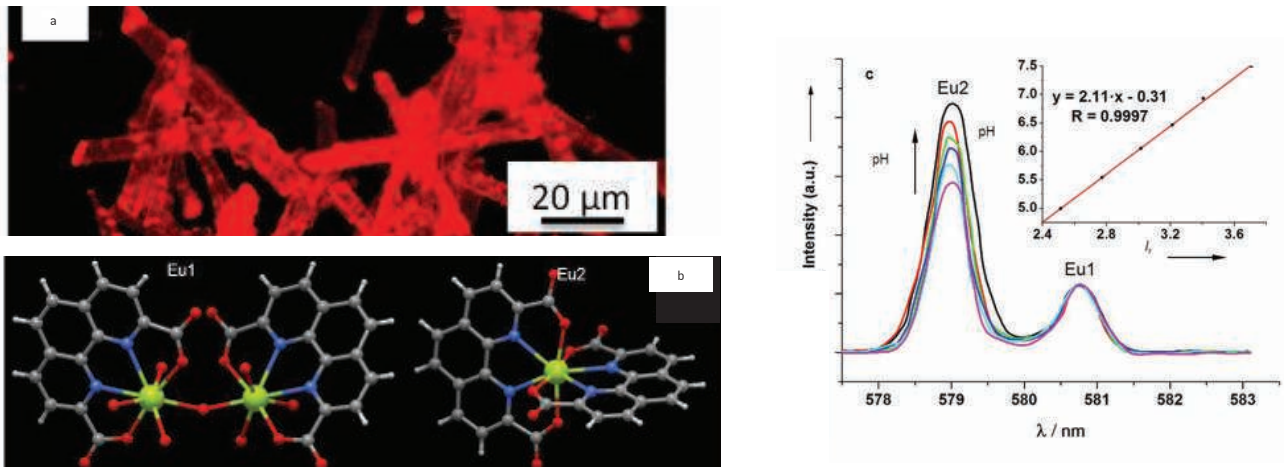

Figure 1. a) Optical microscopy image of the studied material under UV light. **b)** Eu1 and Eu2 coordination environments, C gray, N blue, O red, Eu yellow. **c)** Intensity variation of the Eu2 $^5D_0 \rightarrow {}^7F_0$ transition from high (pH 7.5) to low (pH 5) pH values; the inset shows the linear variation of I_r with the pH value.

MOLECULE-LIKE Eu^{3+}-DIMERS EMBEDDED IN AN EXTENDED SYSTEM EXHIBIT UNIQUE PHOTOLUMINESCENCE PROPERTIES

Ananias D[1], Kostova M[1], Paz FAA[1], Neto ANC[2], De Moura RT[2], Malta OL[2], Carlos LD[1], Rocha J[1]

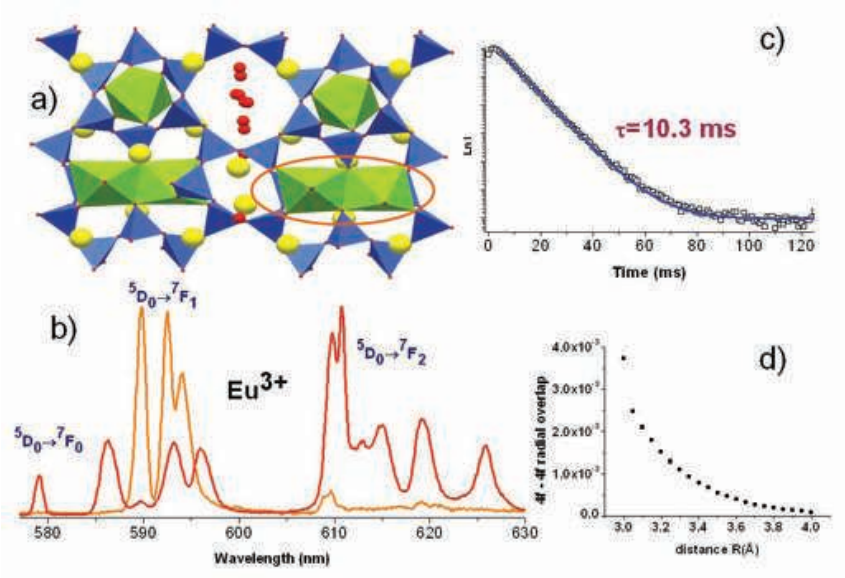

Figure 1. **(a)** Crystal structure of Eu-AV-24 viewing along the direction [100]. **(b)** Time-resolved emission spectra of Eu-AV-24 at 12 K excited at 393 nm. Red line - initial delay of 0.05 ms and sample windows of 0.5 ms; orange line – initial delay of 25 ms and a sample windows of 10 ms. **(c)** Dimmer decay curves of Eu-AV-24 detected at 12 K on the $^5D_0 \rightarrow {}^7F_1$ transition (589.8 nm) and excited at 229 nm. **(d)** Dependence of the overlap integral S_{4f} with the Eu-Eu distance R.

Trivalent lanthanide ions (Ln^{3+}) hold a special place in photonics because of their exceptional luminescence features, especially with respect to their application as phosphors in the generation and amplification of light in lasers and optical amplifiers. To explore new multifunctional materials we have focused our attention on the development of new microporous lanthanide silicates, which combine microporosity and photoluminescence, and present excellent thermal stability.

Much is known about the photoluminescence of lanthanide-containing systems, particularly amorphous silicates or organic-inorganic hybrids, and crystalline metal-organic frameworks. Comparatively, stoichiometric microporous Ln-silicates, are poorly studied. As a result of collaboration between CICECO and Departamento de Química Fundamental in Recife, Brazil, we have recently reported the exceptional photoluminescence properties of a microporous lanthanide silicate, known as AV-24[1].

This material, formulated as $K_7[Ln_3Si_{12}O_{32}]\cdot xH_2O$ (Ln^{3+} = Sm^{3+}, Eu^{3+}, Gd^{3+}, Tb^{3+}), is the first silicate possessing Ln^{3+}—O—Ln^{3+} dimers (inter-Ln distance *ca.* 3.9 Å), *i.e.,* two edge-sharing (LnO_6) octahedra embedded in a crystalline matrix (Fig. 1a). It is totally unprecedented that in AV-24 (maximum absolute emission quantum yield of 0.52) Eu^{3+}—O—Eu^{3+} dimers behave like discrete entities, *i.e.,* molecules: they (i) have a unique emission signature, with pseudo-point group symmetry (C_i), different from the symmetry (C_1) of each individual constituent Eu^{3+} ion, and (ii) exhibit a $^5D_0$ lifetime of 10.29 ms at12 K, among the longest so far observed in solids (due to the forbidden character of the $^5D_0 \rightarrow {}^7F_2$ transition) (Figs. 1b, c).

In accord with the experimental evidence, a simple molecular orbital model shows that the Eu^{3+}—O—Eu^{3+} dimers are energetically more stable than the individual metal ions. In accord with the experimental evidence, this model predicts for the $^5D_0 \rightarrow {}^7F_0$ transition an energy *ca.* 15 cm^{-1} lower than the corresponding energy of each individual constituent Eu^{3+} ion. The calculations also show that stability of the Eu^{3+}—O—Eu^{3+} dimmer entity is strongly dependent on the Eu^{3+} interatomic distance and negligible for a distance as short as 4.2 Å (Fig. 1d). A complex and unusual energy transfer dynamics between the distinct Eu^{3+} ions is also present. While non-radiative energy transfer from the isolated Eu(1) ions to the Eu(2)-Eu(2) dimers occurs at 12 K, at temperatures above 50 K a second, thermally-activated, energy transfer process from the dimers to the isolated Eu(1) ion is in operation, for time delays larger than 25 ms.

[1] Departments of Chemistry and Physics, CICECO, University of Aveiro, 3810-193 Aveiro, Portugal

[2] Departamento de Química Fundamental, CCEN-UFPE, Recife-PE (Brazil)

Funding

This work was financed by the FCT.

Reference paper

[1] Ananias D, Kostova M, Paz FAA, Neto ANC, De Moura RT, Malta OL, Carlos LD, Rocha J, "Molecule-Like Eu^{3+}-Dimers Embedded in an Extended System Exhibit Unique Photoluminescence Properties" *J. Am. Chem. Soc.*, **2009**, *131*, 8620-8626.

SYNTHESIS, SPECTROSCOPIC PROPERTIES, AND STABILITY OF TERNARY EUROPIUM COMPLEX COVALENTLY GRAFTED ON SBA-15 AND PERIODIC MESOPOROUS ORGANOSILICA

Fu L[1], Guo X[2], Guo H[2], Deng R[2], Chen W[2], Feng J[2], Dang S[2], Zhang H[2]

Lanthanide complexes are a very useful and important class of luminescent systems. So far, however, they have been excluded from practical applications essentially due to their low chemical, optical, and thermal stabilities. In order to overcome these shortcomings, lanthanide complexes can be incorporated into mesoporous materials to form organic/inorganic luminescence hybrids. SBA-15 is one of the mesoporous silicas with large uniform pore size, thick wall, and good stability. In recent years, periodic mesoporous organosilicas (PMO) have also been synthesized.

In order to compare the effect of the different hosts on the luminescence properties the ternary europium complex $Eu(tta)_3phen$ was covalently bonded to SBA-15 and PMO materials by impregnation of $Eu(tta)_3{\cdot}2H_2O$ into phen-functionalized SBA-15 and PMO, respectively, through a ligand exchange reaction. The resulting hybrids were designated as $Eu(tta)_3phen$-S15 and $Eu(tta)_3phen$-PMO for SBA-15 and PMO host, respectively (Fig.1).

The results show that, compared to $Eu(tta)_3phen$-PMO, $Eu(tta)_3phen$-S15 exhibits a longer luminescent decay time and higher $^5D_0$ emission quantum efficiency (0.45), and absolute quantum yield (0.22). The molecular high-energy vibration of the main flexible framework groups (-CH2-CH2-) in $Eu(tta)_3phen$-PMO results in very strong nonradiative transition and less efficient intramolecular energy-transfer process (from ligand to Eu^{3+} ion) and lower quantum efficiency in $Eu(tta)_3phen$-PMO. Meanwhile, the results of thermal treatment show that the europium complex in $Eu(tta)_3phen$-S15 possesses a better thermal stability than that in $Eu(tta)_3phen$-PMO. The above photoluminescence and thermal stability features indicated that SBA-15 is a better host for lanthanide complex than PMO.

[1] Department of Physics, CICECO, University of Aveiro, 3810-193 Aveiro, Portugal

[2] Changchun Institute of Applied Chemistry, China

Reference paper

J. Phys. Chem. C, 2009, 113, 2603-2610.

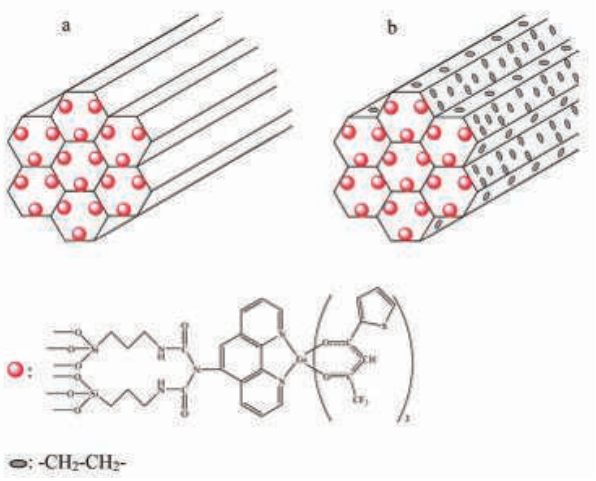

Figure 1. $Eu(tta)_3phen$-S15 (a) and $Eu(tta)_3phen$-PMO (b).

LANTHANOPOLYOXOTUNGSTATES IN SILICA NANOPARTICLES: MULTI-WAVELENGTH PHOTOLUMINESCENT CORE/SHELL MATERIALS

Granadeiro CM[1], Ferreira RAS[2], Soares-Santos PCR[1], Carlos LD[2], Trindade T[1], Nogueira HIS[1]

Core/shell systems have been widely used in recent years, considering a series of advantages for specific applications which include new clinical diagnosis platforms. The encapsulation of several types of nanoparticles with amorphous SiO_2 shells, using either the Stöber method or the microemulsion synthesis, has become a widespread technique. The high surface area-to-volume ratio, along with the relatively ease of surface functionalization of core/shell SiO_2 nanoparticles, allows their extensive use in the fabrication of biosensors, cell labelling and drug delivery systems. Lanthanopolyoxometalate-based materials have been

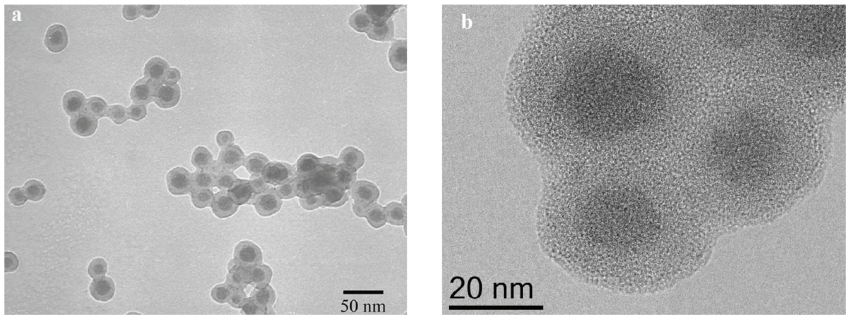

Figure 1. TEM (a) and HRTEM (b) images of $[Eu(W_5O_{18})_2]/SiO_2$ nanocomposite showing the core/shell structure of the particles.

investigated in particular due to their photoluminescent properties. Lanthanopolyoxometalates have been assembled by us in Langmuir–Blodgett films and in layer-by-layer deposition films, or incorporated in double layer hydroxides, envisaging new optically active materials. Polyoxometalates (POMs) have also been used in the fabrication of siliceous sol-gel hybrid materials. The preparation of POM-containing dense core/shell nanoparticles, with a well-defined polyoxometalate core, was reported for the first time in this work. Following our studies of coupling lanthanide complexes, mainly of Eu(III) and Tb(III), to SiO_2 nanoparticles, in this work we have prepared core/shell POM/SiO_2 nanocomposites. Comparing to previous work with Ln(III) 3-hydroxypicolinate complexes, here the use of microemulsions as nanoreactors and Ln(III) polyoxometalate compounds allowed a better control of the morphological properties of the composite nanoparticles (Fig.1).

Photoluminescent lanthanopolyoxotungstate core/shell nanoparticles were prepared by the encapsulation of lanthanide-containing POMs with amorphous silica shells (Fig.2). The preparation of morphological well-defined core/shell nanoparticles is achieved by the hydrolysis of tetraethoxysilane in the presence of POMs using a reverse microemulsion method. The POMs used are lanthanopolyoxotungstates of $[Ln(W_5O_{18})_2]^{9-}$ type (Ln(III) = Eu, Gd and Tb). Photoluminescence studies show that there is efficient emission from the POM located inside the SiO_2 shells, through excitation paths that involve O → Eu/Tb and O → W ligand-to-metal charge transfer. It was also shown that the excitation of the POM containing europium(III) may be tuned towards longer wavelengths *via* an antenna effect, by coordination of an organic ligand such as 3-hydroxypicolinate (HpicOH; sample of $[Eu(W_5O_{18})_2(picOH)_4]/SiO_2$ in Figure 3). The POM/SiO_2 nanoparticles form stable suspensions in aqueous solution having the advantage of POM stabilization inside the core and the possibility of further surface grafting of chemical moieties *via* well known derivatization procedures for silica surfaces. These features together with the possibility of tuning the excitation wavelength by modifying the coordination sphere in the lanthanopolyoxometalate, make this strategy promising to develop a new class of optical biotags composed of silica nanobeads with multi-wavelength photoluminescent lanthanopolyoxometalate cores.

[1] Department of Chemistry, CICECO, University of Aveiro, 3810-193 Aveiro, Portugal

[2] Department of Physics, CICECO, University of Aveiro, 3810-193 Aveiro, Portugal

Funding

This work has been funded by FCT (Portugal).

Reference paper

[1] Granadeiro CM, Ferreira RAS, Soares-Santos PCR, Carlos LD, Trindade T, Nogueira HIS, "Lanthanopolyoxotungstates in silica nanoparticles: multi-wavelength photoluminescent core/shell materials", *Journal of Materials Chemistry* **2010**, 20, 3313-3318.

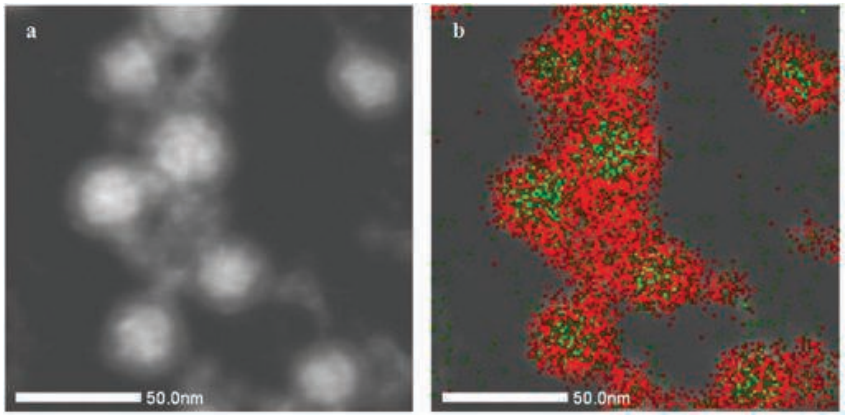

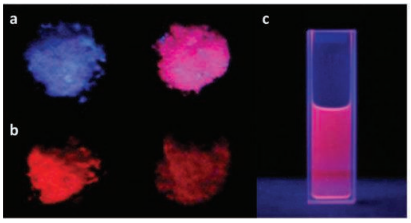

Figure 2. (left) HRTEM image of $[Tb(W_5O_{18})_2]/SiO_2$ nanocomposite in dark field mode (a) and with overlapping of EDX mapping for Si (red) and W (green) (b).

Figure 3. (top) Digital photographs of solid nanocomposites $[Eu(W_5O_{18})_2]/SiO_2$ (left) and $[Eu(W_5O_{18})_2(picOH)_4]/SiO_2$ (right) under **(a)** 366 nm and **(b)** 254 nm radiation; and **(c)** a suspension of $[Eu(W_5O_{18})_2]/SiO_2$ in ethanol under 254 nm radiation. The blue shadow is due to reflection of the UV light.

ORGANIC–INORGANIC HYBRID MATERIALS FOR THE NEXT GENERATION OF OPTICAL NETWORKS

Ferreira RAS[1], Pecoraro E[2], André PS[2,3], Carlos LD[1]

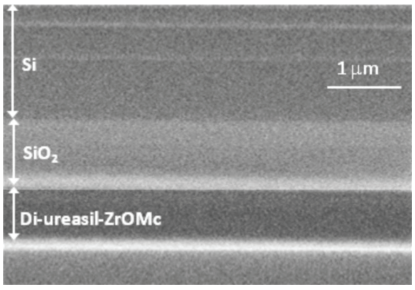

Figure 1. SEM photo of the cross-section of a di-ureasil planar waveguide.

In the framework of a collaboration with Instituto de Telecomunicações (IT), we focused our attention on the production of sol-gel derived organic-inorganic hybrids (OIH) based on methacrylic acid (McOH) modified zirconium tetrapropoxide, $Zr(OPrn)_4$, (di-ureasils-ZrOMc) to be used in integrated optics devices for the next generation of optical networks. Emphasis was given to passive (planar and channel waveguides, couplers and multimode interference splitters) and active (lasers and optical amplifiers) optical architectures. Fig. 1 shows a SEM image of a di-ureasil-ZrOMc planar waveguide deposited silica on silicon substrates, revealing a uniform and crack-pinhole-free dense microstructure for the di-ureasil layer with an average thickness of 0.835±0.028 μm [1].

Direct UV-laser writing was use to pattern channel waveguides and diffraction gratings to produce optical filters and Fabry–Perot cavities with controlled refractive index, filtering wavelength peak, bandwidth, optical rejection and FSR values[2]. The photosensitivity of the di-ureasils–ZrOMc to the UV light was also used to write 1-to-2 Y-splitters (Fig. 2a). Light propagation was optimised for a minimum refractive index contrast value of 10^{-3} and a maximum opening angle for the branches of 2.86º (Fig. 2b). Monomode propagation was achieved for coupling ratios of 50:50 in the NIR (Fig. 2c)[2].

For the first time, the incorporation of Rhodamine 6G into a di-ureasil matrix lead to random laser behaviour. The experimental results in the spectral and temporal domains, obtained by pumping with picosecond laser pulses, show the existence of efficient random laser emission in this OIH-based system (Fig. 3) [3].

OIHs are a technologically key class of advanced multifunctional materials that fulfil the challenging strict requirements of the beginning of the century: higher levels of sophistication, miniaturisation, recyclability, reliability and low energy consumption with potential to be used as low-cost components in optical networks operating at high bit rates, as recently described in a review paper, written by some of us in the context of this fruitfully CICECO-IT collaboration [2].

[1] Department of Physics, CICECO, University of Aveiro, 3810-193 Aveiro, Portugal

[2] Instituto de Telecomunicações, University of Aveiro, 3810-193 Aveiro, Portugal

[3] Department of Physics, University of Aveiro, 3810-193 Aveiro, Portugal

Funding

This work was supported by Fundação para a Ciência e a Tecnologia, FEDER, COMPETE (PTDC/CTM/72093/2006) and COST Action MP0702.

Reference paper

[1] Fernandes VR, Vicente CMS, Wada N, André PS, Ferreira RAS, "Multi-objective genetic algorithm applied to spectroscopic ellipsometry of organic-inorganic hybrid planar waveguides" *Optics Express* **2010**, 18, 16580–16586.

[2] Ferreira RAS, André PS, Carlos LD, "Organic–inorganic hybrid materials towards passive and active architectures for the next generation of optical networks", *Optical Materials* **2010**, 32, 1397–1409, and references therein.

[3] Pecoraro E, García-Revilla S, Ferreira RAS, Balda R, Carlos LD, Fernández J, "Real time random laser properties of Rhodamine-doped di-ureasil hybrids", *Optics Express* **2010**, 18, 7470–7478.

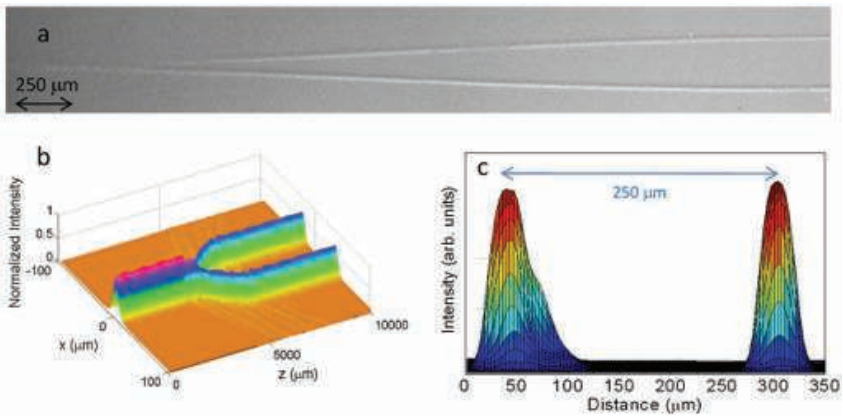

Figure 2. **a)** 1-to-2 Y-splitter optical micrography; **b)** signal intensity propagation along the Y-splitter and **c)** mode field distribution at the Y-splitter output arms for light propagation at 980 nm.

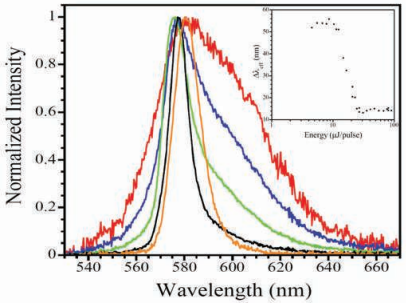

Figure 3. Normalised emission spectra of the ground powder of a Rhodamine 6G-doped di-ureasil obtained at (red) 10.3, (blue) 14.7, (green) 20.7, (black) 24.5, and (orange) 103 μJ/pulse. The inset shows the pump energy dependence of the emission linewidths.

INSIGHT INTO ION DIFFUSION MECHANISMS IN LAYERED OXIDE PHASES WITH HIGH OXYGEN PERMEABILITY: La_2NiO_4-BASED MIXED CONDUCTORS

Naumovich EN[1], Kharton VV[1]

Solid-state ionic conducting materials are the key components of many new and emerging technologies for energy storage, conversion and generation. The discovery of novel materials with enhanced ionic conductivity is crucial to the development of these technologies. New solid-state compounds with high lithium conductivity, for example, are critical to the improvement of all solid-state lithium batteries. Likewise, new oxide ion conductors will play a critical role in making solid-oxide fuel cells (SOFCs), which use hydrocarbons and other chemical fuels far more efficiently than any other device, practical and economically viable as power sources for remote areas, industries that require clean, high-quality, uninterruptible supply (hospitals, high-tech, military), and vehicles. Other important applications include high-temperature electrolysis of gases and dense ceramic membranes for oxygen, hydrogen and CO_2 separation, conversion of fuels and biogas, and waste utilization. Consequently the rational discovery of new materials and their use in electrochemical devices demands detailed structural, thermodynamic and kinetic studies from atomic-scale phenomena up to energy system modeling. In addition to the electrical power generation and conversion of natural gas and biogas, the target processes include CO_2 capture via incorporation of ceramic membrane reactors into the conventional energy systems, hydrogen separation and utilization from hydrocarbon-containing fuels, high-temperature electrolysis of water vapor and carbon dioxide, purification and processing of various fuels, and electrochemical generation of reagents for catalytic reactors.

La_2NiO_4-based solid solutions constitute a very promising group of mixed ionic and electronic conductors (MIECs) for many energy-related applications, such as SOFC cathodes and ceramic membranes. In addition to the attractive electrochemical activity and oxygen semipermeability, their advantages include a high dimensional stability under high gradients of oxygen chemical potential (for example, air/CO_2). This combination of properties is very unusual for the MIECs with high mobility of oxygen anions and high oxygen nonstoichiometry. The high dimensional stability of La_2NiO_4-based materials is, hence, essentially exclusive, originating from the features of crystal structure and defect formation mechanisms in the layered nickelates. The structure of La_2NiO_4 includes two layers, or planes, with the lattices similar to perovskite and rock-salt minerals (Fig.1). Whilst the former structural blocks provide fast electronic transport and may support anion diffusion by vacancy mechanism, the latter layers support migration of the oxygen interstitials formed due to oxidation of the transition metal cations such as nickel. The intercalation of the excess oxygen into rock-salt layers and its key role in ion diffusion processes were studied experimentally, but many reproducible observations had no explanation in framework of conventional defect-chemistry models. In order to fill this gap, a series of computer simulation studies were performed using the molecular dynamics and static-lattice methods[1]. The results were made it possible to identify major mechanisms relevant for the diffusion phenomena in La_2NiO_4-based materials, and their energetic parameters. It was shown, in particular, that the anion jumps in the rock-salt layers are always cooperative, whilst migration through perovskite plane is much more rare event (Fig.2). The simulations output enabled to develop quantitative models for steady-state oxygen permeation through La_2NiO_4-based membranes, and to determine ranges of oxygen nonstoichiometry and doping necessary for optimization of these membranes.

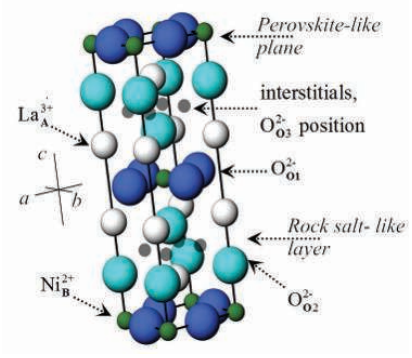

Figure 1. (top) Crystal structure of $La_2NiO_{4+\delta}$, comprising two regular oxygen sites (*01* and *02*) and interstitial *03* positions. The subscripts *A* and *B* correspond to the general formula of K_2NiF_4-type oxide phases, A_2BO_4.

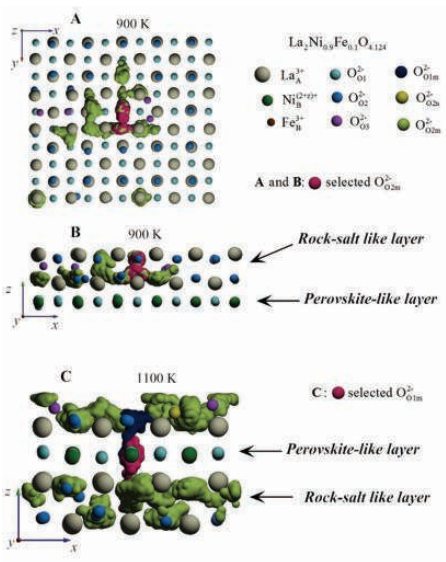

Figure 2. (right) Examples of the oxygen migration pathways in $La_2Ni_{0.9}Fe_{0.1}O_{4.124}$ during 50 ps. Immobile species are presented as spheres. The axes length corresponds to 3 Å.

[1] Department of Ceramics and Glass Engineering, CICECO, University of Aveiro, 3810-193 Aveiro, Portugal

Funding:

This work has been funded by FCT (Portugal).

Reference paper

[1] Naumovich EN, Kharton VV "Atomic-scale insight into the oxygen ionic transport mechanisms in La_2NiO_4-based materials" *Journal of Molecular Structure: THEOCHEM* **2010**, 946, 57–64

CORE-SHELL CERAMIC MIXED CONDUCTORS

Gomes E[1,2], Figueiredo FM[1], Marques FMB[1]

Mixed oxide-ion and electronic conductors are needed for various applications, namely as electrode materials for fuel cells or for permeating membranes for syngas production. Strategies to enhance mixed conduction included mostly doping of electrolytes with mixed valence cations and processing of composites with one electrolyte and one electronic conductor. All these solutions proved to be of limited effectiveness. The levels of electronic conduction obtained by compositional excursions are usually modest and undesirable phase interaction or development of ion-blocking interfaces is frequent in the case of composites. On the other hand, these mixed conductors contain a large of mixed valence cations, which cause important chemical expansion mismatch under large oxygen activity gradients, frequently leading to mechanical failure.

We have demonstrated the possible development of core-shell type materials, with formation of electronically conductive grain boundary regions surrounding the grains of solid electrolytes as an alternative approach to the design of mixed electronic-ionic conductors with minimum amounts of transition metals [1,2]. These mixed conductors are based on a lanthanum gallate solid electrolyte (LSGM) selectively doped in the grain boundaries with Fe. This was achieved using Fe source ($LaFeO_{3-\delta}$) layers screen-printed onto LSGM, after annealing at high temperature in air for several hours to promote Fe diffusion into LSGM. The combined analyses of data on microstructure, composition and electrical behaviour of core-shell Fe-grain boundary doped LSGM was used to assess the electronic conductivity of these heterogeneous materials (Fig.1). The results show that the low temperature (<400°C) total electronic conductivity (in blue) of LSGM may be enhanced by impressive 2 to 3 orders of magnitude by localised doping of the grain boundaries with less than 1 at.% of Fe (see Arrhenius plot). A key point here is that the total concentration of the transition metal in these materials is in the ppm range. The effect is reduced at higher temperature (>800°C), where only a slight improvement of the electron hole conductivity could be measured. The potential of this type of materials with grain-boundary controlled properties is thus particularly appealing for low to intermediate operation temperature, where grain boundaries tend to have a higher impact on the overall behavior of the material.

The concept demonstrated in this work may lead to the development of new mixed ionic-electronic conductors or pure ionic conductors based on the idea of the confinement of dopants to selected microstructural entities.

[1] Department of Ceramics and Glass Engineering, CICECO, University of Aveiro, 3810-193 Aveiro, Portugal

[2] School of Management and Technology, Polytechnic Institute of Viana do Castelo, Portugal

Acknowledgements

Work supported by FCT and PRODEP (Portugal), and CEC (Brussels, Network of Excellence FAME).

Reference paper

[1] Gomes E, Figueiredo FM, Marques FMB. "Grain boundary Fe-doping effects in LSGM". *Solid State Ionics* **2008,**179(21-26):900-903

[2] Gomes E, Marques FMB, Figueiredo FM, "Microstructural effects on the electrical properties of grain boundary Fe-doped LSGM". *Solid State Ionics*. **2008,** 179(27-32):1325-1328.

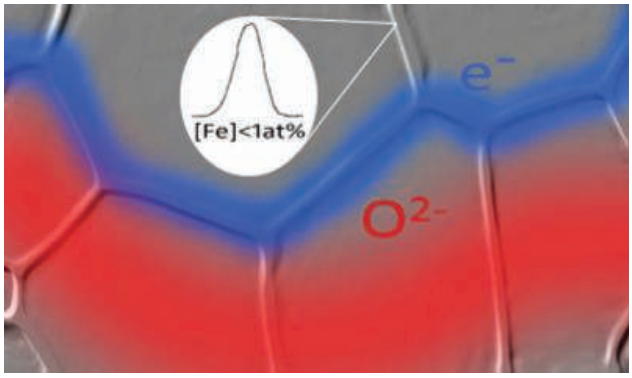

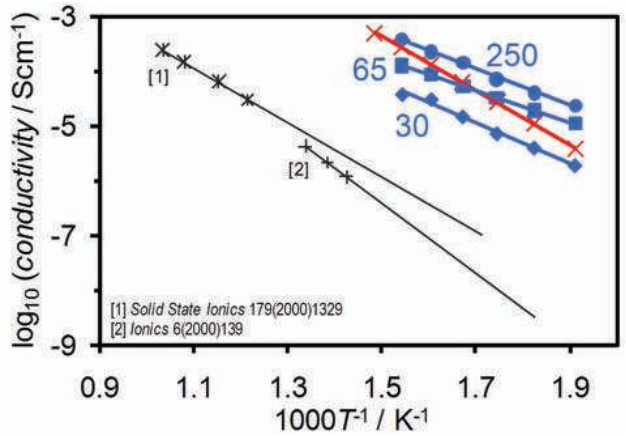

Figure 1. Preferential pathways for electronic (blue) and ionic (red) transport in core-shell Fe-doped LSGM mixed conducting ceramics. Doping levels in the ppm range (30 to 250, at %) enhance the electronic conductivity by up to 3 orders of magnitude in comparison to the undoped materials (black), bringing it to levels of the order of the ionic contribution.

FROM HOMOGENEOUS TO HETEROGENEOUS ZIRCONIAS WITH IMPROVED PERFORMANCE

Figueiredo FM[1], Frade JR[1]

Zirconias are amongst the most performing technical ceramics due to the combination of excellent thermochemical stability and suitable mechanical resistance or ionic conductivity. The number of applications is vast, spanning from biological implants to thermal barriers in high efficiency engines, where the mechanical performance is the key factor. Zirconia is also the state-of-the-art solid electrolyte of the solid oxide fuel cells (SOFCs), where the combination of stability and ionic conductivity justifies the choice. These properties may be optimised by the control of the structure and microstructure upon suitable doping with a trivalent cation, usually Y^{3+}. While the mechanical performance of zirconia-based materials is best for the $(ZrO_2)_{0.97}(Y_2O_3)_{0.03}$ partially stabilized tetragonal zirconia polycrystals (TZP), the ionic conductivity is the highest for the cubic yttria-stabilised composition $(ZrO_2)_{0.92}(Y_2O_3)_{0.08}$ (YSZ).

We have demonstrated that both the mechanical properties and the ionic conductivity of YSZ is enhanced by the dispersion of about 25 wt.% of TZP clusters. These composites show a combination of beneficial effects, including improvements in sinterability, gains in bulk and grain boundary conductivity and, also, enhanced fracture toughness with respect to the pure YSZ. The cubic-tetragonal phase separation is not retained for fractions of TZP higher than about 30% due to Y diffusion from YSZ to TZP, suggesting percolation-type mechanisms. The properties of the composites with TZP loads above the percolation threshold approach the typical features of TZP. The detailed study of these materials by impedance spectroscopy revealed an enhancement of the specific grain boundary conductivity for samples with finer grain sizes, attained by increasing the fraction of TZP. This effect can be rationalised in terms of the reduction of the grain boundary space-charge potential induced by the TZP.

The interesting properties displayed by this new kind of heterogeneous zirconias depend very much on the ability to retain both phases separated during the processing and operation. Further improvements are thus expected from the optimisation of the various steps of the ceramics processing, including, for example, the microstructure of the initial powders or the sintering schedule/method. On the other hand, the better performance at low temperature makes the heterogeneous zirconias to be an alternative to the homogeneous ceramics in the direction of lower temperature (600°C-700°C) SOFC or micro-SOFC operation.

[1]Department of Ceramics and Glass Engineering, CICECO, University of Aveiro, , 3810-193 Aveiro, Portugal

Funding

This work was supported by the CEC, Brussels (Project MAT-SILC-TREP033410.

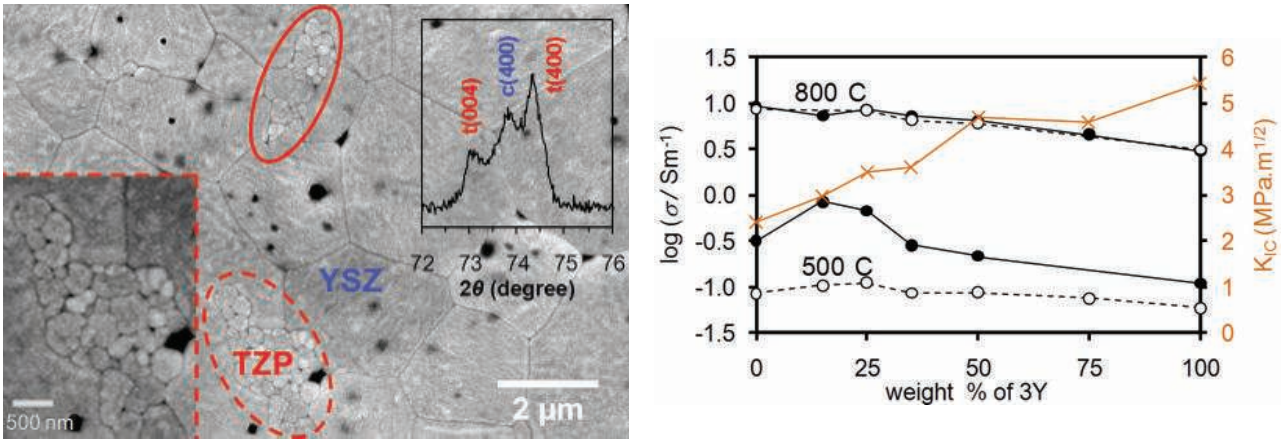

Figure 1. Scanning electron micrograph of a 75 YSZ% / 25 TZP % showing the clusters of TZP small grains (red and inset) dispersed within the coarse-grained YSZ matrix (blue). Both tetragonal and cubic phases are confirmed by X-ray powder diffraction. These composites display higher ionic conductivity (σ) and fracture toughness (K_{IC}) than the pure YSZ cubic phase.

SEE-THROUGH TUBES

Scott JF[1], Fan HJ[1], Kawasaki S[1], Banys J[2], Ivanov M[2], Krotkus A[2], Macutkevic J[2], Blinc R[3], Cevc P[3], Liu JS[4], Kholkin AL[4]

Terahertz frequency radiation possesses a unique combination of desirable properties for noninvasive imaging and spectroscopy of materials[1]. This includes the ability to obtain chemical and structural information about substances concealed within dry packaging, such as paper, plastics, and cardboard. As a result, the application of terahertz frequency spectroscopy for the sensing and identification of materials of security interest, such as explosives and, to a lesser extent, drugs of-abuse, has caught the attention of a number of researchers and security agencies. Nowadays high-energy ultrashort terahertz pulses are strongly desired particularly for the security imaging and nonlinear terahertz spectroscopy applications. Until recently only free-electron laser sources and femtosecond optical pump systems with ferroelectric $LiNbO_3$ emitters have been able to generate terahertz pulses that have at least 1 μJ of energy.

Lead zirconium titanate (PZT) is a most typical ferroelectric material that shows a high potential for piezoelectric device applications due to its high dielectric constant, high Curie temperature, and high breakdown strength. Joint work of researchers from Cambridge University, Vilnius University, J. Stefan Institute, and CICECO discovered that terahertz emitters and detectors based on PZT (via the optical rectification effect) are a viable solution of this problem[2]. The intense terahertz emission was observed from PZT tubular nanostructures, which have a wall thickness around 40 nm and protrude on n-type Si substrates. Such emission is totally absent in flat PZT films or bulk; hence the effect is attributed to the nanoscale geometry of the tubes. The terahertz radiation is emitted within 0.2 ps (Fig.1), and the spectrum exhibits a broad peak from 2 to 8 THz (Fig.2). This is a gap in the frequency spectrum of conventional semiconductor terahertz devices, such as ZnTe, and an order of magnitude higher frequency peak than that in the well-studied p-InAs, due to the abnormally large carrier concentration gradient in the nanostructured PZT. The inferred mechanism is optical rectification within a surface accumulation layer, rather than the Dember effect. The terahertz emission is optically pumped, but since the tubes exhibit ferroelectric switching, electrically driven emission may also be possible. EPR revealed O_2 molecules adsorbed onto the nanotubes, which may play some role in the emission.

The new results are exciting because previously such high frequencies were generated primarily with quantum wells. PZT nanotubes are much cheaper and easier to process, as compared with expensive $Hg_{1-x}Cd_xTe$ nanostructures which is a commercial advantage of PZT for terahertz generators.

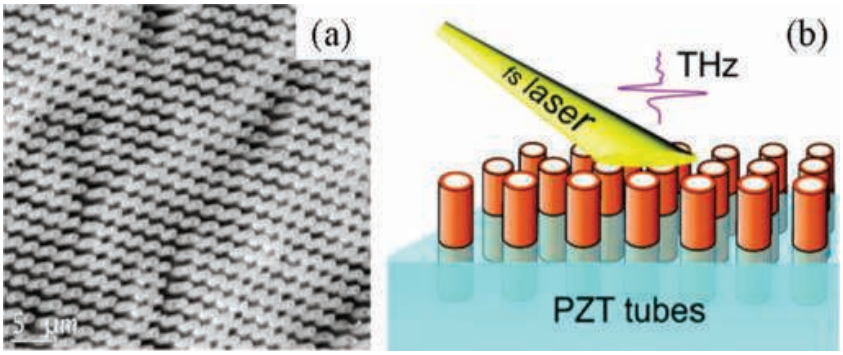

Figure 1. a) SEM of PZT tube array, **b)** Schematic of using PZT tubes as THz emitters.

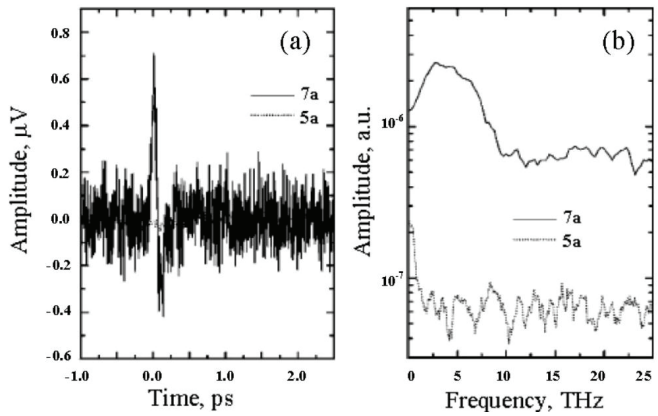

Figure 2. (a) Waveform and (b) spectra of a terahertz pulse generated from PZT nanotubes (sample 7a). The dashed line denotes trace from a sample without PZT nanotubes.

[1] University of Cambridge
[2] Vilnius University
[3] J. Stefan Institute
[4] Department of Ceramics and Glass Engineering, CICECO, University of Aveiro, , 3810-193 Aveiro, Portugal

This work was highlighted in Nature Nanotechnology Research Highlights (Vol. 3, 702, 2008) and funded by EU project NMP3-CT-2006-032616(Multiceral).

Reference paper

[1] Davies AG et al, *Materials Today.* **2008**, 11, 18.
[2] Scott JF et al, *Nano Lett.*, **2008**, 8 , 4404.

Dielectrics and Ferroics

PIEZOELECTRICS GO GREEN: PIEZOACTIVE BIOINSPIRED PEPTIDE NANOTUBES

Kholkin AL[1], Heredia A[1], Bystrov V[1], Bdikin IK[2], Gracio J[2], Mishina E[3], Sigov AS[3]

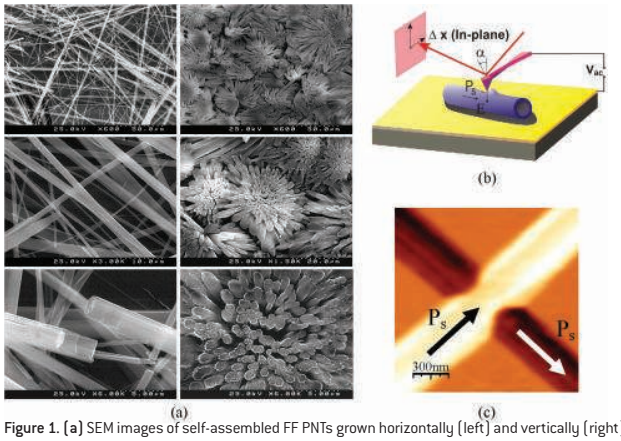

Figure 1. **(a)** SEM images of self-assembled FF PNTs grown horizontally (left) and vertically (right), **(b)** schematic of the PFM measurements and **(c)** representative piezoelectric image of two intergrown tubes showing axial polarization directions.

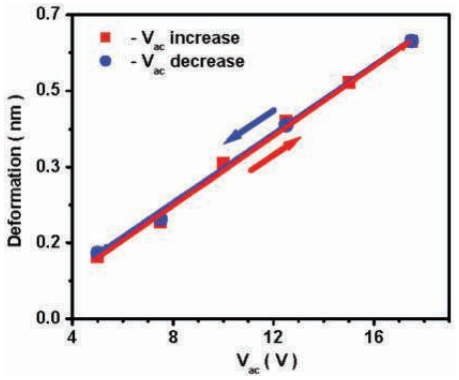

Figure 2. Shear displacements of 100 nm-diameter PNT under increasing (red line) and decreasing (blue line) ac voltage.

Piezoelectricity is the ability of certain materials to produce mechanical stress/strain under an electric field or charge/voltage under a mechanical force. This property is extremely important in many applications including acoustic transducers, sensors/actuators, motors, accelerometers, filters, balances, etc. In view of growing interest in biomedical applications and green technologies, bioorganic materials having significant piezoactivity are required for ever expanding area of piezo devices. Several biologically originated materials were identified to be piezoelectric but their piezoelectric properties were rather weak to be used in applications. Another challenge is to fabricate the nanostructures such as nanotubes for the activation of piezoelectricity at the nanoscale.

Strong piezoelectricity (of the order of that in the classical transducer material $LiNbO_3$) has been recently discovered in bioinspired peptide nanotubes (PNTs) made by a self-assembly process of small diphenylalanine, NH2-Phe-Phe-COOH (FF), peptide monomers[1]. These PNTs are derived from the determination of the smallest recognition motif of the amyloid-β protein, associated with over 30 diseases, mostly neurodegenerative ones such as Alzheimer, Huntington, Parkinson, Creutzfeldt-Jacob and prions. They conveniently self-assemble in unique stable tubes with hydrophilic hollows where piezoelectric polarization is directed along the tube axis (Fig.1). Both horizontal and vertical tubes were grown and their properties were studied by piezoresponse force microscopy (PFM) (Fig.1). Stability of the observed piezoeffect was so high that reversible shear deformations could be excited at 16 V rms without degradation (Fig.2).

Among the recent findings of CICECO group in collaboration with MIREA (Moscow) is the temperature-dependent polarization response in FF PNTs studied via PFM and optical SHG[2]. The polarization gradually decreases from room temperature to 140 °C, and experiences irreversible phase transformation to another (identified as orthorhombic) crystalline phase with zero polarization and antiferroelectric-like structure with opposite polarization orientations in adjacent aromatic rings. Partial polarization switching is observed by the application of a strong electric bias to

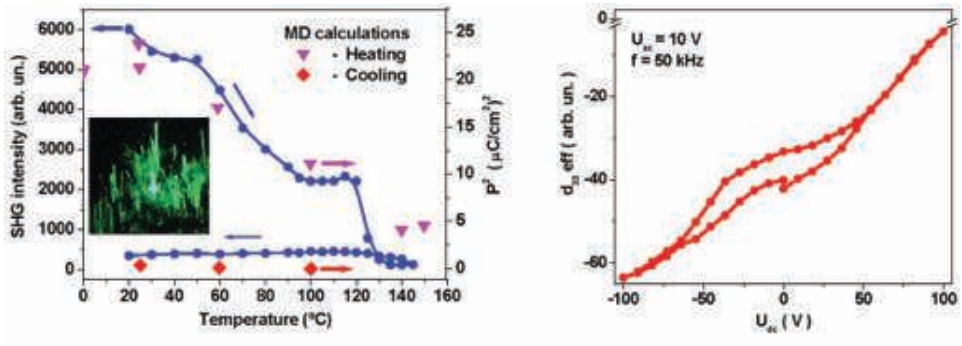

Figure 3. **(a)** Temperature-dependent SHG (inset shows SHG image) and **(b)** ferroelectric-like response on vertical PNTs.

the PFM tip signifying the system is close to ferroelectric state (Fig.3). These findings are supported by rigorous molecular simulations showing that ferroelectric-like behavior is originated from the hydrogen bonds connecting individual FF monomers, which break upon the temperature increase. This phase transformation is extremely important in view of the possible applications of PNTs (currently considered as a dielectric analog of carbon nanotubes) as bio-organic sensors, actuators and molecular motors.

[1] Department of Ceramics and Glass Engineering, CICECO, University of Aveiro, , 3810-193 Aveiro, Portugal

[2] TEMA, University of Aveiro

[3] MIREA, Moscow, Russia

Reference paper

[1] Kholkin AL et al, *ACS Nano* 4, 610 (2010).

[2] Heredia A et al, *J. Phys. D: Fast Track Comm.* (in print).

TEXTURED MICROSTRUCTURE AND DIELECTRIC PROPERTIES RELATIONSHIP OF $BaNd_2Ti_5O_{14}$ THICK FILMS PREPARED BY ELECTROPHORETIC DEPOSITION

Zhi F[1], Vilarinho PM[1], Wu A[1], Kingon A[2]

R&D on the synthesis and characterization of films for high frequency applications is required. Wireless applications (portable phones, blue tooth, office voice, video and data transmission through wireless local area networks, global positioning systems, automotive safety control, etc.) based in part on radio-frequency devices and integrated circuits technology, have expanded quickly and became an important market. Current needs of this rapidly growing wireless industry include high density, small size and lightweight integrated components and packages, and low costs. Hence, thin and/or thick films of dielectric materials have to be considered to replace the dielectric components presently in use in the form of bulk. There are only a few examples of commercial applications of high Q (low loss) films. The inability to reproduce the bulk electrical response in thin layers is a strong limiting factor. In general, thin layers present reductions in permittivity and increases in dielectric losses, associated with extrinsic effects, such as defects, strains, interfacial layers, and generally referred to as size effects. Moreover, there are no commercial near-zero-temperature coefficient of permittivity ($TC\varepsilon_r$), high Q microwave dielectrics with permittivity between 45 and 80.

Within an on going collaboration between the Electroceramics Group (CICECO/UA) and the Group of Prof. Angus Kingon at Brown University (USA) on the exploitation of Electrophoretic Deposition (EPD) for the preparation of thick functional dielectric films, an alternative approach to tailor $TC\varepsilon_r$ of high Q dielectric $BaO–Re_2O_3–TiO_2$ (Re – rare earth) thick films was developed[1]. Densification of thick films on rigid substrates is always constrained. Full densification is hard to achieve and anisotropic grain growth usually occurs. In our approach, taking advantage of the constrained sintering, the raise of the sintering temperature increases markedly the aspect ratio of the grains, decreases the dielectric permittivity and $TC\varepsilon_r$ changes from -114 to +12 ppm/°C, as illustrated in Fig.1. By controlling the sintering temperature, near – zero $TC\varepsilon_r$, high Q thick films can be fabricated with 45< permittivity <70. These findings are of technological relevance since they demonstrate that control of substrate constraint and sintering conditions can be used to control grain anisotropy and thus high frequency properties of $BaO-Re_2O_3-TiO_2$. Thick films facilitate scaling to small device sizes for high-frequency operation. Similar observations are expected in other MW systems thus opening further technological opportunities. These results demonstrate the enormous potential of thick films. Other collaborations are now on going (University of Sheffield) for the preparation of composite thick films and the studies of constrained sintering (University of Darmstadt).

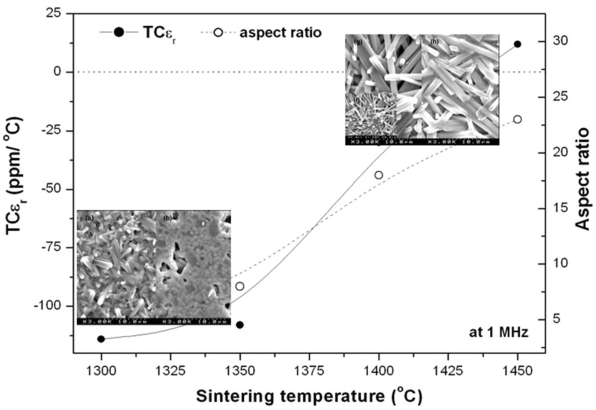

Figure 1. Dependence of $TC\varepsilon_r$ and aspect ratio of BNT films on sintering temperature.

[1]Department of Ceramics and Glass Engineering, CICECO, University of Aveiro, 3810-193 Aveiro, Portugal.

[2] Division of Engineering, Brown University, Providence, Rhode Island, USA

This work has been funded by FCT (Portugal).

Reference paper

[1] Fu Z, Vilarinho PM, Wu A, Kingon A, "Textured microstructure and dielectric properties relationship of $BaNd_2Ti_5O_{14}$ thick films prepared by electrophoretic deposition", *Advanced Functional Materials* **2009**, *19*, 1071–1081

DOPING STRATEGIES FOR INCREASED PERFORMANCE IN $BiFeO_3$

Khomchenko VA[1,2], Karpinsky DV[1], Vieira JM[1], Kholkin AL[1]

$BiFeO_3$ is the only material that is both magnetic and a strong ferroelectric at room temperature. As a result, it is the most studied multiferroic system sometimes called "The Holy Grail" of multiferroicity. A significant disadvantage of $BiFeO_3$ is cycloid-type spatial modulation, superimposed onto G-type antiferromagnetic spin ordering that prevents any net magnetization and magnetoelectric effect. The modulation can be eliminated by strain (either induced by substrate in thin films or by doping). If the modulated magnetic structure is suppressed, the system becomes ferromagnetic and it can be further used in multiferroic applications due to expected magnetoelectric coupling. Release of the latent magnetization was reported in epitaxial $BiFeO_3$ films, but doping possibilities were much less explored and results are contradictory.

In this work, we systematically studied the possibility of A-site doping with diamagnetic alkali-earth[1-5] and magnetically-active rare-earth[5-9] ions. It has been shown that the heterovalent diamagnetic A^{2+} substitution results in the formation of oxygen vacancies. The crystal structure transforms towards cubic-like state, however, a slight rhombohedral distortions characteristic of the parent phase persist up to 30%. In accordance with structural evolution, the polar displacements caused by the stereochemical activity of the $6s^2$ lone pair of Bi^{3+} ions and responsible for ferroelectricity in $BiFeO_3$ are suppressed with increasing doping concentration. However, ferroelectric behavior is retained even for 30%-substituted $BiFeO_3$. Magnetization measurements have shown that the magnetic state of these compounds is determined mainly by the ionic radius of the substituting elements. A-site substitution with the biggest ionic radius ions was found to suppress effectively the spiral spin structure giving rise to the appearance of room- temperature ferromagnetism with magnetic moment of ~1 emu/g (Fig.1). The most significant magnetoelectric response is therefore expected for $Bi_{1-x}A_xFeO_3$ ($0.1 \le x \le 0.2$) solid solutions, where the spontaneous magnetization coexists with ferroelectric polarization (Fig.2).

Intriguing behavior has been found for rare-earth substituted $BiFeO_3$. With increasing doping concentration, $Bi_{1-x}RE_xFeO_3$ undergo a number of structural and magnetic phase transitions, which can be generally described by the following sequence: polar antiferromagnet- polar weak ferromagnet- antipolar weak ferromagnet- nonpolar weak ferromagnet (Fig.3). Concentrational boundaries of the phases depend on kind of the substituting element and are shifted towards lower concentrations with decreasing its ionic radius. Existence of the intermediate ferroelectric and antiferroelectric phases demonstrating increase of magnetization opens an avenue for numerous applications in these systems. Thus, the A-site doping is an effective way to modify and to control crystal structure, magnetic and ferroelectric properties of $BiFeO_3$ to achieve desirable multiferroic behavior.

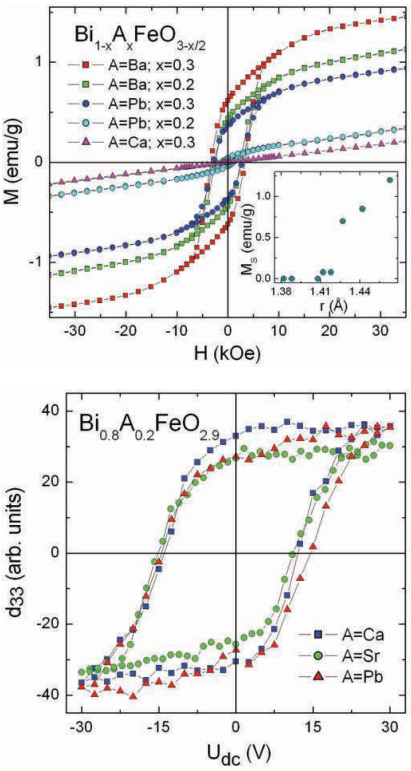

Figure 1. Magnetic hysteresis in doped $BiFeO_3$ demonstrating release of canted magnetization at room temperature. The inset shows the dependence of saturated magnetization on the ionic radius.

Figure 2. Local ferroelectric properties of 20% substituted $BiFeO_3$ (Ca, Sr, Pb).

[1] Department of Ceramics and Glass Engineering, CICECO, University of Aveiro, 3810-193 Aveiro, Portugal.

[2] CEMDRX, Department of Physics, University of Coimbra.

Reference paper

[1] Khomchenko VA et al, *Appl. Phys. Lett.* **2007,** 90, 242901

[2] Khomchenko VA et al, *J. Phys.: Condens. Matter* **2008,** 20, 155207

[3] Khomchenko VA et al, *J. Appl. Phys.* **2008**, 103, 024105

[4] Khomchenko VA et al, *J. Phys. D: Appl. Phys.* **2008**, 41, 102003

[5] Khomchenko VA et al, *J. Phys. D: Appl. Phys.* **2009**, 42, 045418

[6] Khomchenko VA et al, *Appl. Phys. Lett.* **2008**, 93, 262905

[7] Khomchenko VA et al, *Acta Mater.* **2009,** 57, 5137

[8] Khomchenko VA et al, Scripta Mater. 2010, 62, 238

[9] Khomchenko VA et al, *J. Appl. Phys.* **2010,** 108, 074109

Funding

This work was funded by the EU project NMP3-CT-2006-032616 (Multiceral).

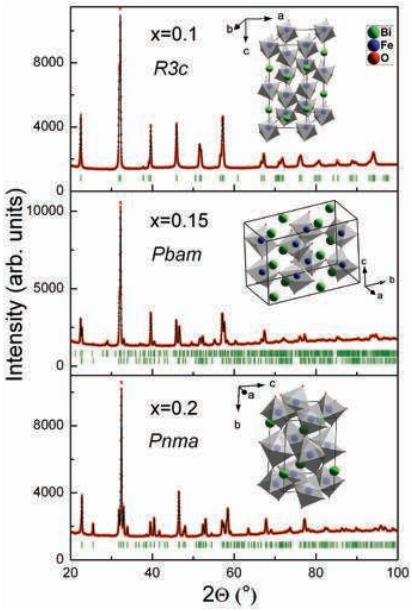

Figure 3. Examples of the structural modifications observed in the $Bi_{1-x}Sm_xFeO_3$ system at room temperature. All the compounds possess a spontaneous magnetization.

THE ROLE OF A DOPANT: X-RAY ABSORPTION FINE STRUCTURE STUDIES OF MN COORDINATION IN DOPED $SrTiO_3$ PEROVSKITES

Tkach A[1], Vilarinho PM[1], Levin I[2], Krayzman V[2], Woicik JC[2]

Multiferroic materials, combining at least two of three properties: ferroelectricity, ferromagnetism and ferroelasticity in the same phase, are currently important due to the high potential for multifunctional applications, although magnetoelectric multiferroics are difficult to obtain. Within this context the role of Mn doping on the dielectric, magnetic and structural properties of perovskite-like $SrTiO_3$ is under discussion. Our recent studies revealed that similarly prepared ceramics having fixed Mn concentration but batched according to $Sr_{1-x}Mn_xTiO_3$ and $SrTi_{1-y}Mn_yO_3$ formulae ($x,y<0.1$) exhibit remarkably dissimilar dielectric responses. In particular, $Sr_{1-x}Mn_xTiO_3$ ceramics displays a co-existence of polar (Fig.1) [1] and spin glass behaviors (Fig.2) [2], whereas no such effect is observed for $SrTi_{1-y}Mn_yO_3$. Additionally, temperature of antiferrodistiortive phase transition, observed in $SrTiO_3$ at 110K increases in $Sr_{1-x}Mn_xTiO_3$ and decreases in $SrTi_{1-y}Mn_yO_3$. *Thus, $Sr_{1-x}Mn_xTiO_3$ is a unique material, revealing antiferrodistortive elastic, polar dielectric, and spin glass magnetic behavior simultaneously.* Moreover, the dielectric and magnetic anomalies were found to be coupled according to so called "multiglass" scenario, where freezing of electric dipoles, created by off-central Mn^{2+}_{Sr} ions in highly polarizable $SrTiO_3$ lattice, initiates the transition of the magnetic Mn^{2+} spin moments into a spin glass state at the dipolar glass temperature T_g = 38 K. However, in spite of a number of indirect confirmations, direct evidence of Mn ions location on Sr-sites, was required.

In a collaboration between CICECO and National Institute of Standards and Technology (NIST) in the US, the confirmation of the lattice site occupancy by Mn in ST was possible by X-ray absorption fine structure (XAFS) measurements, which can probe directly a local coordination environment of dilute species.

Fig. 3a compares near-edge XAFS (XANES) for the differently doped $SrTiO_3$ samples and reference compounds. $MnTiO_3$ and $SrMnO_3$ crystallize with the ilmenite and hexagonal perovskite structures, respectively. Both reference compounds contain Mn in octahedral coordination but exhibit dissimilar Mn-O distances: (3×2.11 Å + 3×2.28 Å) for $MnTiO_3$ and (3×1.88 Å + 3×1.90 Å) for $SrMnO_3$; these distances are commensurate with the distinct ionic radii of Mn^{2+} (0.83 Å, 6-fold coordination, high spin) and Mn^{4+} (0.53 Å). The Mn edge energies (defined at the maximum of the 1st derivative) in these compounds differ by 7.4 eV. Our calculations of a Mn *K*-edge XANES for different coordination environments of Mn in $SrTiO_3$ indicate that the edge position (maximum of the 1st derivative) is determined primarily by the nearest-neighbor Mn-O distances. Thus, a position of the Mn edge in the $SrTi_{0.98}Mn_{0.02}O_3$ sample is consistent with the Mn-O distances of 1.9 Å as observed for Mn^{4+} in $SrMnO_3$. In contrast, comparison of Mn XANES in $Sr_{0.98}Mn_{0.02}TiO_3$ and the reference compounds suggests a mixture of the short (1.9 Å) and long (2.2 Å) Mn-O distances; the latter are consistent with the Mn-O distances in $MnTiO_3$ thus pointing to a Mn^{4+}/Mn^{2+} mixture in this sample. Coexistence of Mn^{4+} and Mn^{2+} in the $Sr_{0.98}Mn_{0.02}TiO_3$ sample was further corroborated by the analysis of the pre-edge peak (Fig.3b) which reflects quadrupolar and dipole excitations of 1s electron to the Mn 3d X-ray exciton states. XANES suggests that a substitution of Mn for Sr stabilizes Mn^{2+}; in contrast, no significant reduction to Mn^{2+} is observed for the $SrTi_{0.98}Mn_{0.02}O_3$ sample, which was annealed under identical conditions.

XAFS provides a direct evidence for the presence of strongly off-centered Mn^{2+} cations on the Sr-sites of $Sr_{1-x}Mn_xTiO_3$ thereby strongly supporting the mod-

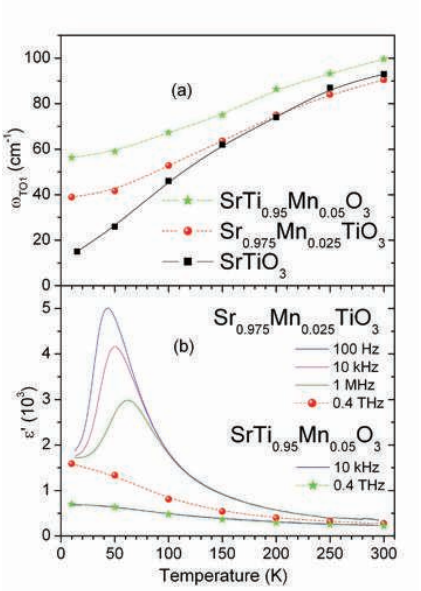

Figure 1. **(right)** Temperature dependence of the soft mode frequency ω_{TO1} of $SrTi_{0.95}Mn_{0.05}O_3$, $Sr_{0.975}Mn_{0.025}TiO_3$, and $SrTiO_3$ ceramics (a) and of the real part of the dielectric permittivity ε' of $Sr_{0.975}Mn_{0.025}TiO_3$ and $Sr_{0.95}Mn_{0.05}TiO_3$ ceramics at selected frequencies (b).

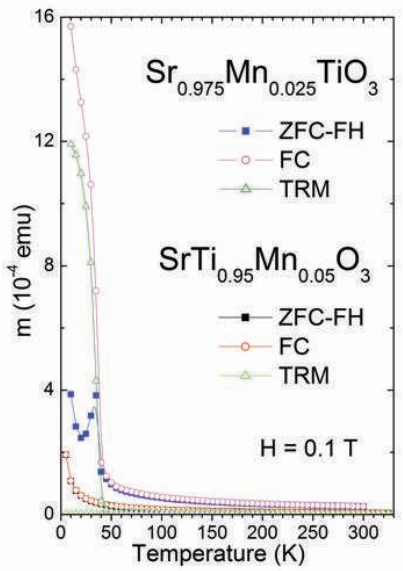

Figure 2. **(left)** Magnetic moment *m* of $SrTi_{0.95}Mn_{0.05}O_3$ and $Sr_{0.975}Mn_{0.025}TiO_3$ ceramics upon 0.1T external-magnetic-field heating after zero-field cooling (ZFC-FH), subsequently upon field cooling (FC), and upon heating after switching off the field (TRM) as a function of temperature *T*.

els previously invoked to explain its "multiglass" behavior [3].

[1] Department of Ceramics and Glass Engineering, CICECO, University of Aveiro, 3810-193 Aveiro, Portugal.

[2] Ceramics Division, National Institute of Standards and Technology (NIST), Gaithersburg, Maryland, USA

Reference papers:

[1] Tkach A, Vilarinho PM, Nuzhnyy D, Petzelt J. "Sr- and Ti-site substitution, lattice dynamics, and octahedral tilt transition relationship in $SrTiO_3$:Mn ceramics" **Acta Mater. 2010**.58:577-582.

[2] Shvartsman V, Bedanta S, Borisov P, Kleemann W, Tkach A, Vilarinho PM. "(Sr,Mn)TiO_3 – a magnetoelectric multiglass", *Phys. Rev. Lett.* **2008**. 101:165704.

[3] Levin I, Krayzman V, Woicik JC, Tkach A, Vilarinho PM. "X-ray absorption fine structure studies of Mn coordination in doped perovskite $SrTiO_3$", *Applied Physics Letters*. **2010.** 96: 052904.

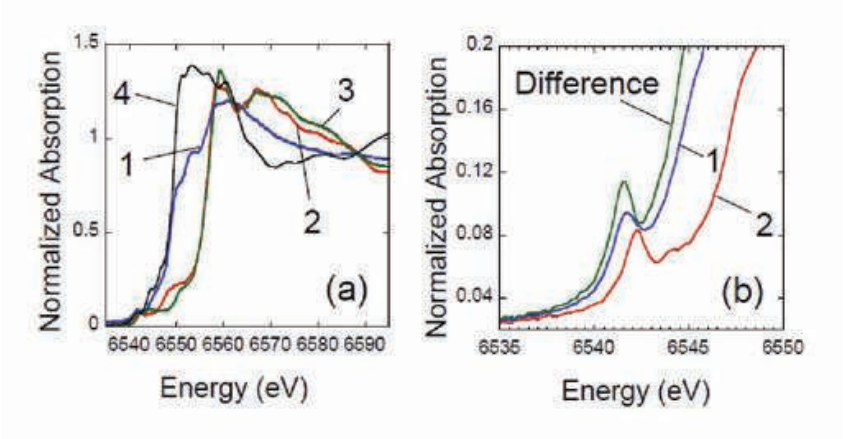

Figure 3. (a) Mn K-edge XANES of spectra for 1-$Sr_{0.98}Mn_{0.02}TiO_3$ (blue), 1-$SrTi_{0.98}Mn_{0.02}O_3$ (red), 3-$SrMnO_3$ (green), and 4-$MnTiO_3$ (black) samples. **(b)** Magnified view of the pre-edge peak. The difference spectrum (green), representing a contribution of Mn^{2+} to spectrum 2 (red), was obtained by subtracting a 0.44 fraction of spectrum 2 from spectrum 1 (blue) and multiplying the result by 0.56. The difference in the pre-edge peak positions in the difference spectrum and spectrum 2 (Mn^{4+}) is 0.7 eV.

MAGNETOELECTRIC CERAMIC COMPOSITES

Pullar RC[1], Karpinsky DV[1], Kisilev DA[1], Bdikin IK[1], Kholkin AL[1]

There has been a great deal of interest in the possibility of coupling between magnetic and electrical properties in multiferroic and magnetoelectric ceramics. Because of the inherent problems in establishing good magnetic and dielectric/ferroelectric properties in a single multiferroic material, we are investigating the manufacture of magnetoelectric composite materials consisting of separate magnetic and dielectric/ferroelectric ceramic components, and potential coupling between such components at microwave (GHz) frequencies. Such coupling will probably involve an applied electrical/magnetic field causing a strain-induced physical change in one of the phases of the composite via piezoelectricity/magnetostriction, which in turn affects the magnetic or dielectric/ferroelectric properties of the other phase in the composite. Such affects may or may not be multiferroic in nature, depending on the properties and type of coupling involved.

The magnetic components in these composites are hexagonal ferrites, which are used in electronics and as adsorbing materials at microwave frequencies, as they do not suffer magnetic losses up to 1-50 GHz, depending upon the formula of the ferrite. The dielectric component is a ferroelectric and piezoelectric ceramic, such as BT ($BaTiO_3$) or BST ($Ba_{0.6}Sr_{0.4}TiO_3$), which are well known microwave dielectrics for tuneable applications, and BT has good piezoelectric properties. Initial investigations of composites consisting of the ferrites BaM ($BaFe_{12}O_{19}$) and SrM ($SrFe_{12}O_{19}$) combined with BT and BST showed that the components do not react, resulting in dual phase ceramics. We have measured the electrical properties of these composites over a range of frequencies (kHz-GHz) and temperatures (10-500 K), and we have shown that the BT/BST composites have retained a degree of ferroelectricity.

In BaM-BT composites examined by PFM (piezo-force microscopy) piezoelectric hysteresis loops were measured, and piezoelectric domains were observed, surrounding large grains/domains which had zero piezoelectric response (Fig.1). This piezoelectricity in the composites clearly allows a good possibility of some degree of tuneability being achievable by applying a contact stimulus. MFM (magneto-force microscopy) measurements revealed clusters of magnetic domains. MFM and PFM images on the same area confirmed that the zero signal parts of the PFM image are indeed magnetic domains, and vice versa (Fig.2). We also have the first evidence of a magnetoelectric effect these materials. A clear change in the magnetic domain structure was observed after localised poling of the surrounding BT – a change

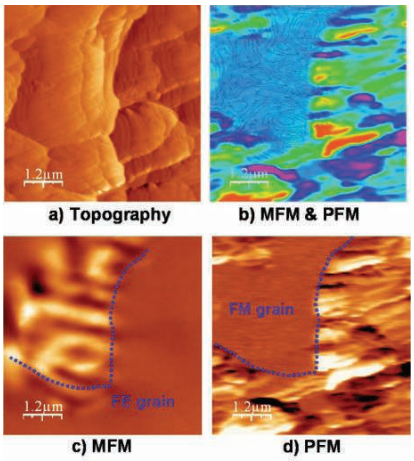

Figure 1. Scanning probe microscopy images of the same 10 μm^2 area of a 50% BaM - 50% BT sample, sintered at 1150 °C: **a)** Topography; **b)** superimposed MFM (contour lines) and PFM (colour map) images, showing distinct magnetic and piezoelectric areas; **c)** MFM image showing large area with zero response containing ferroelectric (FE) grains; d) PFM image showing the ferromagnetic (FM) grain has zero piezo respone.

in a magnetic BaM grain caused by the local application of a voltage to a neighbouring BT grain (Fig.3).
Work is ongoing to improve the density and degree of magnetoelectric coupling in such composites, and reduce the inherent degree of conductivity which arises in ferrites from the existence of some Fe^{2+} ions. We also currently investigating bulk libraries of BaM_xBT_{1-x} and SrM_xBT_{1-x} composites made by high-throughput combinatorial synthesis methods, to enable characterisation of the full compositional range.

[1] Department of Ceramics and Glass Engineering, CICECO, University of Aveiro, 3810-193 Aveiro, Portugal

Reference paper

Karpinsky DV, Pullar RC, Fetisov YK, Kamentsev KE, Kholkin AL, "Local scale probe of magnetoelectric coupling in $BaFe_{12}O_{19}$-$BaTiO_3$ multiferroics" *Journal of Applied Physics,* **2010**, 108, 042012

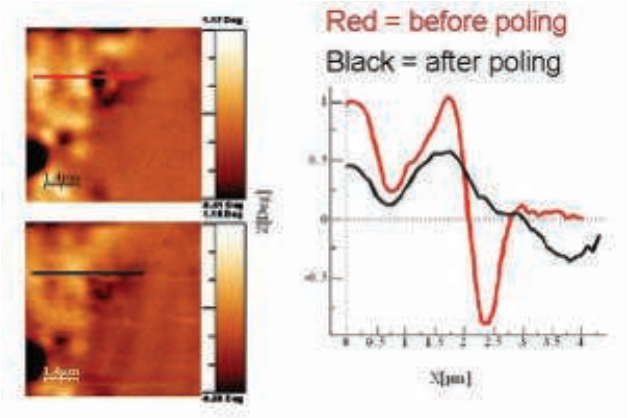

Figure 2. Variation in MFM images and MFM phase measured acros the line on the image before (red) and after (black) poling of neighbouring piezoelectric grains with a voltage.

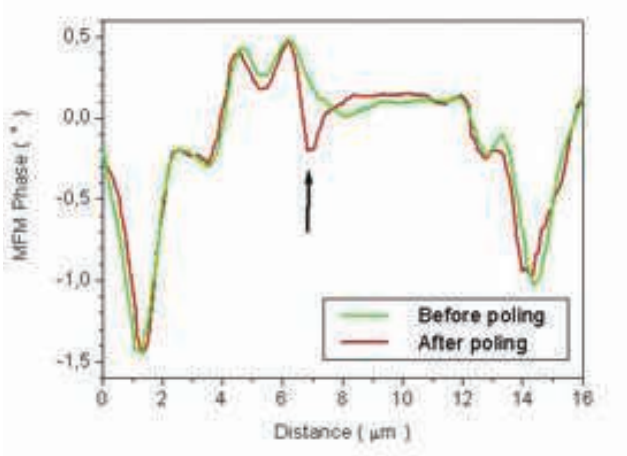

Figure 3. Comparison of MFM signal cross-sections before and after electrical poling for 50% BaM – 50% BT sample, sintered at 1150 °C.

Catalysis and Separation

GRAFTING OF MOLECULARLY ORDERED MESOPOROUS PHENYLENE-SILICA WITH MOLYBDENUM CARBONYL COMPLEXES: EFFICIENT HETEROGENEOUS CATALYSTS FOR THE EPOXIDATION OF OLEFINS

Coelho AC[1], Balula SS[1], Bruno SM[1], Alonso JC[2], Bion N[1], Ferreira P[2], Pillinger M[1], Valente AA[1], Rocha J[1], Gonçalves IS[1]

The transition-metal catalysed epoxidation of olefins is one of the most effective ways to prepare epoxides. In the Arco-Lyondell process for the epoxidation of propene, $Mo(CO)_6$ is used as a precursor, being oxidised *in situ* by the oxidant *tert*-butylhydroperoxide (TBHP) to a molybdenum(VI) complex. Our laboratory has been actively engaged in investigating a series of molybdenum carbonyl complexes as precursors to catalysts for the epoxidation of olefins. Despite the high activities and selectivities exhibited by these systems, they suffer from the usual drawbacks of homogeneous catalysts, i.e., they cannot be easily recovered and reused, and are not suitable to perform reactions under continuous flow operation mode. Devising heterogeneous versions of these catalysts is therefore highly desirable. In a collaboration involving researchers from 3 of the 8 research groups of CICECO, we have successfully functionalised a periodic mesoporous organosilica (PMO) with molybdenum tricarbonyl complexes and used the resultant materials as recyclable heterogeneous catalysts for olefin epoxidation under mild conditions and in the absence of co-solvents [1].

The key characteristic of the PMO used in the present work is the molecular-scale ordering of phenylene groups within the pore walls. Up to 14% of these groups could be converted to arenetricarbonyl complexes, $-C_6H_4Mo(CO)_3-$, by liquid-phase deposition of $Mo(CO)_6$ (Fig.1). These materials gave outstanding epoxide selectivity in the liquid phase catalytic reaction of cyclic and linear olefins with TBHP at 55 °C. No metal leaching was detected and the catalytic reaction was heterogeneous in nature. The oxidation of (*R*)-(+)-limonene gave limonene oxide as the only product in 95% yield at 3 h (Scheme1), which reveals an outstanding regioselectivity to the epoxidation of the endocyclic double bond. Limonene oxide is a key raw material for the synthesis of fine chemicals, pharmaceuticals, fragrances, perfumes, food additives, and polymers. In catalyst recycling experiments carried out with cyclooctene as the substrate, quite similar epoxide yields were obtained in consecutive runs. For limonene, slowing down of the reaction was observed in recycling runs, although conversion continued to increase with time, without changes in product selectivity.

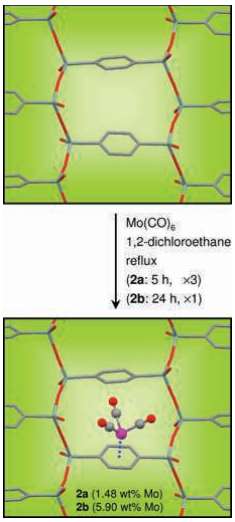

Figure 1. Derivatisation of the crystal-like mesoporous phenylene-silica with molybdenum tricarbonyl complexes.

To conclude, this work has demonstrated the great potential of crystal-like PMOs as catalyst supports. The presence of organic groups in defined positions allows grafted guest species to be spatially organised along the wall surface. Furthermore, the unique hydrophobic pores may facilitate the adsorption of olefins close to the active sites and/or reduce the adsorption of the more polar epoxide and by-products (*tert*-butanol).

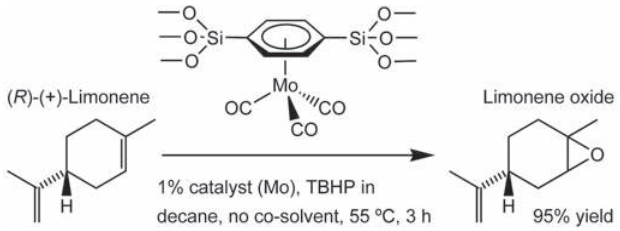

Scheme 1. The selective epoxidation of limonene using the derivatised PMO as a heterogeneous catalyst precursor.

[1] Department of Chemistry, CICECO, University of Aveiro, 3810-193 Aveiro, Portugal

[2] Department of Ceramics and Glass Engineering, CICECO, University of Aveiro, 3810-193 Aveiro, Portugal

Funding

This work was funded by the Portuguese Foundation for Science and Technology (POCI/CTM/55648/2004, PTDC/QUI/71198/2006 and REDE/1509/RME/2005).

Reference paper

[1] Coelho AC, Balula SS, Bruno SM, Alonso JC, Bion N, Ferreira P, Pillinger M, Valente AA, Rocha J, Gonçalves IS, "Grafting of Molecularly Ordered Mesoporous Phenylene-Silica with Molybdenum Carbonyl Complexes: Efficient Heterogeneous Catalysts for the Epoxidation of Olefins", *Advanced Synthesis and Catalysis* **2010**, *352*, 1759-1769

INVESTIGATION OF MOLYBDENUM TETRACARBONYL COMPLEXES AS PRECURSORS TO Mo^{VI} CATALYSTS FOR THE EPOXIDATION OF OLEFINS

Amarante TR[1], Neves P[1], Coelho AC[1], Gago S[1], Valente AA[1], Paz FAA[1], Pillinger M[1], Gonçalves IS[1]

In recent years very efficient homogeneous catalysts for the epoxidation of olefins have been obtained by fine-tuning the first-sphere ligands in dioxomolybdenum(VI) complexes of the type $[MoO_2X_2(L)]$ (X = halide, alkyl, alkoxide, etc, and L = bidentate N-donor ligand). Attention was then drawn to immobilising the molecular catalysts onto inorganic or organic supports in order to facilitate catalyst recycling and reuse. The conversion of oxomo-

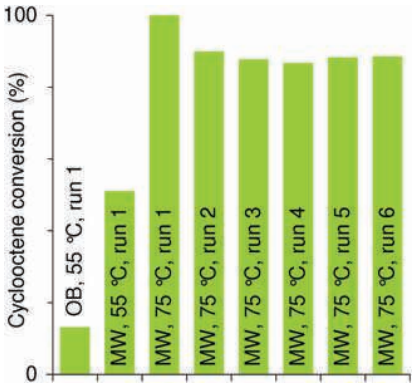

Figure 1. The catalytic performance of $[MoO_3(bipy)]$ in the liquid-phase epoxidation of *cis*-cyclooctene with TBHP using an oil bath (OB) or a microwave (MW) oven for heating and 1,2-dichloroethane as a co-solvent (reaction time = 1 h).

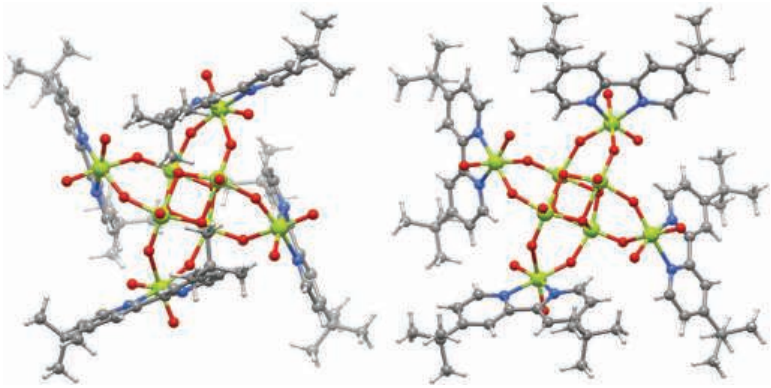

Figure 2. Schematic representation of the two crystallographically distinct octamers present in the crystal structure of $[Mo_8O_{24}(di\text{-}t\text{-}Bu\text{-}bipy)_4]$.

lybdenum complexes into heterogeneous catalysts without the need of a support would be of immense interest. One potentially interesting candidate is the molybdenum oxide/bipyridine hybrid material $[MoO_3(bipy)]$, which was originally obtained by the hydrothermal treatment at 160 °C of a mixture of MoO_3, 2,2'-bipyridine and water. Since the structure of $[MoO_3(bipy)]$ consists of 1-dimensional chains of corner-sharing $\{MoO_4N_2\}$ octahedra, it can be viewed as a polymeric version of $[MoO_2(OR)_2(bipy)]$ complexes. Unfortunately, the hydrothermal method suffers from a low yield (ca. 10%) and the material has to be mechanically separated from other phases. We have recently discovered a far more convenient and efficient route to $[MoO_3(bipy)]$, paving the way to the catalytic application of this compound.

The new synthetic method is based on the oxidative decarbonylation of tetracarbonyl complexes of the type $[Mo(CO)_4(L)]$, which are available effortlessly and in high yields by the microwave-accelerated reaction of $Mo(CO)_6$ with the bidentate ligand (L). Treatment of $[Mo(CO)_4(bipy)]$ with excess *tert*-butylhydroperoxide (TBHP) at room temperature gives $[MoO_3(bipy)]$ rapidly and in quantitative yield (Scheme 1). The hybrid material can be used as the basis for an active, selective and stable catalytic system for the liquid-phase epoxidation of *cis*-cyclooctene with TBHP as the oxidant, giving the corresponding epoxide as the only product. Notably higher activities, with no change in selectivity, are possible by using microwave-assisted heating instead of conventional oil bath heating and/or by increasing the reaction temperature (Fig.1). Moreover, the stable parent tetracarbonyl can be used as a catalyst precursor since it is transformed into $[MoO_3(bipy)]$ under the operating catalytic conditions.

Ongoing work in our laboratory is focused on applying the new synthetic method to other tetracarbonyl complexes with different ligands and geometries, which is expected to provide a series of novel compounds with different structures. For example, the oxidative decarbonylation of the complex with L = 4,4'-di-*tert*-butyl-2,2'-bipyridine leads to the isolation of the polynuclear complex $[Mo_8O_{24}(di\text{-}t\text{-}Bu\text{-}bipy)_4]$ with a structure containing a central $Mo_4(\mu_3\text{-}O)_4$ cubane (Fig.2).

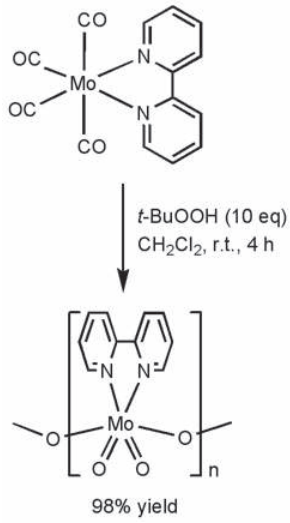

Scheme 1. Oxidative decarbonylation of $[Mo(CO)_4(bipy)]$ to give $[MoO_3(bipy)]$.

[1] Department of Chemistry, CICECO, University of Aveiro, 3810-193 Aveiro, Portugal

Funding

This work was funded by the Portuguese Foundation for Science and Technology (PTDC/QUI/71198/2006).

Reference paper

[1] Amarante TR, Neves P, Coelho AC, Gago S, Valente AA, Paz FAA, Pillinger M, Gonçalves IS, "Investigation of molybdenum tetracarbonyl complexes as precursors to Mo^{VI} catalysts for the epoxidation of olefins", *Organometallics* **2010**, *29*, 883-892.

MODIFIED ELECTRODES WITH IRON – AND COBALT – SUBSTITUTED POLYOXOTUNGSTATES FOR ELECTROCATALYSIS

Cavaleiro AMV[1]

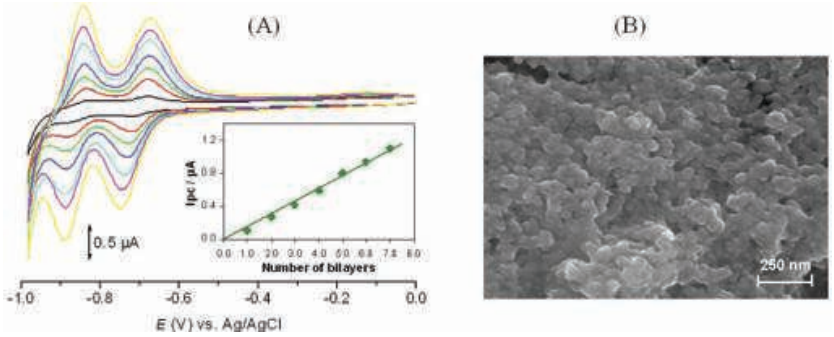

Figure 1. **(A)** Cyclic voltammograms for $(PEI/SiW_{11}CoO_{39})_n$ multilayer films in a pH 4 solution The insets show the peak currents vs. the number of bilayers; **(B)** Representative SEM micrograph of two $(PEI/SiW_{11}CoO_{39})$ bilayers.

Materials scientists are often interested in modifying surfaces of objects while keeping its basic shape and functionalities. Fabrication of uniform and ultrathin films by the layer-by layer (LbL) technique, carried out by the alternate immersion of a solid substrate into solutions containing oppositely-charged species, is an attractive technique. Thin films of well-defined thickness, composition, and structure may be built up through self assembly of anionic and cationic polyelectrolytes. The incorporation in an orderly manner of other functional components, namely transition-metal complexes, can also be achieved.

Great interest has arisen in the production of new devices using polyoxometalates, a well-known class of metal-oxygen clusters with a vast variation in structure, size, composition, and properties. One of the most important features of some polyoxometalate anions is their ability to accept a large number of electrons, which makes them very attractive for the preparation of modified electrodes to be used as sensors or in electrocatalysis.

In CICECO we have been exploiting the potentialities of electrode modification by polyoxotungstates in which one or more tungsten atoms are substituted by 1st row transition metals. In our work we were able to prepare electrostatically-assembled films with positively charged poly(ethylenimine) (PEI) and the polyoxometalates $[PW_{11}Fe(H_2O)O_{39}]^{4-}$, $[SiW_{11}Fe(H_2O)O_{39}]^{5-}$ and $[SiW_{11}Co(H_2O)O_{39}]^{6-}$. The films' growth was monitored by UV–Vis absorption spectroscopy and by cyclic voltammetry (Fig.1A). The surface morphology of the thin films on a glassy carbon electrode was examined by scanning electron microscopy (Fig.1B). It was found that the amount of polyoxotungstate adsorbed per deposition step is almost constant up to a certain number of layers, and that the electrochemical properties of the studied polyoxometalates are maintained in the multilayer films. Surface coverages were evaluated and the interfacial properties of the modified electrodes were studied. These studies showed that the charge of the outermost layer of the multilayer assembly has a significant effect on the electron transfer of soluble species. The prepared electrodes were found to be quite stable and reproducible.

Depending on the polyoxoanion used, it was found that the prepared multilayer films exhibit electrocatalytic activity towards the reduction of nitrite, bromate or iodate, with good dynamic linear ranges and detection limits. The determination of these anions is an important goal, due to their environmental and health implications, and the study of possible probes for their determination is receiving significant attention.

[1] Department of Chemistry, CICECO, University of Aveiro, 3810-193 Aveiro, Portugal

Acknowledgements

This work is being performed in collaboration with Prof Christopher M. A. Brett of the University of Coimbra. It was started at CICECO by the late Prof. Helena Carapuça, who delineated the main lines of this effort.

Reference paper

Fernandes DM, Carapuça HM, Brett CMA, Cavaleiro AMV. *Thin Solid Films*, **2010**, 518, 5881–5888

Fernandes DM, Brett CMA, Cavaleiro AMV, *J. Solid State Electrochem.*, in press, DOI: 10.1007/s10008-010-1154-1.

SULFONIC FUNCTIONALIZED CRYSTAL-LIKE MESOPOROUS BENZENE-SILICA AS A REMARKABLE WATER-TOLERANT ACID CATALYST

Karam A[1], Alonso JC[2], Gerganova TI[2], Ferreira P[2], Bion N[1], Barrault J[1], Jérôme F[1]

The utilization of water as a solvent for acid catalyzed reactions has become of growing interest either in industry or academia. In this context, the search of water-tolerant acid solid catalysts has emerged as a challenging task. Within an on going collaboration between CICECO and the Laboratoire de Catalyse en Chimie Organique, Université de Poitiers/CNRS on the design of new acid-functionalized periodic mesoporous organosilica material for reactions with/in water, we have tested sulfonic acid functionalized mesoporous benzene-silica (Ph–PMO–SO_3H) material in a model reaction of indole with benz-

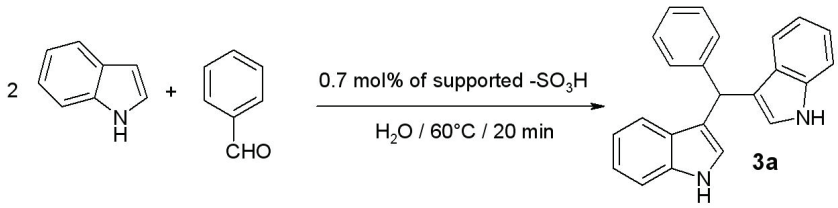

Figure 1. Aqueous synthesis of bis(indolyl)methanes over different type of solid acid catalysts.

aldehyde (Fig.1). This reaction gives access to the bis(indolyl)methane derivatives which constitute an important class of compounds that display diverse pharmacological activities.

We found that Ph–PMO–SO_3H was far more active (TOF= 943h^{-1}) than sulfonic acid functionalized SBA-15 (SBA-15–SO_3H) catalysts (TOF = 257 h^{-1}), affording 3a (Fig.1) with 95% yield against 50% of SBA-15-SO_3H. We compared the stabilities of sulfonic acid functionalised periodic mesoporous silicas (PMS–SO_3H) and Ph–PMO–SO_3H catalyst in water (Fig.2). As shown in Fig. 2, cycle after cycle, an important drop in catalytic activity was observed with HMS–SO_3H since only 15% yield of 3a was recovered after 5 cycles. Further inspections of the reused HMS–SO_3H catalyst revealed a total collapse of the mesoporous structure and a decrease of the proton exchange capacity, thus showing the instability of such catalyst in water. As expected, owing to a higher hydrothermal stability, the mesoporous structure of SBA–SO_3H was preserved after 5 catalytic runs in water. However, a significant drop of yield was still observed (50 to 22% yield of 3a). Titration of the reused SBA–SO_3H showed that the amount of acid sites remained unchanged, thus confirming the superior stability of SBA–SO_3H over HMS–SO_3H in water. Remarkably, over Ph–PMO–SO_3H, no drop of yield was observed since, after 6 successive catalytic cycles in water, 90% yield of 3a was still recovered (Fig.2). The hydrophobic environment created by the presence of the phenyl rings in the pore wall of Ph–PMO–SO_3H should protect the grafted sulfonic sites against water. XRD patterns and BET surface area of the reused Ph–PMO–SO_3H were similar than those of the fresh Ph–PMO–SO_3H confirming the remarkable tolerance of this catalyst for water (Fig.3).

[1] Laboratoire de Catalyse en Chimie Organique, Université de Poitiers/CNRS, 40 Avenue du recteur Pineau, 86022 Poitiers, France

[2] Department of Ceramics and Glass Engineering, CICECO, University of Aveiro, 3810-193 Aveiro, Portugal

Funding

This work was highlighted in *Synfacts*, 2010, *2*, 0248-0248. The authors acknowledge CNRS, POCI 2010, FEDER and FCT for financial support (POCI/CTM/ 55648/2004 and PPCDT/CTM/55648/2004).

Reference paper

Karam A, Alonso JC, Gerganova TI, Ferreira P, Bion N, Barrault J, Jérôme F, "Sulfonic acid functionalized crystal-like mesoporous benzene–silica as a remarkable water-tolerant catalyst", *Chemical Communications* **2009**, 7000–7002.

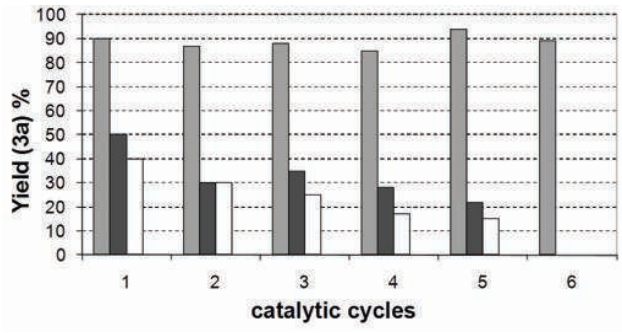

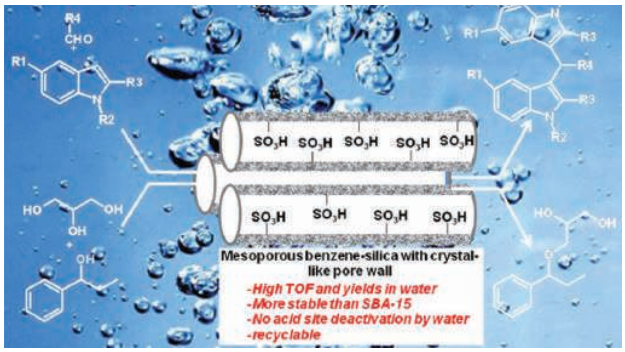

Figure 2. Catalytic recycling over Ph-PMO-SO3H (grey), SBA-SO3H (black), HMS-SO3H (white) (20 min, 60°C, 0.7 mol% of supported –SO3H).

CERAMIC TILES WITH PHOTOCATALYTIC ACTIVITY

Pires RR[1], Lobo P[1], Seabra MP[1], Labrincha JA[1]

The functionalisation of ceramic surfaces, besides meeting the new needs of consumers, helps to differentiate products from those of competitors, extend the set of product attributes and expand fields of application. Thus, ceramic companies have put an effort on the development of new ceramic materials with innovative features, like tiles with photocatalytic activity. This has represented an opportunity for technology transfer from CICECO to a ceramics company.

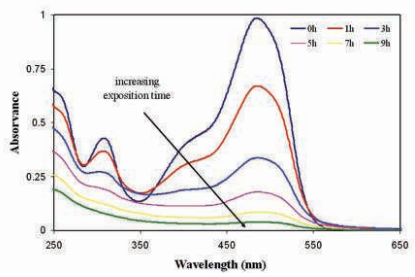

Figure 1. Decolourisation of Orange II dye aqueous solution (20 mg/L) in contact with ceramic tiles with TiO_2 active layers.

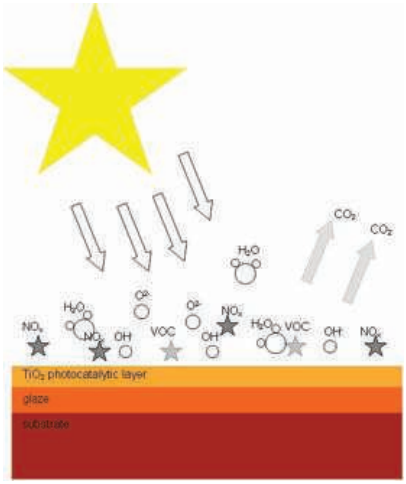

Scheme 1.

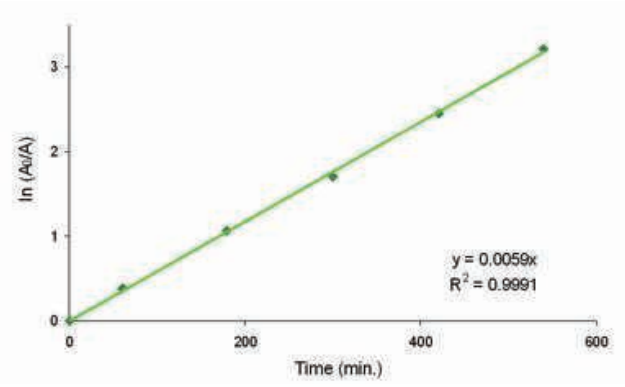

Figure 2. Linear transform ln $A_0/A = f(t)$. The slope is the reaction rate (k_a) and R^2 is the correlation factor.

The technology consists in active surfaces which transform organic and inorganic polluting substances (nitrogen oxide and dioxide, organic particulates, volatile aromatic compounds, carbon monoxide and ozone) into soluble salts (sodium and calcium nitrate) and CO_2 (Scheme1). Furthermore, the break down of bacterial cells can prevent the development of microbes and foul smells, and the tiles also have self-cleaning properties due to their super hydrophilicity.

The collaboration between CICECO and Revigrés (a Portuguese ceramic tiles manufacturer) lead to the industrial-scale production of ceramic tiles having a photocatalytic active surface. The application of layers, on glazed ceramic tiles, was performed by jet spraying of TiO_2 suspensions. This is an inexpensive technique, normally used in the ceramics industry for glazes application.

After adjusting several parameters (type and amount of TiO_2, suspension conditions, firing temperature, etc.) ceramic tiles with good photocatalytic properties were obtained. When in contact with an aqueous solution of the Orange II dye they promoted its photodegradation (Fig.1). After 3 hours of exposure to artificial visible light, a decolouration of 50% was obtained. Almost-total degradation (96%) is reached after 9 hours. The photocatalytic reaction follows a Langmuir-Hinshelwood mechanism, and it is possible to determine the apparent rate constant value (k_a; Fig.2).

The antibacterial properties and the degradation of air pollutants (NO_x, SO_x) are under study.

The resulting tiles have a good adhesion between the functionalised layer and the main tile body, an aesthetically pleasing surface, and are easy to clean, thus fulfilling the industrial/commercial requirements. In these tiles, technical, functional and esthetical requirements are combined. The commercialisation of this product is expected to happen in a near future and it will represent a step forward in the development of environmentally friendly products.

[1] Department of Ceramics and Glass Engineering, CICECO, University of Aveiro, 3810-193 Aveiro, Portugal

SMALL PORE TITANOSILICATE AM-3 MEMBRANE

Lin Z[1], Silva CM[1], Rocha J[1]

It is well known that petroleum and coal fuels generate green house gases while hydrogen fuel only produces water. The development of advanced hydrogen technologies requires high efficient processes and materials for purification, separation and storage. Several techniques for hydrogen separation are already available or under study. The palladium membrane is used due to its high hydrogen permeability and catalytic surface, as well as good mechanical characteristics. However, palladium and its alloys are extremely expensive and highly sensitive to chemicals. Therefore, the search for new membrane materials is an active field of research. Inorganic membranes generally consist of a microporous separation layer on a thicker mesoporous support. They generally exhibit high thermal and chemical stabilities, and resistance to high transmembrane pressure differences making them promising materials for gas separation applications.

Microporous titanosilicates are novel materials that may broaden the scope of application of classical zeolites. The structure of AM-3 consists of a three-dimensional framework with six-membered ring channels, which are partially occupied by Na^+ cations and water molecules. The small pore of AM-3 is particularly important in the separation of small molecules like H_2 from its mixtures.

Small pore titanosilicate AM-3 were prepared as a continuous layer on po-

rous α-alumina and stainless steel tubular supports by seeded hydrothermal synthesis, and pure AM-3 membranes *ca.* 12 μm thick were obtained, exhibiting a good intergrowth of crystals (Fig.1) and preferential orientation. AM-3 is the only crystalline porous phase present in the membranes, and the homogeneous AM-3 membrane forms on the support surface rather than inside the pores of the α-alumina support [1]. The channels of AM-3 align along the [100] direction (the inset in Fig.1b) and perpendicular to the support surface. The dynamic characterisation was carried out by permeation assays and the obtained results were modelled taking into account the various transport mechanisms involved in such microporous materials. The representation of the experimental data was achieved successfully with absolute average relative deviations between 1.5 and 2.5%. The membranes present a desired predominance of the activated diffusion mechanism for H_2 at increasing temperatures[2]. The available evidence shows that the titanosilicate AM-3 membrane is a potential candidate for H_2 separation.

[1]Department of Chemistry, CICECO, University of Aveiro, 3810-193, Aveiro, Portugal

Funding

This work was financed by FCT.

Reference paper

[1] Li XW, Zhou CF, Lin Z, Rocha J, Lito PF, Santiago AS, Silva CM, "Titanosilicate AM-3 membrane: a new potential candidate for H_2 separation"; Microporous and Mesoporous Materials, **2011**, *137*, 43-48.

[2] Lito PF, Zhou CF, Santiago AS, Rodrigues AE, Rocha J, Lin Z, Silva CM, "Modelling gas permeation through new microporous titanosilicate AM-3 membranes"; Chemical Engineering Journal, (2010, 165, 395-404).

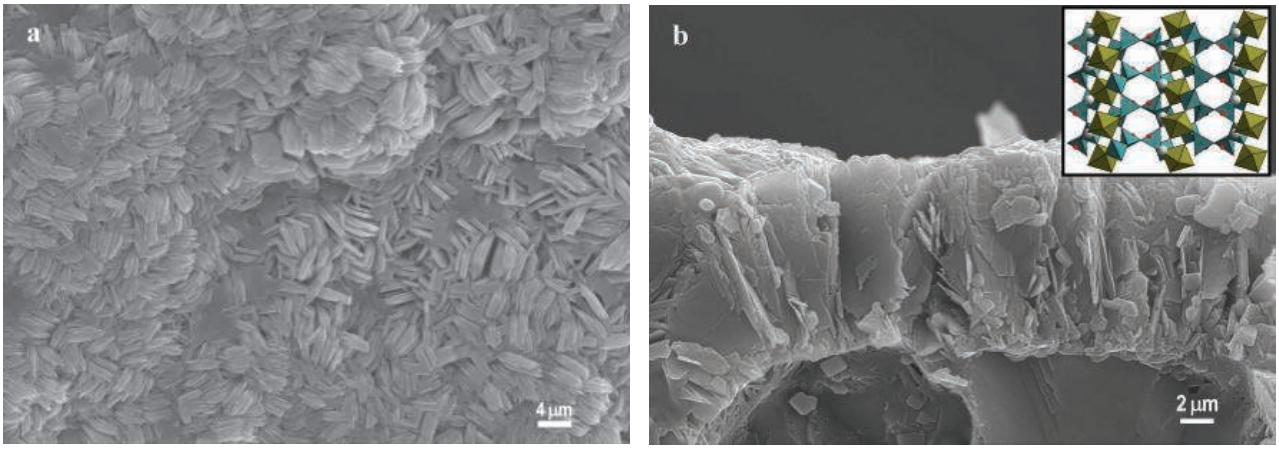

Figure 1. Top view **(a)** and cross-section **(b)** of AM-3 membrane. The inset in (b) shows the channel in the AM-3 structure along [100] direction.

Biorefineries and Materias from Renewable Sources

NOVEL GREEN AND FUNCTIONAL NANOCOMPOSITES BASED ON CHITOSAN AND NANOCELLULOSE FORMS

Fernandes SCM[1], Freire CSR[1], Silvestre AJD[1], Pascoal Neto C[1], Gandini A[1]

In recent years there has been an increasing interest in the search for new functional materials based on renewable resources and prepared through sustainable and green processes that might replace those derived from petrochemistry. In this perspective, polysaccharides, like cellulose, starch and chitosan due to their natural abundance, ubiquity and unique properties are among the most promising starting raw materials. Cellulose has been widely used in the paper and textile industries. Relatively new nanocellulose forms, namely nanofibrillated cellulose (NFC) obtained from the vegetal counterpart, and bacterial nanocellulose (BC) an exopolysaccharide produced by certain bacteria (Fig.1), have emerged as very promising materials due to their singular physicochemical and mechanical properties (e.g. tensile strength and Young modulus), making them particularly suitable as reinforcing elements in composite materials.

Chitosan, is obtained by deacetylation of chitin, the main component of the exoskeleton of crustaceans and considered as the second most abundant natural polymer on earth. Chitosan exhibits unique physicochemical properties like biocompatibility, antimicrobial activity, biodegradability and excellent film-forming ability. However, its films display poor mechanical performance, which limits their applications in several fields.

New chitosan nanocomposites with NFC or with BC can be prepared under environmentally friendly conditions, using water as solvent and converted into films by a simple casting procedure. Due to their natural compatibility, the reinforcing nanofibers (NFC or BC) are perfectly dispersed in the chitosan matrix (Fig.2) which together with their nanometric dimensions, allow the resulting films to keep their high transparency (Fig.2) while imparting substantial improvements in terms of mechanical properties and thermal stability.

The notable properties of these new nanocomposite transparent films allow their application in transparent biodegradable antibacterial packaging, medical and electronic devices.

1 Department of Chemistry, CICECO, University of Aveiro, 3810-193 Aveiro, Portugal

Funding

This work was financed by FCT (PTDC/QUI/68472/2006)

Reference paper

[1] Fernandes SCM, Freire CSR, Silvestre AJD, Pascoal Neto C, Gandini A, Berglund LA, Salmén L. "Transparent Chitosan Films Reinforced With a High Content of Nanofibrillated Cellulose". *Carbohyd. Polym*. **2010**, 81, 394–401

[2] Fernandes SCM, Oliveira L, Freire A.J.D. Silvestre, C. Pascoal Neto, A. Gandini, J. Desbriéres, "Fully-green Transparent Nanocomposite Films Based on Chitosan and Bacterial Cellulose". *Green Chem*. 2009, **11**, 2023

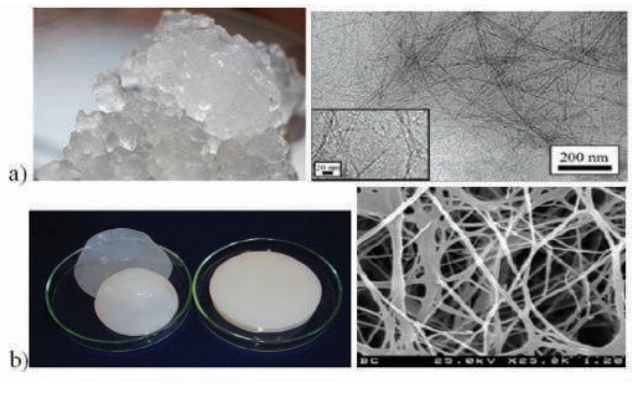

Figure 1. Visual aspect and SEM micrographs of a) nanofibrillated cellulose (adapted from http://www.innventia.com/ and Biomacromolecules, 2007, 8(6), 1934-1941); b) bacterial cellulose.

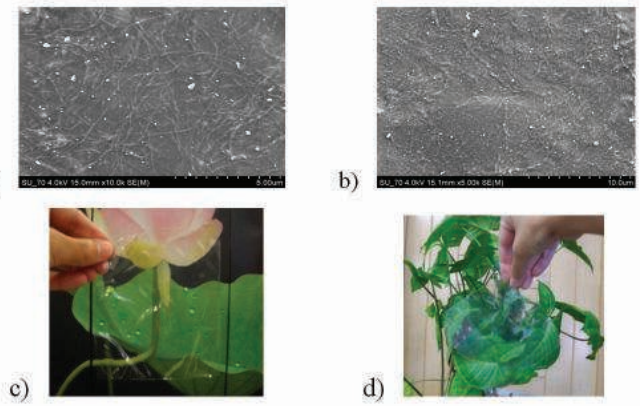

Figure 2. SEM micrographs of chitosan nanocomposites with bacterial (a) and nanofibrillated (b) cellulose; and images of the corresponding (c) and (d) transparent films.

BACTERIAL CELLULOSE, PRODUCTION AND APPLICATIONS: GETTING THE BEST OF A NATURE' MASTER PIECE

Trovatti E[1], Serafim LS[1], Freire CSR[1], Silvestre AJD[1], Pascoal Neto C[1], Gandini A[1]

Cellulose is the most abundant organic polymer on earth and is considered as an inexhaustible source of raw materials for a wide variety of applications. Although wood fibres are the most important source of cellulose some microorganisms, in particular several *Glucanacetobacter, Rhizobium*, or *Agrobacterium* bacteria, among others, are able to produce an extra-cellular form of cellulose known as bacterial (or microbial) cellulose (BC).

BC is produced as a highly swollen gel (~90% water) (Fig.1) which can be dried to

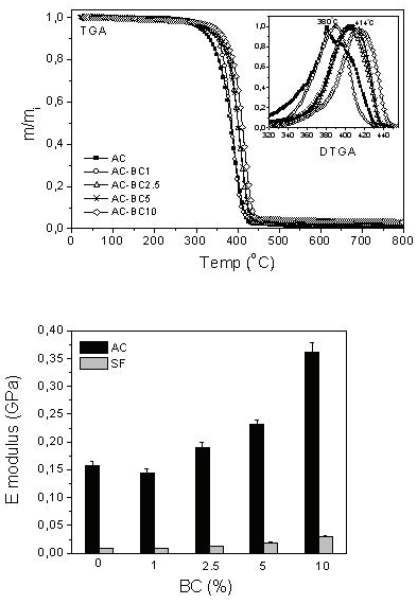

Figure 2. Thermograms and Elastic modulus of acrylic resins reinforced with different BC contents.

form thin films. BC has DPs of 2000-8000 and forms 3D network of highly crystalline nano- and microfibrils with a 10-100 nm width (Fig.1). The high purity and unique physical and mechanical properties of BC make it a very promising material. The applications of BC in the form of dry or wet membranes have increased considerably in the last decade, particularly in the biomedical area, namely as wound healing membranes, substituting natural skin, chirurgical implants and specific applications such as audio membranes and composite materials.

Our group was the first research team in Portugal working on the development of new materials based on BC. Our strategy involved firstly the implementation of the laboratorial production of BC, by a progressive selection and isolation of a high productivity bacterial strain of Gluconaacetobacter. This ensured both unlimited access to this raw material and the possibility to manipulate and to optimize the production conditions and parameters aiming to obtain materials with specific properties, eventually with incorporation of other components during the BC biosynthesis and deposition process. The BC production optimized in our laboratory attained at least about 5g/L during 96 hours of cultivation that is a considerable high productivity.

At the moment we are mainly engaged in the (i) optimization of the BC production using agro-forest industry residues as the carbon source aiming to decrease the production costs of this raw material; (ii) development of new materials and applications, namely nanocomposite films and coatings with other polysaccharides such as chitosan and starch as well as with synthetic acrylic resin emulsions, new functional paper coating formulations and in biomedical applications, for this promising biopolymer, calling-upon its unique properties and, when necessary, adjusting such properties by controlled chemical modification. For example, bacterial cellulose–acrylic resin nanocomposites prepared by a simple and green approach, based on the dispersion of the BC nanofibers into acrylic aqueous emulsions followed by casting showed improved mechanical and thermal properties (Fig.2).

1 Department of Chemistry, CICECO, University of Aveiro, 3810-193 Aveiro, Portugal

Reference paper

[1] Fernandes SCM, Oliveira L, Freire CSR, Silvestre AJD, Pascoal Neto C, Gandini A, Desbriéres J, "Novel transparent nanocomposite films based on chitosan and bacterial cellulose", *Green Chemistry*, **2009**, 11, 2023–2029.

[2] Fernandes SCM, Freire CSR, Silvestre AJD, Pascoal Neto C, Gandini A, "Lars Berglund, Lennart Salmén, Transparent chitosan films reinforced with a high nanocellulose content" *Carbohydrate Polymers*, **2010**, 81,394-401.

[3] Martins IMG, Magina SP, Oliveira L, Freire CSR, Silvestre AJD, Pascoal Neto C, Gandini A, "New biocomposites based on thermoplastic starch and bacterial cellulose" *Composite Sci.Technol*, **2009**, 69, 2163-2168

[4] Trovatti E, Oliveira L, Freire CSR, Silvestre AJD, Pascoal Neto C, Cruz Pinto JJC, Gandini A, "Novel bacterial cellulose-acrylic resin nanocomposites", *Composite Science and Technology*, **2010**, 70, 1148-1153.

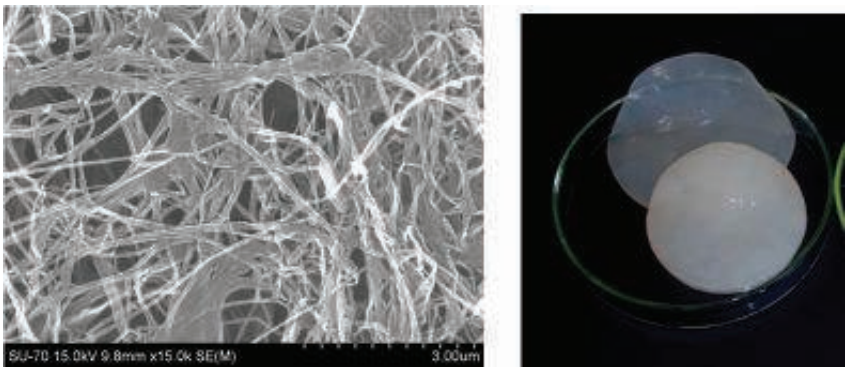

Figure 1. SEM micrograph and visual aspect of a BC mat.

THE FURAN COUNTERPART OF POLY(ETHYLENE TEREPHTHALATE): AN ALTERNATIVE MATERIAL BASED ON RENEWABLE RESOURCES

Gandini A[1], Silvestre AJD[1], Pascoal Neto C[1], Sousa AF[1], Gomes M[1]

Polymers from renewable resources constitute a major research and development issue because they represent a potentially viable alternative to homologues prepared from fossil counterparts. In the course of the last decade, both public and industrial institutions have progressively increased their involvement in this growing realm, which covers the rational exploitation of natural polymers through appropriate processing and/or chemical modifications, as well as the synthesis of monomers from natural sources, the study of their polymerization and the optimization of the ensuing materials.

One of the most promising approaches within this strategy consists in converting sugars or polysaccharides into two readily accessible first-generation furan derivatives, *viz.* furfural and hydroxymethylfurfural and using them as precursors to a wide variety of furan monomers, which are polymerized or copolymerized to generate new macromolecular architecture.

Our laboratory has been actively engaged in pursuing this type of investigation using different chemical routes based on original ideas. The present study[1] was conducted with the specific aim of taking advantage of one of these monomers to synthesize and characterize a novel polyester, whose structure simulates that of the most important petroleum-based counterpart on the world market, namely poly(ethylene terephthalate), PET.

Figure 1 illustrates the synthetic procedure adopted, and the solid poly(ethylene 2,5-furancarboxylate) – PEF- obtained. The characterization studies showed that PEF was a highly crystalline polymeric material, with a DPn of about 250.

The characterization of this material showed that it bore a regular structure and physical properties entirely comparable with those of PET, particularly in terms of melting and glass-transition temperatures, thermal stability and film-forming aptitude. These results provided further clear-cut evidence that abundant and ubiquitous renewable resources can be rationally exploited to prepare high-tech macromolecular materials capable of replacing fossil-based counterparts.

[1] Department of Chemistry, CICECO, University of Aveiro, 3810-193 Aveiro, Portugal

Funding

This work was financed by the FCT.

Reference paper

[1] Gandini A, Silvestre AJD, Pascoal Neto C, Sousa AF, Gomes M, "The Furan Counterpart of Poly(ethylene terephthalate): an Alternative Material Based on Renewable Resources", *Journal of Polymer Science Part A: Polymer Chemistry* **2009**, *47*, 295-298.

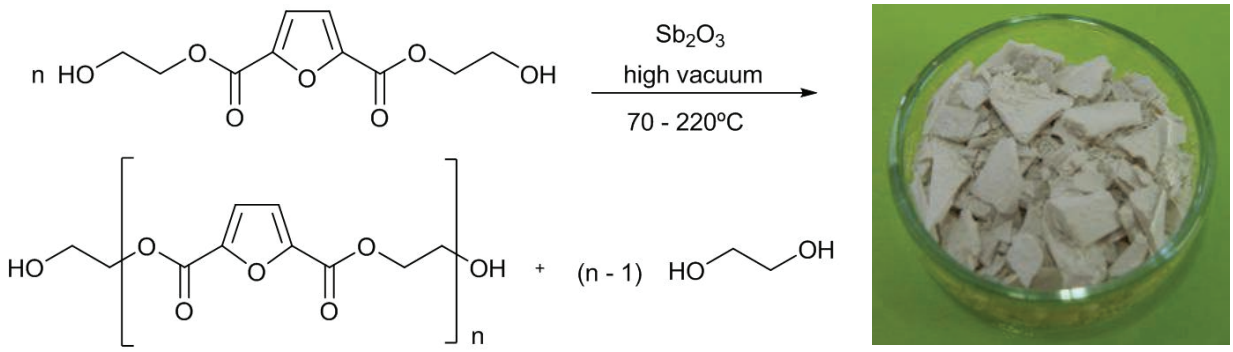

Figure 1. Synthetic procedure adopted to prepare poly(ethylene 2,5-furancarboxylate) – PEF- and a visual aspect of the polymeric material.

POLYOXOMETALATES AS UNIVERSAL MEDIATORS FOR BIOMIMETIC AND ELECTROCHEMICAL OXIDATIONS OF LIGNIN

Evtyugin DV[1], Xavier AMRB[1]

Polyoxometalates (POMs) are composed primarily by early transition metal cations in their high oxidation states and oxoanions with a variety of structures. The oxidative catalysis with POMs is considered a new perspective trend in bleaching of cellulosic pulp fulfilling the environmental concerns. While POMs are used as catalysts, they oxidize residual lignin in pulp and are re-oxidized in turn by oxygen, or some other appropriate oxidiser, in the same process step. Besides high selectivity of lignin oxidation, POM can be reused. Therefore, the catalyzed oxygen bleaching is potentially adapted for the Total Effluent Free (TEF) bleaching plants concept. The high potential of polyanions $[SiW_{11}V^{V}O_{40}]^{5-}$ ($SiW_{11}V^{V}$) and $[SiW_{11}Mn^{III}(H_2O)O_{39}]^{5-}$ ($SiW_{11}Mn^{III}$) in pulp bleaching is difficult to realise in practice because of their very low re-oxidation rate with molecular oxygen even at high temperature (150-200°C). The solution was found while using the naturally occurring oxidative enzymes as biocatalysts for the reoxidation of POMs. Thus, $SiW_{11}V^{V}$ may be effectively reoxidised by laccase and oxygen (Fig.1) [1] and $SiW_{11}Mn^{III}$ by versatile manganese peroxidase and hydrogen peroxide (Fig.2)[2] at low temperatures (40-60 °C). Alternatively POMs may be reoxidised electrochemically (Fig.3)[3].

The technical feasibility of biomimetic delignification of cellulosic pulps with POMs and enzymes, as well as the electrochemical bleaching, were confirmed in the laboratory scale[1-3] . It was shown that implementation of POM-catalysed biomimetic allows significant savings (40-60%) of environmentally hazardous ClO_2 in kraft pulp

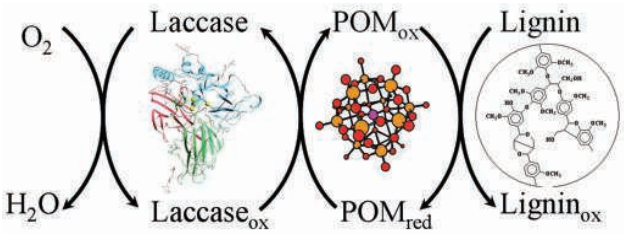

Figure 1. Lignin oxidation by oxygen in presence of laccase and mediated by $SiW_{11}V^{V}$.

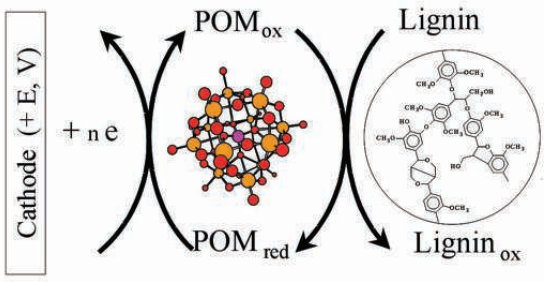

Figure 3. Schematic representation of electrochemical delignification with $SiW_{11}V^{V}$.

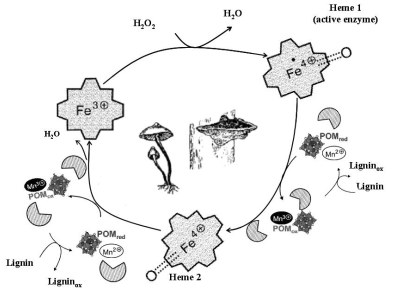

Figure 2. Proposed catalytic cycle for $SiW_{11}Mn^{III}$ reoxidation with versatile peroxidase and H_2O_2.

bleaching (90%ISO) without deterioration of pulp mechanical strength. The electric cost for the electrochemical delignification was more than 50 times lower than the cost of ClO_2 saved, thus demonstrating the economical feasibility of the former technique.

[1] Department of Chemistry, CICECO, University of Aveiro, 3810-193 Aveiro, Portugal

Reference paper

[1] Gamelas JAF, Pontes ASN, Evtuguin DV, Xavier AMB, "New polyoxometalate-laccase integrated system for kraft pulp delignification." *Biochem. Eng. J.* **2007**, 33, 141-147.

[2] Marques G, Gamelas JAF, Ruiz-DueñasFJ, del Río JC, Evtuguin DV, Martínez AT, Gutiérrez A, "Delignification of eucalypt kraft pulp with manganese-substituted polyoxometalate assisted by fungal versatile peroxidise." *Bioresource Technology* **2010**, 110, 5935-5940.

[3] Martins MR, Gamelas JAF, Evtuguin DV, Carapuça HM, "Electrochemical bleaching of kraft pulp employing polyoxometalates." *J. Pulp & Paper Can*. **2009**, *110*, 18 (www.paptac.ca).

ADVANCES IN COMPREHENSIVE UTILIZATION OF SIDE PRODUCTS FROM SULPHITE PULP PRODUCTION

Evtyugin DV[1], Xavier AMRB[1], Silva CM[1]

Acidic sulphite pulping of *Eucalyptus globulus* wood allows sustainable production of Total Chlorine Free (TCF) bleached dissolving pulps and pulps for the paper manufacturing. Sulphite spent liquor (SSL) and condensate (SC), obtained from SSL evaporation before its burning at the recovery boiler, are major liquid side products from acidic sulphite pulp production. The processing of SSL and SC is a necessary term from the technical and environmental points of view. A three years consortium contract between the CAIMA Indústria de Celulose S.A. (ALTRI group) and CICECO (UA), supported by the Portuguese Innovation Agency with total funds of 260 k€ prompted a comprehensive study of the chemical composition of SSL and SC from acidic sulphite pulping of *Eucalyptus globulus* aiming to develop new approaches for the chemical/biochemical processing of SSL and SL allowing a series of commercial products.

The study on the chemical composition of SSL [1,2] lead to several ideas for its utilization, for example: (i) bioprocessing of SSL to produce high quality single cell proteins (SCP) or bioethanol[3] and (ii) SSL oxidation with oxygen resulted in *ca.* 20% yield of vanillin and syringic aldehyde (flavours). The fermentation of SSL with the filamentous fungus *Paecillomyces variotii* revealed a 52% yield of biomass based on consumed acetic acid and sugars. The expected production of SCP may reach up to 160 kg of protein per ton of produced cellulosic pulp. Alternatively, the fermentation of SSL after the ennoblement procedure allowed about 49% yield of ethanol, based on consumed xylose in fer-

Figure 1. Profits from valorisation of sulphite spent liquor.

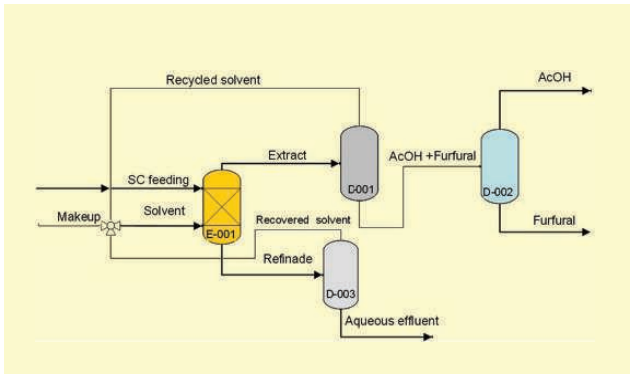

Figure 2. Diagram for the acetic acid and furfural recuperation from SC by liquid-liquid extraction with MTBE.

mentation with *Pichia stipitis* yeasts[3]. The fermentation of SSL to ethanol, according to laboratory results, is estimated to be as high as 100 L per ton of pulp. The gross profits from SSL valorisation may reach 800 € per ton of produced sulphite pulp (almost twice the pulp price) (Fig.1).

It was also verified that acetic acid (10 g/L) and furfural (2 g/L) are the main constituents of industrial SC. The recovery method using liquid-liquid extraction has been developed using an efficient agent - methyl *tert*-buthyl ether (MTBE) (Fig.2). This allowed the estimation of production costs and economical feasibility of the recovery process. It was concluded that concentration of acetic acid in SC of ca 10 g/L is critical for the economic viability of the process while the market price for acetic acid round to 0.5 €/L.

1 Department of Chemistry, CICECO, University of Aveiro, 3810-193 Aveiro, Portugal

Reference paper

[1] Marques AP, Evtuguin DV, Magina S, Prates A, "Chemical Composition of Spent Liquors from Acidic Magnesium-Based Sulphite Pulping of *Eucalyptus globulus*." *J. Wood Chem. Technol*. **2009**, 29, 322-336.

[2] Marques AP, Evtuguin DV, Magina S, Prates A, Amado F, Prates A, "Structure of Lignosulphonates from Acidic Magnesium-Based Sulphite Pulping of *Eucalyptus globulus*." *J. Wood Chem. Technol*. **2009**, 29, 337-357.

[3] Xavier AMRB, Correia MF, Pereira SR, Evtuguin DV, "Second generation bioethanol from eucalypt sulphite spent liquor." *Bioresource Technol*. **2010**, 101, 2755-2761.

VALORIZATION OF A SIDE PRODUCT OF PULP INDUSTRY UNDER THE CONCEPT OF BIOREFINERY

Pereira SR[1], Fernandes D[1], Evtuguin DV[1], Serafim LS[1], Xavier AMRB[1]

Sulphide spent liquors (SSLs) are the side products from acidic sulphide wood pulping and are normally converted to energy by combustion. The annual production of bleached sulphite eucalypt pulp is around 1 million tons and SSLs are normally burned for energy recovery. SSLs contain lignosulfonates and hemicellulose hydrolysis products, with 40-45 g/L sugars, mainly xylose[1]. Using SSL to produce added value products fits well to the biorefinery concept invoked to decrease the dependence from fossil resources and to improve the economic sustainability of pulp mills. The possibility of valorization of sulphite spent liquor (SSL) in the context of biorefinary is the main objective of this project. The rising oil prices and the limited capacity of oil sources prompt the search for renewable sources of energy, like wastes or industrial by-products. The European Union strongly promotes the research focusing on the biotechnological generation of energy and sources of energy, including cellulosic biofuels from non-food crops and agro-forestry wastes, as SSL, the so-called "Second generation" of biofuels.

One of the drawbacks of microbial growth in SSL is the presence of high amounts of acetic acid and lignosulphonates[2]. Despite the presence of inhibitory compounds in SSLs some microorganisms as the filamentous fungus *Paecilomyces variotii*, are able to grow, producing single cell protein (SCP) and consuming acetic acid. *P. variotii* biomass can be sold as Single Cell Protein, an added-value product for animal nutrition. *P. variotii* was cultivated directly in the liquor supplemented with salts attaining a high biomass concentration. The biomass yield obtained in batch tests was 0.13 mg biomass/mg carbon consumed and protein yield was 0.11 mg protein/mg biomass. The batch SCP obtained was composed by 82 ± 14 % protein and only 8 ± 2 % of nucleic acids, in accordance with the specificities of SCP for commercial use.

Another alternative process to remove acetic acid from SSL is the use of microbial mixed cultures (MMC) under aerobic dynamic feeding conditions (ADF). Under these conditions MMC can utilize volatile fatty acids like acetic acid for polyhydroxyalkanoates (PHA) production. PHA are biodegradable biopolymers recognized as good

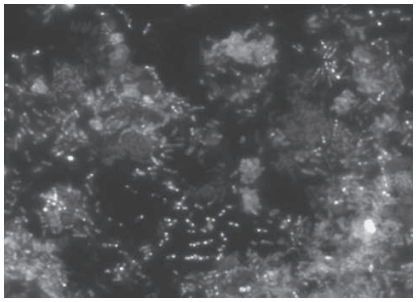

Figure 1. PHA granules inside MMC cells (bright white small dots) after staining with Nile Blue under epyfluorescence microscopy (1000×).

candidates for synthetic polymers partial replacement. PHA production by activated sludge can contribute for a decrease in production costs, since no sterilization is required and bacteria can adapt quite well to the complex substrate present in low cost feedstocks. A MMC culture was selected in a sequenced batch reactor (SBR) under ADF conditions. After 36 days of operation the selected culture was able to produce 29% of PHA per cell dry weight.

The microorganisms were able to uptake the acetic acid and xylose and store them as poly-3-hydroxybutyrate with some xylose was also consumed. Figure 1 shows the PHA granules inside the cells after appropriate staining under epyfluorescence microscopy.

Pichia stipitis is one of the most efficient yeasts to ferment pentoses and it can grow and produce bioethanol from xylose present in SSL after *P. variotii* detoxification. Batch fermentation of *P. stipitis* free cell vs. calcium alginate immobilized beads showed that immobilization is a good strategy for bioethanol production. Certainly *Pichia stipitis* is more protected in beads and less exposed to other inhibitors from HSSL. The time course of this fermentation is present in Figure 2 and an ethanol yield of 91% was obtained.

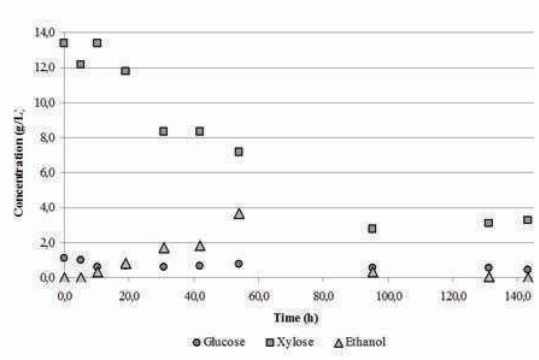

Figure 2. Time course for immobilized *Pichia stipitis* bioethanol bioproduction in detoxified HSSL (T = 28ºC, 180 rpm).

1 Department of Chemistry, CICECO, University of Aveiro, 3810-193 Aveiro, Portugal

Reference paper

[1] Marques AP, Evtuguin DV, Magina S, Prates A, "Chemical Composition of Spent Liquors from Acidic Magnesium-Based Sulphite Pulping of *Eucalyptus globulus*." *J. Wood Chem. Technol.* **2009**, 29, 322-336.

[2] Xavier AMRB, Correia MF, Pereira SR, Evtuguin DV, "Second generation bioethanol from eucalypt sulphite spent liquor." *Bioresource Technol.* **2010**, 101, 2755-2761.

FOREST BIOREFINERIES: ADDED-VALUE CHEMICALS FROM EUCALYPTUS BIOMASS RESIDUES THROUGH GREEN SEPARATION TECHNOLOGIES

Silvestre A, Silva C, Freire C, Pascoal Neto C, Silva A, Oliveira E, Domingues R, Santos S

The forest–based industry is a significant industrial sector in Europe converting wood to pulp, paper, cardboard, energy, and other wood derived products. To increase its competitiveness the pulp and paper industry needs to maximize the value addition of raw materials in its fibre refining processes and to find new and profitable businesses alongside the traditional product lines.

Today, only part of the valuable wood biomass ends up in high-value applications (paper and cardboard), whilst a significant part is channelled into different "side-streams", such as logging residues, debarking residues and pulping liquors. Bark and pulping liquor organic materials are currently incinerated and thereby converted into heat and electricity, or left in the forest partially to provide nutrients, prevent soil erosion and regulate the ecosystem. All of these side-streams contain, however, chemically appealing and reactive constituents (cellulose, hemicelluloses, lignin, extractives and chemicals converted thereof in processing) that could be further refined to value-added chemicals, polymers, materials, and fuels alongside with the sustainable forestry and paper fibre production.

The *Eucalyptus globulus* forest and corresponding pulp and paper sectors play a key role in the Portuguese economy, however as referred above, huge amounts of biomass residues are generated by these activities and are still underexploited. We found that *E. globulus* barks are very rich in high value and bioactive triterpenic acids (e.g. ursolic, oleanolic and betulinic acids) [1-3] as well as phenolic compounds [4] that have a range of unique and potentially usable biological effects and pharmacological activities. A single pulp mill, producing 500 000 ton of pulp per year generates some 100 000 of bark from which some 500 ton of these valuable compounds could be extracted.

The development of methodologies for the efficient extraction of these compounds will be carried out within AFORE, a large collaborative FP7 project, bringing together 20 Research and Industrial Institutions, which aims at developing novel, industrially adaptable and techno-economically viable bio-based solutions for the separation, fractionation, and primary upgrading of green chemicals from forest residues, wood chips, and chemical pulping liquors to be used as starting materials for current and novel value-added applications.

The role of the CICECO Research Team in AFORE Project is mainly centered in:
the detailed characterization of high value triterpenic and phenolic components from eucalyptus bark;
the development of environmentally friendly processes, based on supercritical fluid extraction [5], for the extraction and fractionation of those components
to model and design the scale-up of the extraction/fractionation processes for selected fractions to the demonstration level, integrated in existing pulp mills.
the search for new applications and identification of the more valuable fractions/components;

Research Financial support

AFORE Project is financed by FP7 (CP-IP 228589-2 AFORE): http://www.eu-afore.fi.

Reference papers

[1] C.S.R. Freire, A.J.D. Silvestre, C. Pascoal Neto e J.A.S. Cavaleiro. "Lipophilic Extractives of the Inner and Outer Bark of *Eucalyptus globulus*" *Holzforschung* 2002, **56**, 372-379

[2] R. M. A. Domingues, G. D. A. Sousa, C. S. R. Freire, A. J. D. Silvestre, C. Pascoal Neto, "*Eucalyptus globulus* Biomass Residues from Pulping Industry as Source of High Value Triterpenic Compounds". *Ind. Crops Prod.* 2010, **31**, 65–70.

[3] R. M. A. Domingues, G. D. A. Sousa, C. M. Silva, C. S. R. Freire, A. J. D. Silvestre, C. Pascoal Neto, "High Value Triterpenic Compounds from the outer barks of several Eucalyptus species cultivated in Brazil and in Portugal", *Ind. Crops Prod. In press*

[4] S.A.O. Santos, C.S.R. Freire, M.R.M. Domingues, A.J.D Silvestre, C. Pascoal Neto· "Identification of phenolic components in *E. globulus* bark polar extracts by high performance liquid chromatography–electrospray ionization mass spectrometry and ion–trap tandem mass spectrometry" accepted

[5] E. L. G. Oliveira, A. J. D. Silvestre and C.M. Silva "Review of kinetic models for supercritical fluid extraction", *accepted*

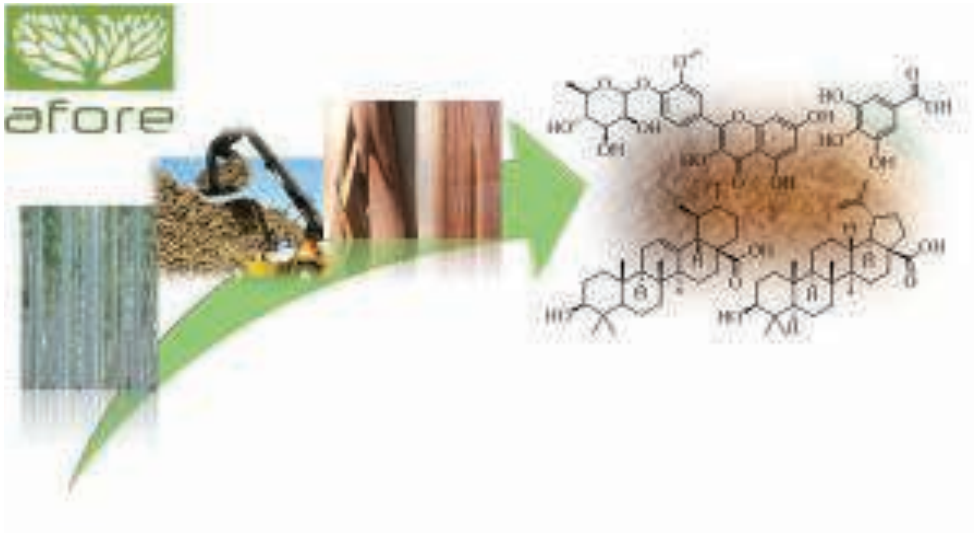

Biomedical Materials and Applications

INSIGHTS INTO METABOLIC DERANGEMENTS AND DIAGNOSTIC MARKERS OF LUNG CANCER AND PREGNANCY DISORDERS THROUGH NMR-BASED METABONOMICS

Duarte IF[1], Barros AS[2], Goodfellow BJ[1], Gil AM[1]

Metabonomics is concerned with the assessment of endogenous metabolites within a biological system (metabolome) and the study of their variations upon different stimuli, such as disease or toxic exposure (Fig.1). Metabolite levels reflect upstream activities of genes and proteins, as well as being modulated by several factors unrelated to the genome (e.g. interaction with commensal microorganisms and environmental agents, nutritional and other lifestyle-related aspects). Therefore, by reflecting the complex interplay between the genome and the environment, the metabolome closely expresses cellular function and the overall physiological status of an organism. Our group has been applying NMR-based metabonomics to the investigation of different disease processes, in order to characterise their metabolic signatures in tissues and biofluids and assess their potential value in disease diagnosis and follow up.

Lung cancer is one of the diseases studied, in collaboration with the Faculty of Medicine and the University Hospitals of Coimbra. Tumour and non-involved adjacent tissues retrieved at surgery were directly analyzed by ^{1}H High Resolution Magic Angle Spinning (HRMAS) NMR, which, in tandem with multivariate statistics, allowed discrimination between the two tissue types to be achieved (Fig.2), providing biochemical information on different histological classes, not available through conventional histopathology[1,2]. Furthermore, consistent alterations were found in the metabolic composition of blood plasma and urine from lung cancer patients, compared to a control group of healthy subjects, thus showing the potential of NMR-based metabonomics for the minimally invasive detection and monitoring of the disease[3]. Some of the metabolites found to be altered in tissues and biofluids related to known cancer biochemical hallmarks, such as the Warburg effect, increased glutaminolysis, and deregulated lipid metabolism, whereas others, like elevated short chain fatty acids and creatinine in urine, were unexpected, paving the way to formulate new pathophysiological hypotheses.

Another subject extensively investigated by our group, in collaboration with Bissaya Barreto Maternity and the Faculty of Medicine of Coimbra, is the search for metabolic markers of pregnancy disorders, through NMR-based metabonomics of amniotic fluid (AF)[4,5]. Among the disorders studied, foetal malformations were found to have the highest impact on AF metabolite composition, enabling statistical validation to be achieved by several multivariate analytical tools (Fig.3). Results confirmed previous indications that malformed foetuses seem to suffer altered energy metabolism and kidney underdevelopment. Moreover, newly found changes (namely in R-oxoisovalerate, ascorbate, creatinine, isoleucine, serine, threonine) suggested possible

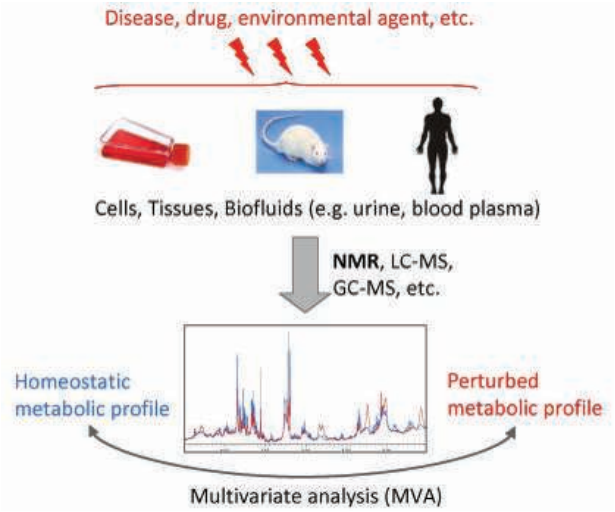

Figure 1. Overview of the typical strategy followed in metabonomic studies.

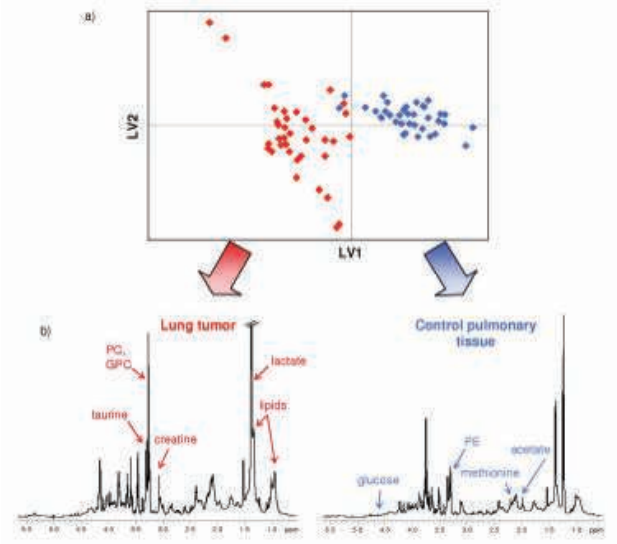

Figure 2. **a)** Scores scatter plot of PLS-DA applied to ^{1}H HRMAS NMR spectra of lung control (♦) and tumour (♦) tissues, **b)** average spectra of control and tumour tissues, with main metabolic differences highlighted.

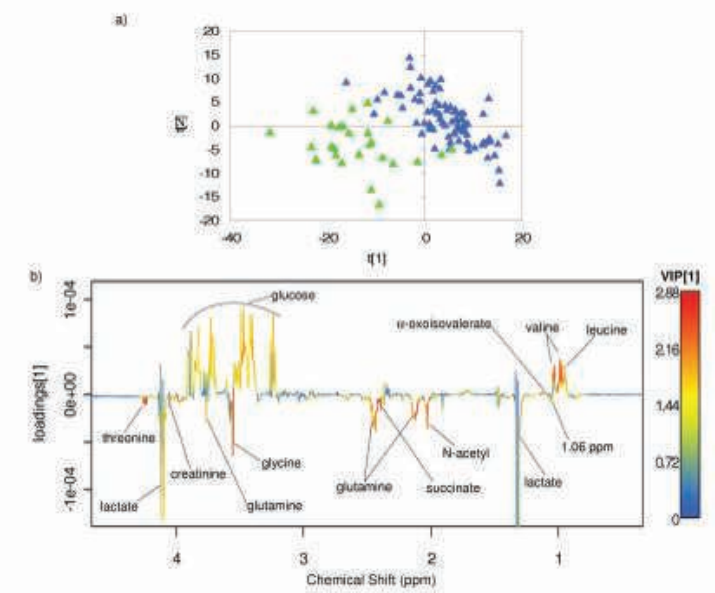

Figure 3. PLS-DA of ^{1}H NMR spectra of amniotic fluid samples from healthy pregnancies (▲) and those affected by several foetal malformations (▲): **a)** scores scatter plot LV1 vs. LV2, **b)** LV1 loadings plot coloured according to variable importance in the projection (VIP), showing the metabolites responsible for sample discrimination.

additional effects on protein and nucleotide sugar biosynthesis. Gestational diabetes was also found to induce detectable metabolic changes in AF composition, prior to medical diagnosis, which were consistent with higher demand for protein and nucleotide biosynthesis, as well as possible changes in renal function and lipid metabolism. Finally, small changes were observed in the second trimester AF of women presenting with preterm delivery or early rupture of membranes, whereas no relevant changes were found for chromossomopathies. The extension of this approach to the analysis of blood and urine from pregnant women is currently ongoing and may help not only to obtain a more accurate picture of the overall metabolic perturbations related to pregnancy but also lay the basis for less invasive follow up and diagnostic methods during pregnancy.

[1] Department of Chemistry, CICECO, University of Aveiro, 3810-193 Aveiro, Portugal

[2] QOPNA, Department of Chemistry, University of Aveiro, Portugal

Funding

This work has been funded by FCT (Portugal) and CIMAGO, University of Coimbra (Portugal).

Reference paper

[1] Rocha C, Barros AS, Gil AM, Goodfellow BJ, Humpfer E, Spraul M, Carreira IM, Melo JB, Bernardo J, Gomes A, Sousa V, Carvalho L, Duarte IF, "Metabolic profiling of human lung cancer tissue by 1_H High Resolution Magic Angle Spinning (HRMAS) NMR spectroscopy", *Journal of Proteome Research*, **2010**, 9, 319-332.

[2] Duarte IF, Rocha CM, Barros AS, Gil AM, Goodfellow BJ, Carreira IM, Bernardo J, Gomes A, Sousa V, Carvalho L, "Can Nuclear Magnetic Resonance (NMR) spectroscopy reveal different metabolic signatures for lung tumours?", *Virchows Archiv*, **2010**, 457, 715-725.

[3] Carrola J, Rocha CM, Barros AS, Gil AM, Goodfellow BJ, Carreira IM, Bernardo J, Gomes A, Sousa V, Carvalho L, Duarte IF. "Metabolic signatures" of lung cancer in biofluids: NMR-based metabonomic study of urine, *in press*.

[4] Graça G, Duarte IF, Barros AS, Goodfellow BJ, Diaz S, Carreira IM, Couceiro AB, Galhano E, Gil AM, "1H NMR based metabonomics of human amniotic fluid for the metabolic characterization of foetus malformations", *Journal of Proteome Research*, **2009**, 8, 4144-4150.

[5] Graça G, Duarte IF, Barros AS, Goodfellow BJ, Diaz S, Pinto J, Carreira IM, Galhano E, Pita C, Gil AM, "The impact of prenatal disorders on the metabolic profile of 2nd trimester amniotic fluid: a Nuclear Magnetic Resonance (NMR) metabonomic study", *Journal of Proteome Research*, **2010**, 9, 6016-6024.

NMR METABOLIC PROFILING OF CELLS FOR ASSESSING THE BIOLOGICAL EFFECTS OF CHEMOTHERAPY DRUGS

Duarte IF[1], Marques MP[2], Gil AM[1]

The use of cell cultures as *in vitro* models for studying physiological and pathological processes, as well as testing drugs and other exogenous substances, has gained refreshed interest given the emerging metabolic profiling approach based on advanced analytical tools, in particular NMR spectroscopy, and multivariate statistics[1]. Indeed, by providing a holistic view of metabolic changes and seeking consistent variation patterns triggered by certain conditions or external influences, rather than following discrete changes in individual compounds, this strategy (metabonomics) has the potential to reveal hidden biological events and allow a deeper understanding of cellular metabolism and its modulation. In our group, we have been using this approach to assess the effects induced by chemotherapy drugs on different cell lines, aiming at elucidating mechanisms of action and identifying putative toxicity/efficacy biomarkers.

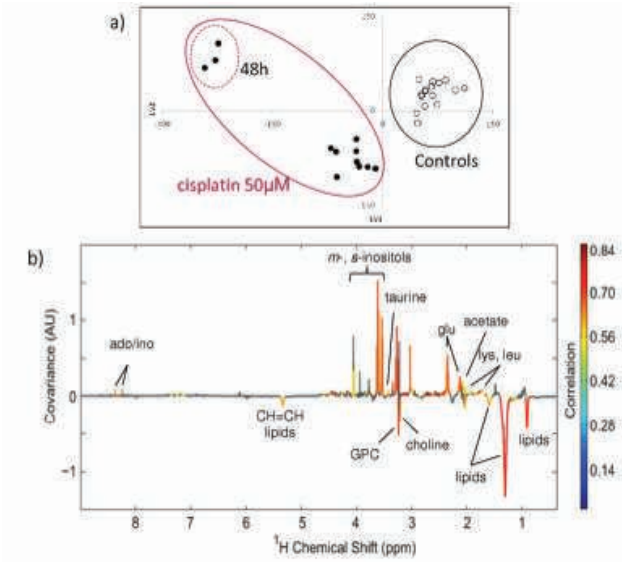

Figure 1. PLS-DA of ^{1}H HRMAS NMR spectra of controls (○) and 50μM cisplatin-treated cells (•): a) scores scatter plot LV1 vs. LV2; b) SRV-LV1 loadings with colour scale reflecting the statistical relevance of each signal.

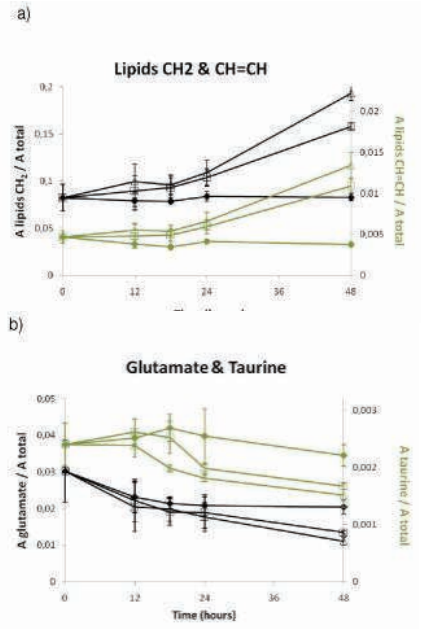

Figure 2. Plots of area ratios (to total spectral area) for a) lipids (CH2)n and CH=CH and b) glutamate and taurine, as a function of cisplatin exposure time. Control cells (◆), 30μm CDDP-treated cells (□) and 50μm CDDP-treated cells (Δ).

At a first stage, the influence of sampling and storage procedures on the integrity and metabolic composition of different cell lines (osteosarcoma and lung cancer) has been systematically evaluated, and optimized protocols have been established[2]. Thereafter, studies of exposure of these cells to the alkylating agent cisplatin have been carried out. The cells' metabolic profiles, measured by ^{1}H High Resolution Magic Angle Spinning (HRMAS) NMR and subjected to multivariate modelling (Fig.1), were found to be exquisitely sensitive to drug exposure, showing evidence of specific time-dependent changes in several metabolic pathways. For instance, in the case of the osteosarcoma cell line MG-63, cisplatin induced significant changes in lipids and choline-containing compounds (Fig.2a)[3], suggesting the occurrence of apoptosis and alterations in lipid metabolism regulation. The levels of some amino acids were also significantly altered (Fig.2b), the decreases in glutamate and taurine possibly reflecting, respectively, effects of oxidative stress overtime and activation of cell DNA-related defence mechanisms. Moreover, significant decreases in osmoregulatory compounds *myo*- and *scyllo*-inositols were consistent with their role in cellular stress response, whereas the decrease in nitrogenated bases ado/ino possibly reflected reduced DNA synthesis. Further biochemical interpretation of the observed metabolic changes is currently underway through stable isotope tracer studies. In this approach, the biotransformation of labelled substrates (e.g. uniformly or atom-specific ^{13}C-labelled glucose) is monitored through the NMR analysis of the isotopomer patterns of their metabolic products. By comparing these patterns in control and drug treated cells, information on specific pathways altered due to drug exposure may arise.

In the short-term future, this analytical strategy will be extended to assess cellular responses to nanoparticles of different chemical composition, size and surface chemistry.

1 Department of Chemistry, CICECO, University of Aveiro, 3810-193 Aveiro, Portugal

2 R&D Unit "Molecular Physical-Chemistry", Department of Life Sciences, Faculty of Science and Technology, University of Coimbra, Portugal

Funding

This work has been funded by FCT (Portugal).

Reference paper

[1] Duarte IF, Lamego I, Rocha C, Gil AM, "NMR metabonomics for mammalian cell metabolism studies", *Bioanalysis*, **2009**, 1(9), 1597-1614.

[2] Duarte IF, Marques J, Ladeirinha AF, Rocha C, Lamego I, Calheiros R, Silva TM, Marques MPM, Melo JB, Carreira IM, Gil AM, "Analytical approaches towards successful human cell metabolome studies by NMR spectroscopy", *Analytical Chemistry*, **2009**, 81, 5023-5032.

[3] Duarte IF, Lamego I, Marques J, Marques MPM, Blaise BJ, Gil AM, "A Nuclear Magnetic Resonance (NMR) study of the effect of cisplatin on the metabolic profile of MG-63 osteosarcoma cells", *Journal of Proteome Research*, **2010**, 9, 5877-5886.

A DOOR WITH MULTIPLE LOCKS. SEARCHING THE KEY TO OSTEOSARCOMA CHEMOTHERAPY WITH NOVEL RUTHENIUM(II) AMINO ACID COMPLEXES

Marques J[1], Santos TM[1], Marques MP[2], Braga SS[1]

Osteosarcoma, the sixth most prevalent cancer for ages below 15 years, develops in long bones requiring surgical removal and limb amputation in severe cases. It is a highly aggressive cancer, able to metastasise to the lungs, thus surgery is accompanied by chemotherapy. The active drugs for osteosarcoma are limited (*cis*-platin, doxorubicin, ifosfamide and high-dose methotrexate) and no new ones have appeared since the 1980´s, in spite of a very active research. This fact illustrates quite well both the interest and the difficulties in the quest for such compounds.

One of the most promising drug design strategies is to introduce a metal centre into a natural compound with intrinsic antitumoural activity. Two patent examples of this approach (though not targeting osteosarcoma) are ferrocifene, a ferrocenyl tamoxifen derivative in which the action of the natural drug against estrogen-dependent breast cancers is expanded to include some estrogen-independent ones, and a family of staurosporin-derived ruthenium complexes for lymphoma. Staurosporin is a natural inhibitor of protein kinases, which are heavily studied targets by the pharmaceutical industry (30% of the global protein research).

The contribution of the Biomaterials Group at CICECO to these novel biomimetic metal drugs is based on Ru(II) complexes with trithiacyclononane, a face capping ligand, to protect from *in vivo* inactivation, and an amino acid fragment directed to receptors found in bone cells. Key amino acids or their biochemically relevant derivatives were strategically selected, comprising (i) glycine, a co-agonist for osteoblastic glutamate receptors, (ii) serotonin, for which osteocytes and osteoblasts have specific receptors, and (iii) its biochemical amino acid precursor tryptophan (Fig.1). Further protection and biocompatibility is achieved by the molecular encapsulation of these complexes with cyclodextrins – naturally occurring D-glucose rings – and their derivatives.

The ruthenium glycine complex was tested first on a common breast cancer cell line (MDA-MB-231) and proved able to instil some antiproliferative action (Fig.2), prompting further studies. Thus, the complex and its inclusion compounds with four different cyclodextrins were tested against osteosarcoma using the MG-63 cell line (Fig.3), but exhibited a mild and time-delayed activity (appearing only after 72h of incubation). The glycine key did, thus, not suffice to open a new path toward the treatment of this cancer.

Renewed hopes lie on the recently-prepared tryptophan and serotonin Ru(II) complexes, currently undergoing cytotoxicity tests on the same cell line (MG-63). Results will reveal if these are the keys unlocking the door to osteosarcoma chemotherapy.

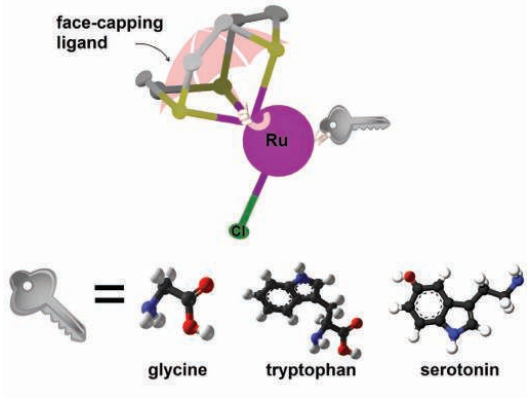

Figure 1. Structure rationale for the ruthenium trithiacyclononane complexes with the amino acids glycine, tryptophan and serotonin.

[1] Department of Chemistry, CICECO, University of Aveiro, 3810-193 Aveiro, Portugal

[2] Science and Technology Faculty, Molecular Physical Chemistry Research Group, Department of Chemistry, University of Coimbra, PO Box 3126, 3001-401 Coimbra, Portugal

Reference paper

[1] Marques J, Santos TM, Marques MP, Braga SS, "A glycine ruthenium trithiacyclononane complex and its molecular encapsulation using cyclodextrins", *Dalton Transactions* **2009**, 9812-9819.

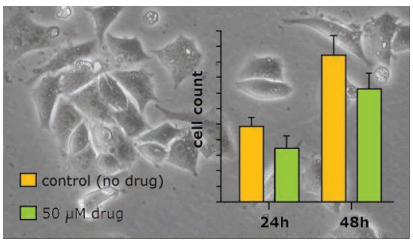

Figure 2. Cytotoxicity of the complex [RuCl(glycine)(trithiacyclononane)] in a 50 μM solution against the MDA-MB-231 breast cancer cell line, shown in the background as a photograph (image from optical microscopy).

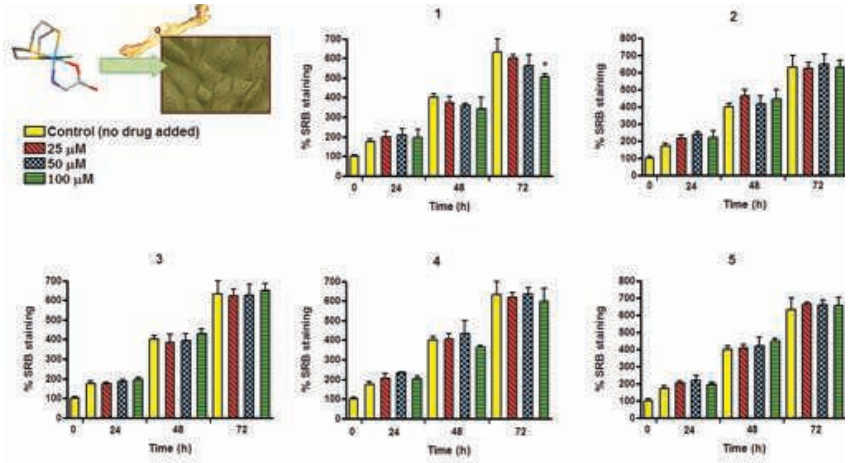

Figure 3. Cytotoxicity of **1**) the complex [RuCl(glycine)(trithiacyclononane)] and its inclusion compounds with **2**) β-cyclodextrin or β-CD, **3**) hydroxypropylated β-CD, **4**) permethylated β-CD and **5**) partially methylated β-CD on the osteosarcoma cell line MG-63 at concentrations ranging from 25 to 100 μM.

CYCLODEXTRIN CARRIERS FOR ANTIMICROBIALS: MOLECULAR LIFEBOATS TO SAIL THE POOLS OF PATHOGENICITY

Marques J[1], Braga TM[2], Ramos A[1], Santos TM[1], Paz FAA[1], Lopes MFS[2], Braga SS[1]

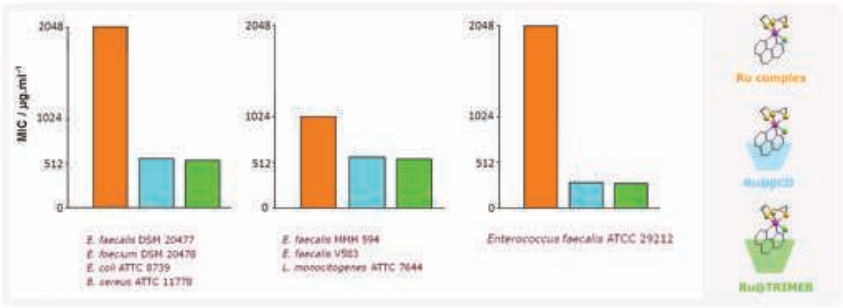

Figure 1. Minimal inhibitory concentrations for the ruthenium complex and its cyclodextrin inclusion compounds against selected bacteria. Below each chart are listed the pathogens for which the results were obtained.

The use of cyclodextrins (CDs) as a drug carrier system is strongly explored, with about 30 different CD-containing marketed products worldwide, including pharmaceuticals, cosmetics, and also numerous food products. Incorporation of CDs in these products is mostly associated with their solubilising, taste ameliorating and stabilising actions.

Recent investigations in our group have shown that the role of CDs can extend beyond these mere physico-chemical abilities. In fact, upon inclusion of selected cytotoxic compounds into CDs, we have observed improved biological activity[1,2].

In search for a novel metal based antimicrobial agent, we have developed the complex [RuCl(trithiacyclononane)(phenanthroline)]Cl and two inclusion compounds with native β-CD and the permethylated derivative TRIMEB, which were tested for their antimicrobial action on a selection of bacterial strains implicated in human infections[3]. The minimal inhibitory concentrations (MIC) of the free complex (with values of 2048 to1024 mg/ml, as shown on Figure 1) are indicative of a mild activity, which is increased up to eight times by inclusion into the cyclodextrins (Figure 1, chart on the right). Bacterial resistance to cytotoxic agents is often dose-induced. Evidence of the cyclodextrins' ability to reduce the amount of drug needed for the antimicrobial action is an encouraging start towards a new strategy to fight bacterial resistance.

Further application of this beneficial action of CDs on the commercial antimicrobials triclosan and chloramphenicol is presently under study. Early results are quite promising, showing that TRIMEB induces selectivity on triclosan, making it more active towards infection-related bacteria and less toxic on environmental bacteria isolated from Portuguese waters and coastal sands.

[1] Department of Chemistry, CICECO, University of Aveiro, 3810-193 Aveiro, Portugal

[2] ITQB/IBET Antibiotic Stress and Virulence of Enterococci Laboratory, ITQB and IBET, Av. República, Estação Agronómica Nacional, 2780-157 Oeiras, Portugal.

Reference paper

[1] Braga SS, Marques MPM, Sousa JB, Pillinger M, Teixeira-Dias JJC, Gonçalves IS," Inclusion of molybdenocene dichloride (Cp_2MoCl_2) in 2-hydroxypropyl- and trimethyl-β-cyclodextrin: Structural and biological properties", *Journal of Organometallic Chemistry*, **2005**, 690, 2905–2912.

[2] Pereira CCL, Diogo CV, Burgeiro A, Oliveira PJ, Marques MPM, Braga SS, Paz FAA, Pillinger M, Gonçalves IS, "Complex Formation between Heptakis(2,6-di-O-methyl)- -cyclodextrin and Cyclopentadienyl Molybdenum(II) Dicarbonyl Complexes: Structural Studies and Cytotoxicity Evaluations", *Organometallics* **2008**, 27, 4948–4956.

[3] Marques J, Braga TM, Paz FAA, Santos TM, Lopes MFS, Braga SS, "Cyclodextrins improve the antimicrobial activity of the chloride salt of Ruthenium(II) chloro-phenanthroline-trithiacyclononane", *Biometals*, **2009**, 22, 541–556.

IONIC LIQUIDS MEET SPORTS: USING IONIC LIQUIDS IN DRUG ANALYSIS

Freire MG[1,2], Neves CMSS[1], Marrucho IM[2], Canongia Lopes JN[2], Rebelo LPN[2], Coutinho JAP[1]

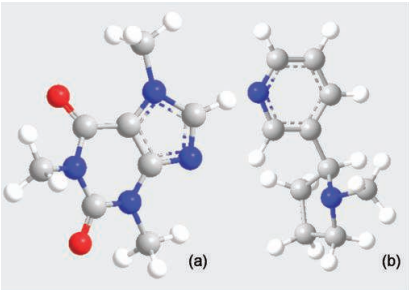

Figure 1. Molecular structures of caffeine **(a)** and nicotine **(b)**.

The use of doping agents by athletes to improve athletic performance is a crucial concern in endurance sports. The International Olympic Committee listed caffeine and nicotine, two easily obtainable alkaloids (Fig.1), as stimulant, ergogenic and restricted drugs.

In anti-doping tests, quantitative determinations of strictly forbidden drugs are regularly accomplished by chromatographic and spectroscopic methods, which require the pretreatment of the biological fluids to increase the drug concentration from the original sample. Liquid-liquid extractions to enhance the metabolites concentration commonly use volatile organic solvents. These solvents present however accrued risks due to their toxicity, volatility and flammability, contributing thus for environmental and occupational hazards. Ionic liquids are novel solvents that display enhanced extraction abilities, can minimize solvent

Figure 2. Experimental procedure applied for the alkaloids extraction.

waste, reduce the exposure to hazardous vapors and generally present low toxicities.
A large number of different ionic liquids was tested and in most of them it was achieved a complete extraction of caffeine and nicotine (Fig.2). After the fine-tuning of ionic liquids, and respective mass fraction compositions, the direct extraction of alkaloids from a synthetic biological sample - artificial human urine - was additionally evaluated. Quantitative extraction of caffeine and nicotine into the ionic-liquid-rich phase from human urine samples showed that the extraction performances of both alkaloids were significantly improved using these more complex matrixes. The presence of urea and sodium chloride enhanced the alkaloids partitioning, and in some particular examples, lead to the complete extraction of caffeine and nicotine not previously observed with simpler aqueous phases. This approach replaces volatile organic solvents with a relatively small quantity of (recyclable) ionic liquid solvent in a second aqueous phase and opens new avenues for the separation and concentration of other bioactive drugs.

We are now actively engaged in pursuing studies aiming at finding suitable ionic liquids for the extraction of added-value products from biomass. Biomolecules, such as amino acids, terpenoids and phenolic compounds, along with caffeine, are being investigated.

[1] Department of Chemistry, CICECO, University of Aveiro, 3810-193 Aveiro, Portugal

[2] Instituto de Tecnologia Química e Biológica, UNL, Av. **República**, Ap. 127, 2780-901, Oeiras, Portugal

Funding

This work was financed by the FCT.

Reference paper

[1] Freire MG, Neves CMSS, Marrucho IM, Canongia Lopes JN, Rebelo LPN, Coutinho JAP, "High-performance Extraction of Alkaloids using Aqueous Two-phase Systems with Ionic Liquids", *Green Chemistry* **2010**, 12, 1715-1718.

POROUS HYBRID SPHERICAL GRANULES FOR CONTROLLED DRUG DELIVERY

Lemos AF[1], Marques AC[1], Bettencourt A[2], Ferreira JMF[1]

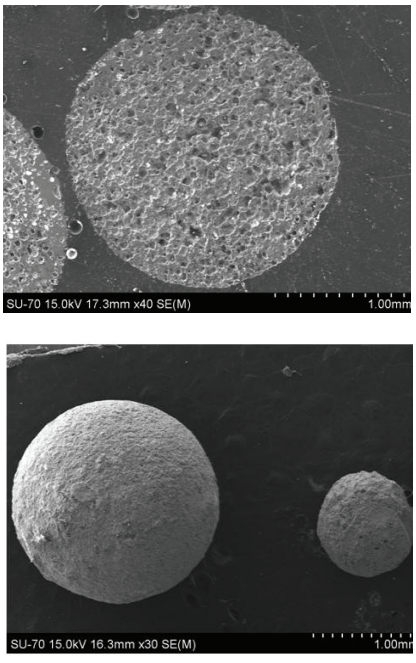

Figure 1. SEM photographs of porous hybrid spherical granules.

A rapidly aging population and a changing in lifestyle habits, which increases the incidence of typically age-related diseases among the younger population, are driving the demand for orthopaedic biomaterials all over the world, being bone grafts often necessary to provide support, fill voids, and enhance biologic repair of skeletal defects.

Porous granules have received much attention from the research field, and depending of their size, microstructure pores content and distribution, they can find application in dental, periodontal, oral/maxillofacial surgical procedures and skeletal bone surgery. Their behaviour in the body depends on morphology and microstructure, and it is known that irregular morphology causes inflammatory reactions, so the rounded forms with smooth geometry are preferable for defect filling. There are some new methods under development for the granules processing, namely one based on the liquids immiscibility effect[1], and other based on the ionotropic gelation[2]. Nowadays, composite materials of organic/inorganic origin are studied extensively because they can combine the tailored degradability and high release efficiencies of the polymer with the osteoconductivity and delayed/sustained release characteristics of the ceramic material.
Levofloxacin is a synthetic chemotherapeutic anticancer of the fluoroquinolone drug class and is used to treat severe or life-threatening bacterial infections or bacterial infections that have failed to respond to other antibiotic classes. This drug can be incorporated in the organic or inorganic part of the composite, depending on the desired release profile.
Under a close collaboration between DECV/CICECO and the Pharmacy Faculty, Lisbon University, porous hybrid spherical granules of doped calcium phosphates[3] were tailored as controlled levofloxacin delivery systems, taking advantage of the expertise valences of each group. The granules preparation was based on the ionotropic gelation[4] with some improvements[5], in order to better control the porosity size, amount and intercon-

nectivity degree. Figure 1 shows SEM photographs of granules with spherical shape and interconnected porosity. These interconnections enable to cover the granules with natural polymers, like chitosan and collagen, by a simple vacuum immersion method, freezing and lyophilisation. The type, amount and degree of polymerization of the polymer used enable to tailor the drug release kinetics. The amount of drug absorbed by the granules was about 100%. The release profiles were studied by UV- Visible spectroscopy and the levofloxacin release was optimised by varying the porosity of the granule, and the amount and type of polymer.

1 Department of Ceramics and Glass Engineering, CICECO, University of Aveiro, 3810-193 Aveiro, Portugal

2 Faculty of Pharmacy, Lisbon University, Av. das Forças Armadas, 1600 -083 Lisbon, Portugal.

References

[1] Komlev VS, Barinov SM, Koplik EV. *Biomaterials*, **2002,** 23, 3449

[2] Lamprecht A, Shafer U, Lehr C. *AAPS PharmSciTech*, **2000,** 3 (1), 17

[3] Kannan S, Lemos IAF, Rocha JHG, Ferreira JMF. *Journal of Solid State Chemistry*. **2005**.178, 3190

[4] Lemos AF, Rocha JHG, Ventura JM, Ferreira JMF. *Key Engineering Materials,* **2005.** 284-286, 309

[5] Lemos AF, Ferreira JMF. *Key Engineering Materials*. **2004.** 254-256, 1041

DESIGNING NANOSTRUCTURED MATERIALS FOR CANCER THERAPY

Costa MEV[1], Almeida MM[1], Santos C[1]

The importance and usefulness of calcium phosphates (CaP) for bone repair, osteologic implant coating, cements and scaffolds is nowadays unquestionable and well established. Taking advantages from CaP biocompatibility and nontoxicity, a new interest on the CaP applications as drug carrier and delivery systems (DDS) is now emerging. Since the expectations for the 21st century healthcare improvement are particularly focused on the potentialities of nanosized materials for superior diagnostics and biosensors, improved imaging techniques, better tissue regeneration and repair technologies and innovative therapeutics, a growing attention is being paid to the synthesis of nanosized or nanostructured systems. The concept that a nanosized particle (nP) may be a vehicle carrying into a cell a therapeutic agent for a specific in situ action anticipates a revolution in therapeutics paradigms. However this targeted nP concept still awaits the knowledge that might ensure therapeutic effectiveness, nontoxicity, selectivity, minimum lateral and invasive effects, thus still being at its infancy.

The synthesis of nanosized Hydroxyapatite (HaP) and its viability for a DDS application are a topic of research at CICECO. Despite the many chemical synthesis methods reported for producing successfully HaP particles with varied shape and size, the experimental conditions require a close control in order to achieve the adequate compromise between nucleation and growth rates thus minimizing unpredictable variations on the final particle morphology. Nanosized HAP particles were precipitated at physiological temperature in presence of citrate ions (Fig.1). The chelating ability of citrate species together with solution pH were the key tools for controlling the free calcium availability in the precipitating solution and hence the burst of Hap nuclei. Additionally, citrate adsorption on HAP nuclei allowed to control the nanoparticle stability thereby ensuring final nanosized needle like particles having a surface area as large as 170m^2/g [1]. Since Hap has a good ability to adsorb substances biologically active, this large surface area

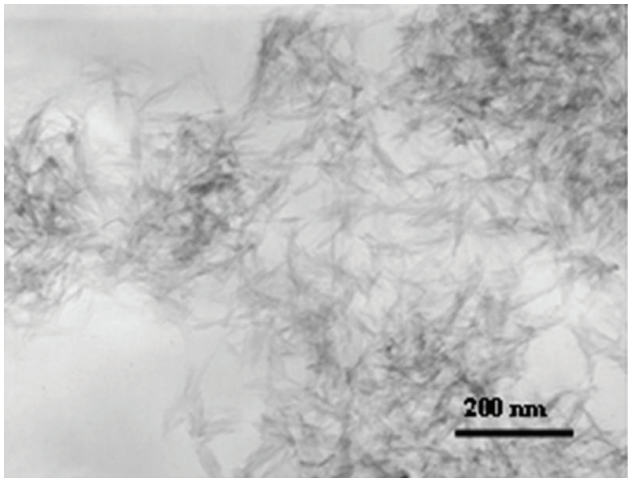

Figure 1. TEM micrograph of hydroxyapatite nanosized particles precipitated in presence of citrate ions at 37ºC.

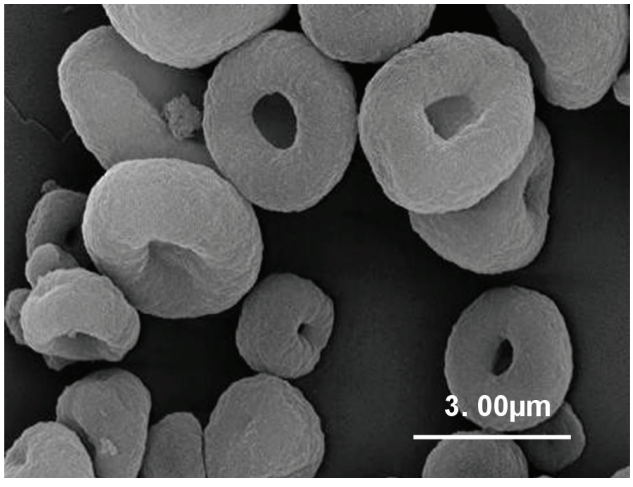

Figure 2. SEM micrograph of hydroxyapatite donut shaped granules obtained by spray drying hydroxyapatite nanosized particle suspensions.

enhanced its attractiveness for DDS application. Hap nanoparticles were further converted by spray-drying into highly porous donnut shaped granules which maintained the surface area as high as 150m²/g (Fig.2). Such nanostructured granules could be easily handled and loaded with the anticancer drug 5-Fluourouracil while ensuring the subsequent drug release in a controlled manner. Moreover it was also shown that the granules drug adsorption and or release profiles could be engineered by manipulating the granules surface reactivity through adequate thermal treatments. In addition, considering that the biological performance of CaP materials is morphology dependent being known that smooth spherical geometries are preferable for minimizing inflammatory processes, the donnut shaped granules may combine geometry advantages with a tailored adsorptive reactivity. *In vitro* studies were already initiated with cells originated from a rat osteosarcoma. The preliminary results revealed that HAP microgranules loaded with 5-FU efficiently reduced the proliferation of cancer cells. In vivo studies are now in progress for assessing the drug carrier ability to overcome several obstacles including uptake, clearance, degradation, non-targeted accumulation, and phagocytosis prior to delivering the therapeutic payload. This study is being carried out within an on going collaboration with the Dentistry Faculty of the University of Oporto.

[1] Department of Ceramics and Glass Engineering, CICECO, University of Aveiro, 3810-193 Aveiro, Portugal

[1] Martins MA, Santos C, Almeida MM, Costa MEV, *Journal of Colloid and Interface Science*, **2008,** 318, 210–216.

POROUS PLLA-BIOGLASS COMPOSITES - A PROMISING APPROACH FOR BONE TISSUE ENGINEERING

Barroca N[1], Daniel-da-Silva AL[1], Vilarinho PM[1], Fernandes MHV[1]

Injured tissues and organs have the innate ability to heal and defend themselves. However in some cases they cannot heal or repair on their own. Regenerative Medicine, linked to Tissue Engineering may help to restore structure and function of damaged tissues.
Strategies to correct bone defects for instance are critically dependent on the proper combination of cells, cell signals and three-dimensional porous structures (or scaffolds) to work as extracellular matrix while the cells proliferate and secrete their own extracellular matrix.
Requirements for these 3D structures are manifold and depend on the specific application. For bone tissue, scaffolds should be biocompatible, have adequate mechanical properties, a controllable biodegradability as the degradation and resorption rates should match cell/tissue growth, and also a pore size >100 μm and good pore interconnectivity.
Usually, 3D structures for bone regeneration consist of polymer/ceramic composites, such as a polymeric matrix filled or coated with bioactive glasses, glass ceramics and calcium phosphates. The use of a bioactive phase allows the *in vivo* bonding with bone due to the development of a bone-like apatite layer on the surface of the material. Additionally, they have been found to enhance the mechanical properties of scaffolds, improve osteoblast growth, differentiation and function.
The processing technique to prepare this kind of structures is determinant in obtaining a morphology that satisfies the above mentioned requirements. Thermally induced phase separation (TIPS) followed by freeze-drying may be one of them. It basically consists in the preparation of a solution that comprises the polymer and a mixture of a polymer miscible solvent and an imiscible solvent to favour phase separation. The resultant morphology of the scaffold depends on the final thermodynamic state of the polymer solution and on the rate of heat transfer during phase separation. TIPS allows the production of porous structures with higher porosity (>95%) comparing with other existing techniques, thus facilitating vascularization and tissue ingrowth.

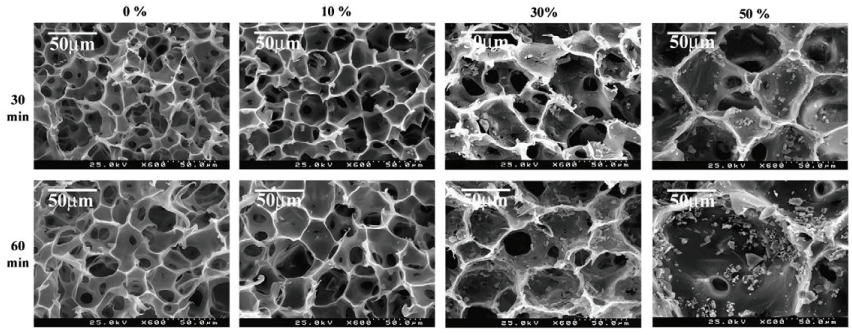

Figure 1. Scanning electron microscopy photographs of PLLA scaffolds with varying bioactive glass contents (0, 10, 30 and 50 wt.%) and different phase separation times (30 and 60 minutes).

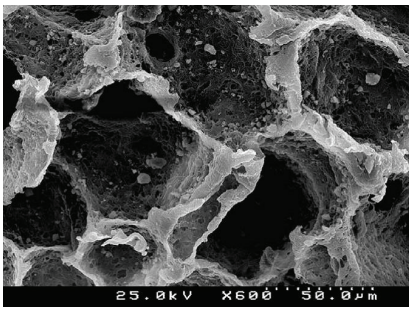

Figure 2. Scanning electron microscopy photograph of the composite scaffold PLLA/50 wt.% crystallized bioactive glass (phase separation of 60 minutes).

Its handicap lies on the reduced pore size that can be achieved maintaining a reasonnable interconnectivity of the pores, normally overpast by the use of toxic surfactants.

In this work, we developed a modified TIPS process to produce PLLA scaffolds with designed pore size without the use of surfactants, in which the bioactive phase itself, a surface active glass from the $3CaO\text{-}P_2O_5\text{-}MgO\text{-}SiO_2$ system produced in our laboratory, is used as a pore growth inductor. The bioactive glass is introduced in the polymer solution and is allowed to dissolve for a certain time to vary the thermodynamic state of the solution prior to the phase separation. As a consequence of the dissolution of the bioactive phase, ion–dipole interactions between alkaline earth ions leached from the bioglass surface and water molecules will increase the surface tension of the water-rich phase and, subsequently, increase the interfacial tension between the polymer-rich and the polymer-poor phases, resulting in a large pore size in the composite scaffold matrix. Due to an increasing concentration of leached ions in the system, enlargement of the pores becomes more pronounced as the bioglass content increases (Fig.1). This result is of particular relevance, since by varying parameters such as the amount of bioactive glass, its solubility and time for its dissolution, it is possible to design the pore morphology (Fig.2)[1]. We believe that this approach can be broaden to other polymers and other bioactive phases namely within the family of calcium phosphates.

[1] Department of Ceramics and Glass Engineering, CICECO, University of Aveiro, 3810-193 Aveiro, Portugal

Reference paper

[1] Barroca N, Daniel-da-Silva AL, Vilarinho PM, Fernandes MHV, "Tailoring the morphology of high molecular weight PLLA scaffolds through bioglass addition". *Acta Biomater* **2010,** 6, 3611-3620

[2] "Método de Preparação de Suportes Porosos Compósitos de Base Polimérica para Aplicação em Engenharia de Tecidos", Maria Helena V Fernandes, Nathalie Barroca, Ana Luísa Silva, Paula Maria Vilarinho, Pedido de Patente de Invenção National nº 104 136 de 22 de Junho de 2008.

NOVEL AND SIMPLE DISILICATE GLASS-CERAMIC COMPOSITIONS FOR DENTAL CROWN APPLICATIONS

Fernandes HR[1], Tulyaganov DU[1], Goel A[1], Ferreira JMF[1]

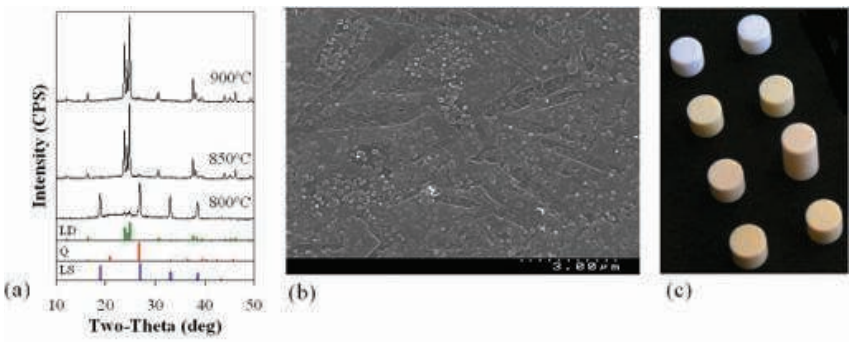

Figure 1. (a). X-ray patterns LD-GCs prepared from glass powder compacts and sintered at 800, 850 and 900ºC (1 h) (LS, Lithium silicate (Li_2SiO_3); LD, Lithium disilicate ($Li_2Si_2O_5$); Q, Quartz (SiO_2)]; **(b)** SEM of LD-GCs sintered at 900 ºC (1 h); **(c)** Photo of LD-GCs ingots prepared from glass powder compacts and sintered at 900 ºC (1 h).

Lithium disilicate (LD) glass-ceramics (GC) in the $Li_2O\text{-}SiO_2$ system feature outstanding mechanical and aesthetic properties, being well suited for dental crown applications. The Ivoclar-Vivadent company has thoroughly developed the IPS Empress®2 material, a multi-component LD-GC system with a wide compositional range of (in wt.%) 57-80 SiO_2, 11-19 Li_2O, 0-13 K_2O, 0-5 Al_2O_3, 0-8 ZnO, 0.1-6 La_2O_3, and 0.1-11 P_2O_5. However, the coefficient of thermal expansion (CTE) of IPS Empress®2 is too high ($100\text{-}110\times10^{-7}$ K^{-1}). Therefore, new LD-GCs featuring CTE values lower than that of IPS Empress®2 without compromising the mechanical and aesthetic properties are needed. This will allow improving the thermal shock resistance of LD-GCs used in dental applications. On the other hand, it would be interesting if the desired properties could be achieved from simpler compositions without changing the production technology.

Attempting to cover all the above mentioned short comings of existing LD-GCs, we have formulated simple and nucleating agent-free glass compositions in the system $SiO_2\text{–}Al_2O_3\text{–}K_2O\text{–}Li_2O$ comprising equimolar amounts of Al_2O_3 and K_2O added to the binary $SiO_2\text{–}Li_2O$ system, which are prone to volume nucleation and crystallisation thus, resulting in the formation of fine $Li_2Si_2O_5$ (LD) crystals within the temperature interval of 650–900 ºC (Fig.1a). We have demonstrated that Al_2O_3 and K_2O also improve the chemical durability of the $Li_2O\text{–}SiO_2$ glasses.

In context of monolithic bulk glasses, liquid–liquid phase separation occurred in all investigated compositions as illustrated by the nanosize droplets precipitated in the glassy matrixes. Al^{3+} acting as network former decreases the volume fraction and mean diameter of droplet phase resulting in transparent glasses. Glass powder compacts sintered at 900 ºC (Fig.1b&c) resulted in well densified fine-grained LD-GCs with enhanced mechanical properties (bending strength = 224 ± 4 MPa) and $CTE_{200\text{-}500\ °C} = 86.9\times10^{-7}$ K^{-1} featured almost monomineral LD composition.

Small additions of Al_2O_3 and K_2O to pure $Li_2O\text{–}SiO_2$ system also enhanced

the densification behaviour, the ultimate mechanical strength and the thermo-physical properties. Moreover, a careful selection Al_2O_3 and K_2O contents promotes internal nucleation and moderates crystal growth.

[1] Department of Ceramics and Glass Engineering, CICECO, University of Aveiro, 3810-193 Aveiro, Portugal

Research financial support

This work was financed by the FCT.

Reference paper

[1] Fernandes HR, Tulyaganov DU, Goel A, Ferreira JMF, "Effect of Al_2O_3 and K_2O content on structure, properties and devitrification of glasses in the Li_2O–SiO_2 system", *Journal of The European Ceramic Society* **2010**, 30, 2017-2030.

NOVEL OSTEOGENIC ION-SUBSTITUTED BRUSHITE CEMENTS FOR CLINICAL APPLICATIONS

Pina S[1], Vieira SI[2], Rego P[3], Torres PMC[1], da Cruz e Silva OAB[2], da Cruz e Silva EF[4], Ferreira JMF[1]

Calcium phosphate cements (CPC) have unique characteristics for bone substitution compared with other biomaterials. Their excellence relies on good biocompatibility, excellent bioactivity, self-setting characteristic, low setting temperature, adequate stiffness, and easy shaping for any complicated geometry. Brushite-based bone cements are well tolerated *in vivo* by the hard and soft tissues and its resorption rate closely matches that of new bone formation.

Trace amounts of Zinc (Zn) and strontium (Sr) elements proved to exert stimulatory outcomes on bone formation, having a direct specific proliferative effect on osteoblasts. Therefore, in order to beneficiate from these important features, the novel brushite cements were doped with Zn (ZnCPC), and with a mixture of Zn+Sr (ZnSrCPC) and their *in vitro* and *in vivo* performances were investigated in MC3T3-E1 osteoblastic-like cell cultures and after injecting the bone cement pastes into trabecular bone cylindrical defects in pigs. It was observed that the presence of Zn and Sr in brushite-forming cements stimulated pre-osteoblastic proliferation and osteoblastic maturation. Indeed, MC3T3-E1 cells exposed to the powdered cements had increased proliferative rates and higher adhesiveness capacity, in comparison to control cells. Furthermore, they exhibited higher alkaline phosphatase (ALP) activity and increased Type-I collagen secretion and fibre deposition into the extracellular matrix (Fig.1).

The *in vivo* studies proved that Zn and Sr are good inductors of osteoprogenitor cell proliferation and differentiation without any evidence of adverse foreign body reactions (Fig.2). Histological and histomorphometrical analyses revealed that the novel cements exhibited a higher rate of bone regeneration and penetration into the implant in comparison to commercial bone cement (Norian SRS®) (Fig.3).

These overall results proved that the novel brushite-forming Zn, Sr-substituted bone cements besides being biocom-

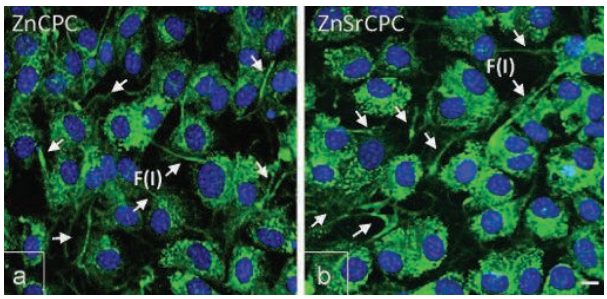

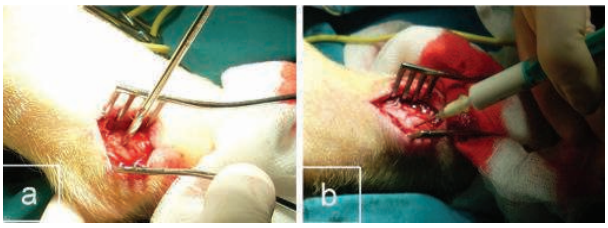

Figures 1. (left) Confocal microscopy analysis of intra and extracellular Type-I collagen (green fluorescence) for (a) ZnCPC and (b) ZnSrCPC). Arrowheads: intracellular granule-like densities. F/arrows: extracellular cell associated collagen fibres.

Figures 2. (bottom left) Surgery procedure: (a) drilling of defect and (b) cement injection.

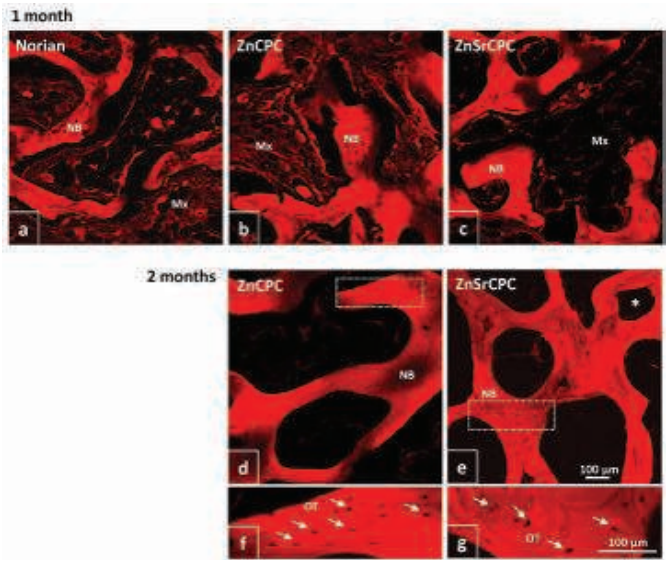

Figures 3. (bottom right) Confocal fluorescent micrographs of histological H&E stained sections, showing the tissue osteogenic response to Norian SRS® (a), ZnCPC (b,d,f) and ZnSrCPC (c,e,g) cements after 1 (a-c) and 2 (d-g) months of implantation. NB: new bone; Mx: protein matrix; arrows/OT in g,h: osteocytes.

patible, bioresorbable and osteoconductive, they beneficiate from the specific proliferative effects of Sr and Zn on proliferation and differentiation of osteoblasts and from their positive roles in mitigating osteoporosis, being an interesting promise for applications in dentistry, orthopaedics and trauma surgeries such as for filling bone defects.

[1] Department of Ceramics and Glass Engineering, CICECO, University of Aveiro, 3810-193 Aveiro, Portugal

[2]University of Aveiro, Health Sciences Dept., Centro de Biologia Celular, 3810-193 Aveiro, Portugal.

[3]University of Lisbon, Orthopaedic Clinic, Medicine Faculty, 1600-190 Lisbon, Portugal.

[4]University of Aveiro, Dept. of Biology, Centro de Biologia Celular, 3810-193 Aveiro, Portugal.

Funding

This work has been funded by FCT (Portugal).

Reference paper

[1] Pina S, Vieira SI, Rego P, Torres PMC, da Cruz e Silva OAB, da Cruz da Silva EF, Ferreira JMF."Biological responses of brushite-forming Zn- and ZnSr- substituted beta-tricalcium phosphate bone cements". *Eur Cell Mater* **2010**, 20, 162-177.

ALKALI-FREE HIGHLY BIOACTIVE GLASSES FOR BONE TISSUE ENGINEERING

Goel A[1], Ferreira JMF[1]

Bioactive glasses and glass-ceramics are a class of biomaterials which elicit a special response on their surface when in contact with biological fluids, leading to strong bonding to living tissues. In the field of bone tissue engineering, bioactivity is defined as the ability of the material to bond to bone tissue *via* the formation of a bone-like hydroxyapatite (HA) layer on its surface. Due to a number of attractive properties for use in tissue engineering and regeneration, for example: enhanced angiogenesis and up-regulation of specific genes that control the osteoblast cell cycle, there is increasing effort in the use of bioactive glasses and glass-ceramics in tissue engineering applications.

Since the discovery of 45S5 Bioglass®, many artificial biomaterials based on, or inspired by, Hench's glasses have been developed and successfully employed in clinical applications for repairing and replacing parts of the human body. Although, the use of 45S5 glass in numerous clinical programs has exhibited favourable healing capability, however, one of the main problems associated with this glass is its high dissolution rate mainly owing to its high alkali content. This causes fast resorption that may negatively affect the balance of natural bone remodelation and in particular the physiologically vital process of angiogenesis, thus leading to gap formation between the tissue and the implant material. Similarly, most of the bioactive glass compositions investigated so far contain significant amount of alkali oxides (Na_2O, K_2O). The incorporation of alkali oxides in bioactive glass although is advantageous for the production of bioactive glass, as they reduce the melting temperature of the glass but the presence of alkali metals, sodium and potassium, in bioactive glass can reduce the usefulness of the glass *in vivo*. In particular, the bioactive glasses having high alkali metal content are susceptible to water uptake by osmosis resulting in swelling and cracking of polymer matrix embedding them in composites and may, in case of degradable polymer composites, exhibit increased levels of degradation. Such, bioactive glasses may also be unsuitable for use as coatings for metal prosthetics due to increased coefficient of thermal expansion owing to the presence of alkali metals. Furthermore, high levels of alkali cations degrade the sintering ability of bioactive glasses by increasing the crystallization tendency of glass, thus, rendering them unfit for use as bioactive porous scaffolds or porous coatings. For example, in case of 45S5 Bioglass®, owing to its poor sintering ability, there have been problems with the manufacture of highly porous scaffolds possessing good mechanical strength from its glass powders as it needs extensive densification to strengthen the solid phase, *i.e.* the struts in the foam-like structure, which would otherwise be made of loosely bonded particles and thus be too fragile to handle. Also, it has been noticed that crystallization of 45S5 Bioglass® turns this glass into an inert material.

In a pursuit to find a feasible solution for the above mentioned long standing problem with bioactive glasses and glass-ceramics, we have synthesized

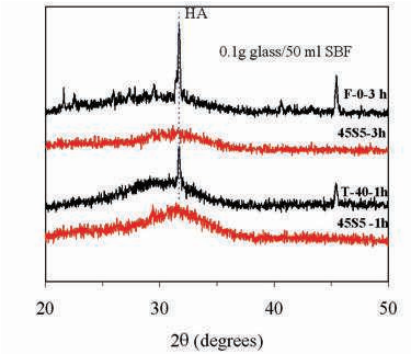

Figure 1. A comparison between in vitro bioactivity of some of the investigated glasses and the 45S5 Bioglass®.

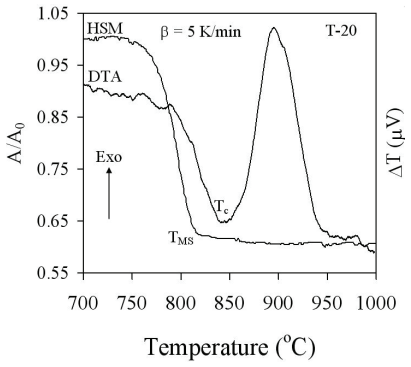

Figure 2. Sintering and crystallization behaviour of an investigated bioactive glass (T-20).

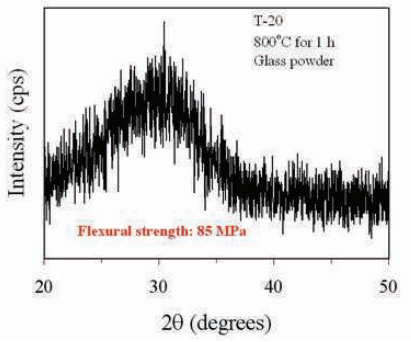

Figure 3. Well sintered, mechanically strong but amorphous glass powder compact obtained from glass (T-20).

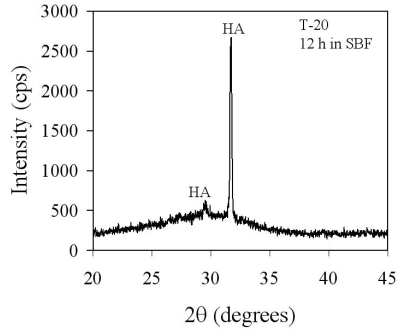

Figure 4. Extensive HA formation on the surface of glass (T-20) after 12 h of immersion in SBF.

a series of alkali-free phosphosilicate glasses in the system CaO-MgO-P_2O_5-SiO_2-CaF_2. The preliminary results on the designed glasses depict high rate of bioactivity and good sintering ability, thus making them potential candidates for applications in bone tissue engineering. Some of the investigated glass compositions exhibit formation of hydroxyapatite on their surface (which is the marker of bioactivity) after 1 h of immersion in simulated body fluid (SBF) (Fig.1) which is comparatively faster than the well known 45S5 Bioglass®. Further, chemical degradation of these glasses (measured by weight loss in Tris-HCl in accordance with ISO 10993-14) is significantly lower in comparison 45S5 Bioglass®. Also, in case of most of the glass compositions, sintering precedes crystallization (Fig.2), thus resulting in dense but amorphous or partially crystalline glass powder compacts (Fig.3) with three point flexural strength varying between 80-150 MPa. The sintered glass powder compacts exhibit the formation of hydroxyapatite layer on their surface in less than 12 h of their immersion in SBF (Fig.4). Therefore, they are ideal as scaffolds in tissue engineering applications. If their performance in cell proliferation *in vitro* and their bone bonding ability *in vivo* will be at the same level as we can expect, this will be a significant breakthrough in the field of biomaterials.

[1] Department of Ceramics and Glass Engineering, CICECO, University of Aveiro, 3810-193 Aveiro, Portugal

Funding

This work was funded by FCT (Portugal) under the post-doc fellowship grant Reference: SFRH/BPD/65901/2009, and by the Department of Ceramics and Glass Engineering, CICECO, University of Aveiro.

Reference paper

[1] Kansal I, Tulyaganov DU, Goel A, Pascual MJ, Ferreira JMF, "Structure and thermal behaviour of diopside-fluorapatite-wollastonite based glasses and glass-ceramics", *Acta Biomater.* **2010,** 6, 4380-4388.

[2] Agathopoulos S, Tulyaganov DU, Ventura JMG, Kannan S, Karakassides MA, Ferreira JMF, "Formation of hydroxyapatite onto glasses of the CaO–MgO–SiO_2 system with B_2O_3, Na_2O, CaF_2 and P_2O_5 additives", Biomater. **2006**, *27*, 1832-1840.

[3] Stan GE, Pina S, Tulyaganov DU, Ferreira JMF, Pasuk I, Morosanu CO, "Biomineralization capability of adherent bio-glass films prepared by magnetron sputtering" , *J. Mater. Sci. Mater. Med.* **2010,** 21, 1047-1055.

Methods and Techniques

SMALL PROBES FOR BIG CHALLENGES

Lopes AML[1,2,3], Araújo JP[1], Amaral VS[2], Correia JG[3,4], Tomioka Y[5], Tokura Y[6]

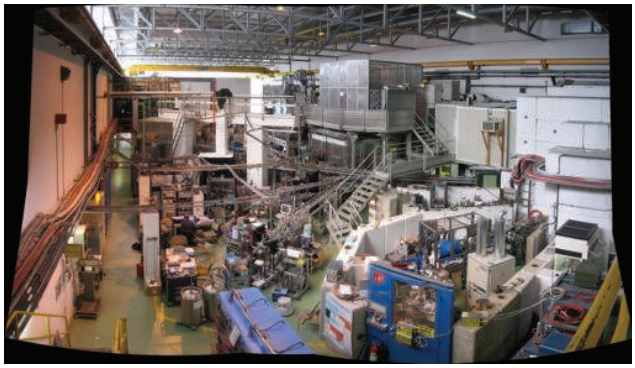

Figure 1. ISOLDE-CERN hall where radioactive ion beams are collected and implantations are performed.

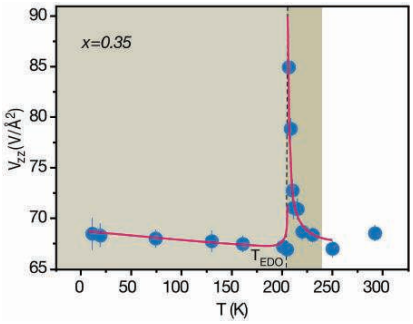

Figure 2. Temperature dependence of the principal component Vzz of the EFG tensor for sample x=0,35 across the C/O transition. The thick line indicates the contribution of local electric polarization.

One of the grand needs of modern research on materials is the possibility to "see and feel" at the nanoscale, to determine the positions and function of all the elements (atoms, electrons, electric and magnetic fields) in a nanoscale solid or structure. Results on the understanding of oxide materials through the use of radioactive ion probe hyperfine techniques with site or element specificity are here briefly described.

Strongly correlated electron oxide materials present a vast variety of physical behaviours. Magnetic, electronic and lattice interactions lead to cooperative phenomena like High-Tc superconductivity, colossal magnetoresistance or ferroelectricity, which are topics of advanced research. The coupling of magnetic and dielectric degrees of freedom has aroused a further interest on multiferroic oxides, on the quest to implement new spintronic device design architectures with magnetoelectric control. In manganite oxides mixed valence of Mn^{3+} and Mn^{4+} ions (due to doping) controls the occurrence of coupled structural, magnetic or charge and orbital (C/O) ordering mechanisms that underlie colossal resistive changes induced by magnetic field, pressure or radiation, or ferroelectricity driven by spatial inversion symmetry breaking due to magnetic or C/O ordering. These phenomena lead to intrinsic and ubiquitous phase separation phenomena and nanoscale inhomogeneities whose spatial extent is still poorly understood, requiring an adequate description down to local atomic length scales: structure of clusters, polaron dynamics, polar distortions and nanoscale ferroelectricity.

Radioactive ions beams are produced at the ISOLDE laboratory at CERN, Geneva and implanted on samples in depths up to 100 nm (Fig. F1), giving access to techniques such as perturbed angular correlations (PAC) which analyses the time/angular dependence of photon pairs emitted from the probe. This provides a sensitive method to detect hyperfine magnetic fields (MHF), local structural distortions through the electric field gradient (EFG) and their fluctuations occurring during PAC time scale, from specific locations using different ions. The analysis of the data requires the study the localization of implanted ions. This is done using the emission channelling (EC) technique: electrons emitted by an implanted probe are collected by a 2D detector providing an image of the lattice.

Such capabilities can be illustrated by recent studies, using ^{111m}Cd PAC in the $Pr_{1-x}Ca_xMnO_3$ manganites. The sensitivity of EFG to delocalized electrons and the charge asymmetry from the lattice ion cores enabled to find large effects both as a function of x and temperature across the C/O ordering transition. Particular features in the EFG that signal the presence of an electrical polarization at local scale, with critical behaviour at the transition, were observed for the first time. Figure F2 shows the principal component Vzz of the EFG tensor for x=0,35 clearly displaying the fluctuations of EFG and the critical temperature for the electric order (TEDO). At lower temperatures, the contribution of the spontaneous polarization gives mild temperature dependence. This predicted polarization had until now been undisclosed in this or similar systems. It is particularly relevant since it results from a new mechanism, where C/O ordering breaks the inversion symmetry, leading to multiferroic behaviour. Our study of the magnetoelectric-structural couplings and short-range order effects using PAC includes other manganite systems and oxides (chromites, nickelates) and magnetic semiconductors (MnAs) and is complemented by detailed calculations using ab-initio density functional theory for the development of reliable theoretical models and multifunctionalities control. Furthermore, a new line of radioactive local probing was initiated with research on the coordination mechanisms of heavy metal ions to functionalized magnetic nanoparticles.

Work at ISOLDE-CERN (http://isolde.web.cern.ch/ISOLDE/) is performed within international collaborations led by Portuguese members and is also supported by Projects from EU and FCT.

[1] Departamento de Física and IN-IFIMUP, Universidade do Porto, 4169-007 Porto

[2] Department of Physics, CICECO, University of Aveiro, 3810-193 Aveiro, Portugal

[3] CERN EP, CH 1211 Geneva 23, Switzerland

[4] Instituto Tecnológico Nuclear, E.N. 10, 2686-953 Sacavém

[5] CERC, National Institute of Advanced Industrial Science and Technology, Tsukuba, Ibaraki 305-8562, Japan

[6] Department of Applied Physics, University of Tokyo, Tokyo, 113-8656, Japan

Reference paper

[1] Lopes AML, Araújo JP, Amaral VS, Correia JG, Tomioka Y, Tokura Y. "New phase transition in Pr1-xCaxMn03 system: evidence for electrical polarization in charge ordered manganites" *Physical Review Letters*/ **2008**,100,155702

HIGH-RESOLUTION ^{1}H NMR TECHNIQUES FOR THE STUDY OF SOLIDS

Mafra L[1], Siegel R[1], Rocha J[1]

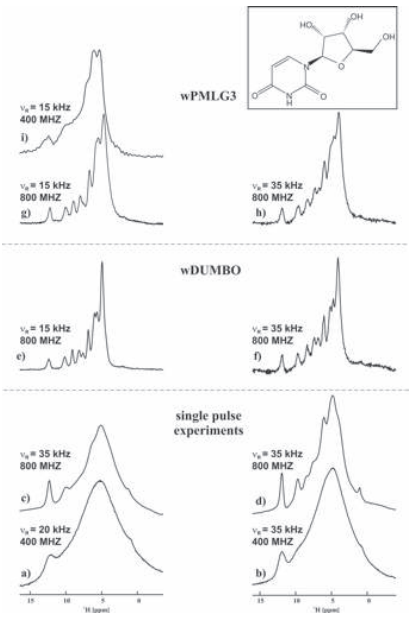

Figure 1. ^{1}H NMR spectra of uridine recorded employing (a–d) ^{1}H single-pulse excitation (SPE); wDUMBO decoupling using (e) ν_1 = 112 kHz, (f) ν_1 = 146 kHz; wPMLG3 decoupling using (g) ν_1 = 112 kHz, (h) ν_1 = 146 kHz and (i) ν_1 = 70 kHz. Recycle delay: 25 s. The experimental scaling factors were (e) λ_{exp} = 0.61; (f) λ_{exp} = 0.61; (g) λ_{exp} = 0.65; (h) λ_{exp} = 0.73 and (i) λ_{exp} = 0.69.

^{1}H NMR spectroscopy is an extremely powerful and now routine tool for studying molecular structure and dynamics in liquids. In contrast, investigating solids by ^{1}H NMR still presents considerable challenges because the strong ^{1}H–^{1}H dipolar coupling (dominant interaction in rigid solids) homogeneously broadens the proton resonances up to a few tens of kHz. The ^{1}H homonuclear dipolar interaction may be partially averaged out using NMR techniques developed since the sixties, which rely on two strategies: (i) periodic radio-frequency (rf) multiple-pulse sequences, acting on the spin part; (ii) magic-angle spinning (MAS) to average the spatial part. Both come together in the so-called Combined Rotation and Multiple-Pulse Spectroscopy (CRAMPS). Recent technological developments in NMR probes (MAS up to 70 kHz) and spectrometer consoles (fast electronics) contributed to a considerable improvement in the quality and resolution of ^{1}H NMR spectra. Although much of the NMR community considered that ^{1}H decoupling would not work at very fast MAS rates, we have shown recently that DUMBO and PMLG ^{1}H homonuclear decoupling techniques perform well at MAS rates up to 35 kHz and magnetic fields of 9.4 and 18.8 T.[1] As an example, Figure 1 shows the ^{1}H spectra of uridine, a biological solid[1].

Double-quantum (DQ) homonuclear recoupling MAS NMR methods are among the most useful techniques available to chemists. Such techniques encode important structural information by restoring the through-space dipole–dipole couplings, such as distance information between interacting nuclei. They also allow estimating torsional angles, filtering signals of mobile or isolated spin species and provide a route to the excitation of higher coherence orders. In addition, the availability of CRAMPS decoupling techniques capable of performing well at very fast MAS, opens up new perspectives in ^{1}H NMR spectroscopy, providing improved resolution in 2D ^{1}H-^{1}H DQ–SQ correlation experiments. Most DQ ^{1}H recoupling techniques are mainly confined to moderate MAS rates (10–15 kHz) because the recoupling part of the sequence requires very large rf field strengths. We have recently shown that RN_n^ν Rrotor-synchronised sequences allow efficient ^{1}H–^{1}H DQ recoupling at MAS rates up to 67 kHz, thus overcoming the difficulties of ob-

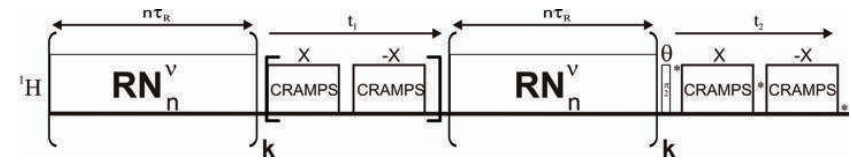

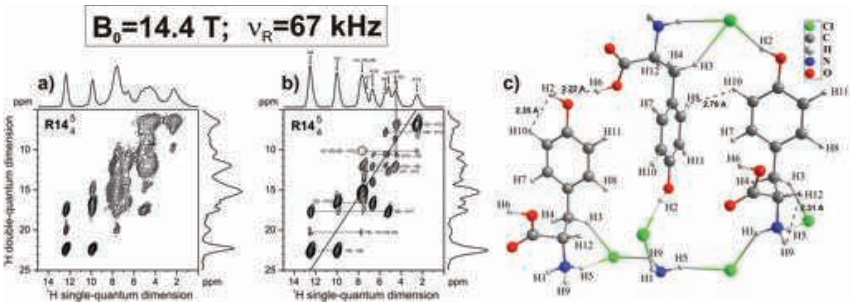

Figure 2. Pulse sequence for 2D ^{1}H-^{1}H DQ homonuclear recoupling Rexperiments. $R12_2^5$ and $R14_4^5$ symmetries are used for DQ excitation/reconversion (k=1). Here, we use the CRAMPS decoupling scheme DUMBO during the t_1 and t_2 evolutions. The flip angle of the read pulse is θ=90°. RN_n^ν recoupling blocks are of the form $[R_\phi R'_{-\phi}]^{N/2}$ where $\phi = \nu\frac{\pi}{N}$ (the rf phase in degrees) and the basic element R is a 180° flip angle. Therefore, for sequences employing a complete $R12_2^5$ recoupling six pairs of building blocks of the type $[R_{.75^\circ}R'_{-.75^\circ}]^6$ were employed, which gives a total of 12 R pulses spanning over two rotor periods during the excitation and reconversion blocks because n=2. In the same way, $R14_4^5$ recoupling employs a $[R_{.75^\circ}R'_{64.29^\circ}]^7$ building block spanning over four rotor periods (n=4). The nutation frequency (ν_1) for any of the RN sequences is detailed in Table 1 and may be calculated using the expression ν_1=(N/2n)*ν_R.

Figure 3. 2D ^{1}H-^{1}H DQ-SQ spectra of Tyr.HCl, recorded at MAS 67 kHz using ν_1=117 kHz and Larmor frequency of 600 MHz (B_0=14.1 T, Bruker wide-bore NMR spectrometer), using the symmetry $R14_4^5$ for ^{1}H-^{1}H recoupling. a) No CRAMPS used, b) DUMBO decoupling in both dimensions (DUMBO shape pulse length = 15 μs; Decoupling power=198 kHz), c) Schematic representation of the solid-state structure of Tyr.HCl.

taining high-quality ^{1}H spectra at fast MAS rates. Although RN_n^v sequences have already been used to recouple ^{13}C–^{13}C dipolar interactions at MAS rates below 22 kHz, our contribution is the first work showing the capability to reintroduce ^{1}H–^{1}H dipolar couplings at ultra-fast spinning rates (67 kHz) [2]. The method was illustrated on two solids of biological interest, amino-acid tyrosine hydrochloride (Tyr·HCl) and tri-peptide glutathione in its reduced form (GSH), at magnetic fields of 14.1 and 18.8 T. ^{1}H homonuclear decoupling (DUMBO) is employed in the DQ (t_1) and SQ (t_2) dimensions using the pulse sequence depicted in Figure 2. The achieved 2D high-resolution ^{1}H DQ-SQ homonuclear correlation spectrum of Tyr·HCl combining such ^{1}H decoupling and ultra-fast MAS shows an outstanding resolution enhancement, allowing its full assignment and the distinction between intra- and intermolecular ^{1}H proximities (Fig.3) [2].

[1] Department of Chemistry, University of Aveiro, CICECO, 3810-193 Aveiro, Portugal

Funding

We thank FCT, FEDER and POCTI for financial support and post-doc grant (RS). The Portuguese NMR Network is acknowledged for granting access to the 18.8 T NMR Bruker spectrometer at ITQB. We are also very thankful to Bruker-Biospin Germany (Rheinstetten) and France (Wissembourg) for allowing us to access their installations and use the ultra-fast MAS probe.

Reference paper

[1] Mafra L, Coelho C, Siegel R, Rocha J, "Assessing the performance of windowed H-1 CRAMPS methods, on biological solids, at high-field and MAS up to 35 kHz", *Journal of Magnetic Resonance* **2009**, 197, 20-27

[2] Mafra L, Siegel R, Fernandez C, Schneider D, Aussenac F, Rocha J, High-resolution H-1 homonuclear dipolar recoupling NMR spectra of biological solids at MAS rates up to 67 kHz, *Journal of Magnetic Resonance* **2009**, 199, 111-114

SOLID-CONTACT ION-SELECTIVE MICROELECTRODES FOR LOCALIZED POTENTIOMETRIC MEASUREMENTS

Lamaka S[1], Taryba M[1], Zheludkevich ML[1], Ferreira MGS[1]

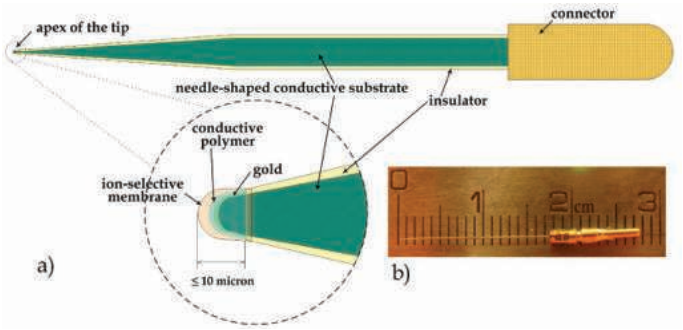

Figure 1. (top) a) A schematic drawing and **b)** an optical image of the solid-contact ion-selective micro electrode.

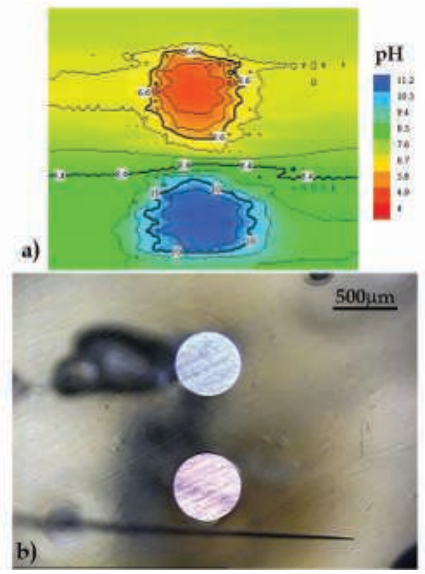

Figure 2. (right) a) pH mapping over the surface of coupled Al and Cu wires embedded into non-conductive holder; **b)** optical microphoto.

Information on the spatial distribution of the ionic species consumed or released on the active sites of various solid/liquid interfaces is of primary importance for understanding many chemical and biological processes. Examples of such processes can be found in biology where living cells exchange ionic species with surrounding liquid media and in corrosion science where localized electrochemical processes occur on the metallic surfaces.

The concentration of different ionic species can be assessed by using ion-selective electrodes (ISEs). Traditional glass-capillary micro electrodes widely used for localised potentiometric measurements suffer from several disadvantages: spontaneous leakage of liquid membrane out of capillary, life time limited to one day at the most and fragility of glass capillary. As in the case of macro ISE, the main characteristics of glass capillary microelectrodes, namely detection limit and selectivity are limited by the flux of primary ions from the ion-selective membrane and inner filling solution that contaminates the near boundary layer of solution which is in contact with the ion-selective membrane. The alternative for liquid-membrane ISE can be solid-contact electrodes. Solid-contact electrodes contain neither liquid membrane nor inner filling solution and represent an alternative to liquid-membrane electrodes.

The novel solid-contact ionophore-based ion-selective microelectrodes for localised scanning potentiometric measurements were recently developed in our group [1]. The design, fabrication procedure, properties and application of solid state micro-ISE are patented. A solid-contact microelectrode is based on an insulated needle-shaped metallic wire

with open 5 micron long apex of the tip plated with gold (Fig. 1). Ion-to-electron transducer that enables transition from ionic to electronic conductivity is made of poly-3-octylthiophene (POT) and placed between ion-selective membrane and the metallic tip. Ion-selective polyvinyl chloride–based (PVC) membrane is deposited atop of the layer of conductive polymer. The diameter of the ion-sensitive part of the electrode is equal or less than 10 micron allowing high spatial resolution. pH and Mg^{2+} -selective microelectrodes of presented design were developed and tested showing high stability, low detection limits and fast response time which are essential for the practical application of such electrodes for localised scanning potentiometric measurements (Fig. 2). Further miniaturization of solid-contact microelectrodes is possible and is considered for future work. Moreover we believe that the life time of the microelectrodes can be extended by using methacrylate-based membrane matrix that lowers the ionic mobility and prevents water penetration through the ion-selective membrane.

[1] Department of Ceramics and Glass Engineering, CICECO, University of Aveiro, 3810-193 Aveiro, Portugal

Funding

This work has been funded by FCT Portugal (PTDC/CTM/65632/2006 and REDE/1509/RME/2005).

Reference paper

[1] Lamaka SV, Taryba MG, Zheludkevich ML, Ferreira MGS, *Electroanalysis*, **2009,** 21, 2447

[2] Patent (WO/2010/076717) ION-SELECTIVE SOLID CONTACT MICROELECTRODE AND ITS PRODUCTION METHOD, 08.07.2010, S.V. Lamaka, M.L. Zheludkevich, M.G.S. Ferreira.

ULTRAMICROELECTRODES MADE OF BORON DOPED NANOCRYSTALLINE DIAMOND

Silva EL[1], Zheludkevich ML[1], Oliveira FJ[1], Silva RF[1]

Usually known by its extreme mechanical properties, CVD diamond becomes a conducting material when heavily doped by boron ([B] >1x10^{20} atoms/cm^3). Potential applications for this kind of coating are small-size electrodes in analytical chemistry (e.g., miniature electrochemical sensors for nucleic acids), biochemistry (in vivo measurements on biological objects, like serotonin secretion in the brain associated to Parkinson's disease) and in scanning electrochemical microscopy (e.g., imaging redox centers present in thin solid films). The superior electrochemical performance of CVD diamond is enabled by properties such as low and stable background current over a wide potential range, good responsiveness for many redox analytes without pretreatment, very good microstructural stability at extreme cathodic and anodic potentials and high current densities, and also resistance to fouling due to the weak adsorption of polar analytes on its non-polar hydrogen-terminated surface[1]. Although B-doped diamond macroelectrodes show all these properties, some advantages arise when the electrode scale is reduced to produce the so called ultramicroelectrodes (UMEs), which have at least one dimension <25 µm. UMEs allow a very efficient hemispherical diffusion thus enabling a high signal-to-noise ratio and the possibility to work in high resistive media, due to the limited ohmic drop within a small area close to the electrode[1].

For the UMEs preparation, tungsten tips with ap. 50nm of curvature radius were obtained by electrochemicaly etching

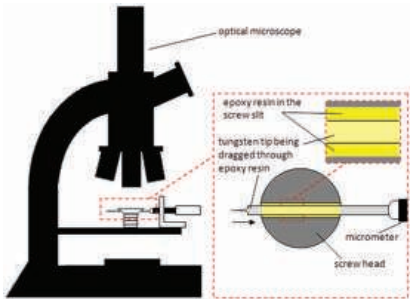

Figure 2. Homemade UME insulating device.[2]

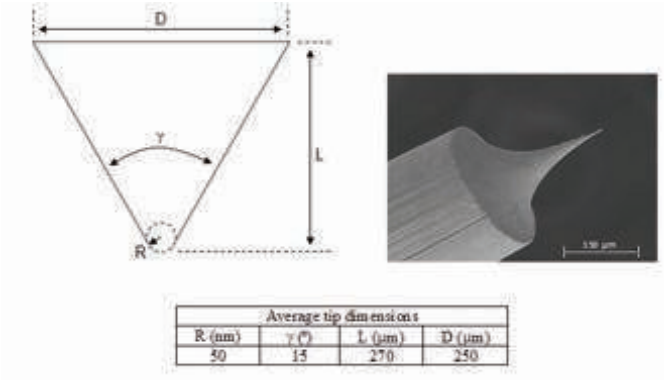

Figure 1. Electrochemically sharpened tungsten tips.[2]

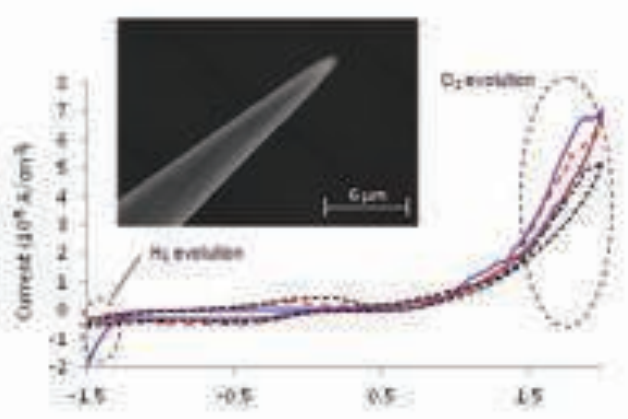

Figure 3. Cyclic voltammograms of a B-NCD coated tip performed in a NaCl 0.05M solution.[2]

tungsten filaments in a 3M NaOH solution[2]. A proper adjustment of the sharpening factors allows the production of nanosized and well shaped tips as shown in Figure 1. Afterwards, the tips were coated with boron doped nanocrystalline diamond (B-NCD) by the hot filament chemical vapour deposition (HFCVD) technique. B-NCD nonporous very thin films (<100nm) ensure two important features at once: the smallest possible size for the UME and the necessary insulation that avoids the analytes from reacting with the substrate material. The insulation of the B-NCD tips was carried out using epoxy resin which covered the whole body of the tip leaving just the final extremity, with the aid of an optical microscope coupled to a manual micrometric controlling device (Fig.2).

The electrochemical response of the UMEs was tested by cyclic voltammetry in a 0.05 M NaCl solution. When submitted to polarization, the cathodic current, due to hydrogen evolution, increases for a potential greater than -1.25V and the anodic current starts to increase for potentials greater than 1V due to oxygen evolution (Fig.3). The cyclic voltammetry for this sample revealed good chemical stability on the first sweep and a potential window of 2.25V. On the following sweeps, a possible insulation failure enabled the electrolyte to react with the tungsten substrate or residual carbon sp^2 phases on the diamond surface.

[1] Department of Ceramics and Glass Engineering, CICECO, University of Aveiro, 3810-193 Aveiro, Portugal

Funding

This work has been funded by FCT Portugal (grant SFRH/BD/61675/2009).

Reference paper

[1] Foord JS, Hu J, Holt KB, Phys. Status Solidi A-Appl. Mater. 204 (2007) 2940.

[2] Silva EL, Neto MA, Fernandes AJS, Bastos AC, Silva RF, Zheludkevich ML, Oliveira FJ, Diam. Relat. Mater. 19 (2010) 1330.

HYDROGEN BOND DYNAMICS OF C–H•••O INTERACTIONS FROM INELASTIC NEUTRON SCATTERING

Ribeiro-Claro PJA[1], Nolasco MM[1], Vaz PD[2], Gil F[3], Tomkinson J[4]

In the last few years, the role of C–H···O hydrogen bonds in crystal engineering and molecular recognition processes has aroused considerable interest. The small binding energy of this interaction, when compared with conventional O–H···O hydrogen bonds, seems to be overcome by the almost ubiquity of C–H bonds and efficient cooperativity effects. One of the open questions concerning this interaction refers to the potential energy curve of the CH···O contact, predicted to be weaker than the conventional OH···O one, but with larger angular freedom, with longer and smoother cut-off distance, but with unexpectedly high H···O stretching frequency (>50 cm^{-1}).

Vibrational spectroscopy presents unique capabilities to assess the potential curve of hydrogen bond contacts, such as weak CH···O bonds, through the direct observation of the motions of the H-atom. However, the detection of vibrational modes involving the H-atom in CH···O contacts is hampered by their weak intensity in both Raman and IR spectra, and the experimental difficulties of the low wavenumber region.

Inelastic Neutron Scattering (INS) spectroscopy turns out to be the unique solution to answer this challenge, overcoming far-IR and Raman limitations, since the large cross-section of the hydrogen nucleus turns this technique particularly sensitive to the motions involving H atoms – in particular, the antitranslational νH···O stretching motion, directly related with the shape of the potential energy curve of the hydrogen bond.

This is clearly illustrated in the case of the chloroform···acetone [Cl_3CH···O=$C(CH_3)_2$, Fig.1] association – historically related with the first experimental evidence of C–H···O hydrogen bonding – , which remained a challenge for vibrational spectroscopists[1]. The "INS view" of the chloroform molecule (Fig.2) allows the detection of the H-atom motions and the determination of the potential energy function profile for the C–H···O hydrogen bonds in the mixture.

The INS spectra of the acetone-chloroform mixtures show strong evidences of the presence of C–H···O hydrogen-bonded complexes. Comparison between the INS spectra of pure samples and their binary mixtures reveals the presence of new bands at *ca.* 82 cm^{-1}, 130 cm^{-1} and 170 cm^{-1}. The new band

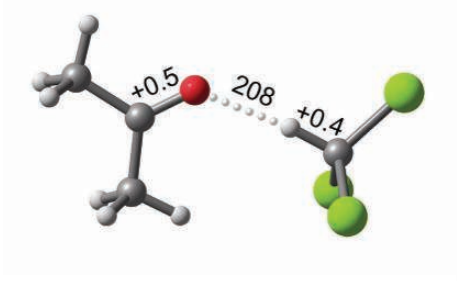

Figure 1. Optimized structure (B3LYP/6-31G*) of the acetone-chloroform complex. (Hydrogen-bond distance and bond length increase upon complexation in pm).

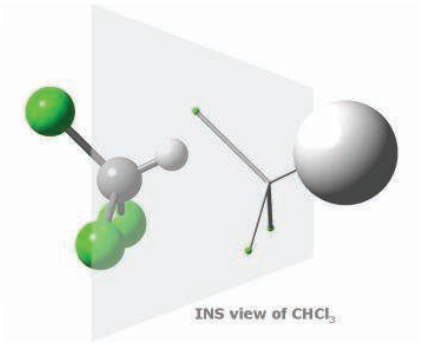

Figure 2. Representation of the $CHCl_3$ molecule based on the H/Cl scattering cross section ratio (79.7/5.2).

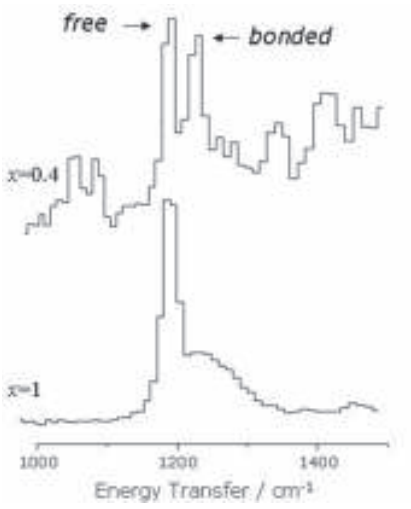

Figure 3. INS spectra of pure chloroform, $x = 1$ and binary mixture ($x = 0,4$) in the fundamental βC–H mode region.

arising at ca. 82 cm^{-1} is assigned to the νO···H antitranslational mode, while the remaining bands are assigned to the out-of-plane and in-plane bending modes of the chloroform···acetone complex. In addition, the βC–H mode of $CHCl_3$ at 1242 cm^{-1} is split in the spectra of the mixtures, and the high wavenumber component is assigned to the hydrogen-bonded complex (Fig.3). The plot of the integrated intensity of this component presents a maximum for $x = 0.5$, in agreement with the 1:1 stoichiometry of the chloroform···acetone complex, with a calculated complexation constant of 0.15±0.02 $dm^3\ mol^{-1}$. Results also show that the complex behaves as an independent entity showing that despite weak such interactions can play a key-role in supramolecular chemistry.

[1] Department of Chemistry, CICECO, University of Aveiro, 3810-193 Aveiro, Portugal

[2] Department of Chemistry and Biochemistry, Faculty of Science, University of Lisbon

[3] Departamento de Física, FCT, Universidade de Coimbra

[4] Science and Technology Facilities Council, Rutherford Appleton Laboratory, UK

Reference paper

[1] Vaz PD, Nolasco MM, Gil FPSC, Ribeiro-Claro PJA, Tomkinson J,*Chemistry – Eur. J.*, **2010**, 16, 1910-1917

NON-POLAR NANOSTRIPED Z_nO THIN FILMS ON M_gO SUBSTRATES STUDIED BY TRIPLE AXIS HIGH RESOLUTION X-RAY DIFFRACTION

Pereira S[1]

Zinc oxide is a wide band-gap semiconductor with unique physical properties and a wide range of potential applications. Until now ZnO-based heterostructures have been mostly grown in the [00.1] direction. Unfortunately, wurtzite ZnO layers exhibit built-in electric fields in this crystallographic orientation, which can be of the order of 1 MV cm^{-1} along the *c*-axis. The large built-in electric field, due to the lack of inversion symmetry of the wurtzite crystal structure, results in a significant separation of electrons and holes in active layers, very long carrier lifetimes and hence very poor light emission efficiencies. The growth on non-polar surfaces such as the *A* plane (11.0) or the *M* plane (1-1.0) has, therefore, been proposed to avoid any built-in electric fields, and non-polar quantum wells. We are investigating ZnO thin

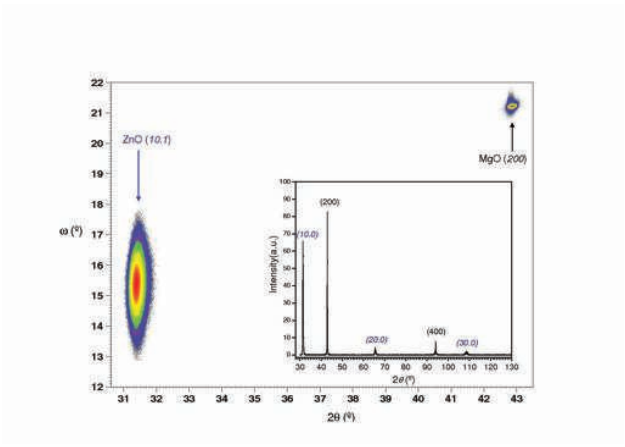

Figure 1. High resolution X-ray diffraction results obtained from the ZnO films grown. The figure shows a θ-2θ map of the symmetric reflections *(10.0)* and *(002)* from the ZnO film and MgO substrate, respectively. The inset shows the results of a conventional (radial) θ-2θ scan on a wide angular range encompassing the *(10.0)*, *(20.0)* and *(30.0)* reflections from the nonpolar film and *(002)* and *(004)* reflections from the MgO substrate.

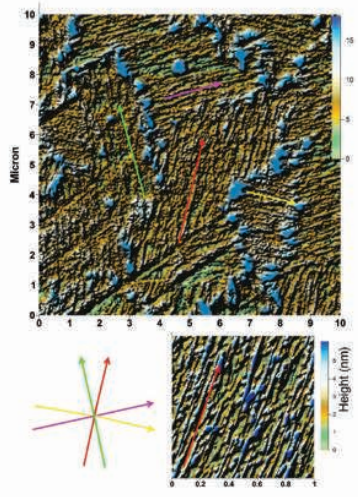

Figure 2. Atomic force microscopy images of the surface of the non-polar ZnO films. Top image shows a large scale image illustrating the rotational nanostripped domains running along the four directions as summarized below by colored arrows. The height scaled AFM image below shows in detail one of the stripped domains. The average ZnO wire height is around 4 nm.

films grown by RF- Magnetron Sputtering (film grown by Dr. A. Lourenço, CICECO) on MgO substrates.

The XRD results shown in Figure 1 show a perfect alignment between the ZnO {10.0} planes and the MgO {001} planes and therefore demonstrate that it is possible to grow epitaxialy non-polar ZnO thin films on cubic MgO substrates. The films thus obtained have peculiar, and quite interesting, morphological properties, as shown in Figure 2. Despite the overall smoothness of the obtained films, self organized "nanowire-like" structures can be observed at the surface. The directions between the stripped domains are highlighted by the colored arrows. The higher magnification AFM micrograph shows in more detail the characteristics of these striped structures. In particular we note the relatively good parallelism between the nanowires and an average height of about 4 nm, i.e. small enough to observe quantum confinement. (AFM performed in collaboration with Dr. A Kholkin, CICECO)

In order to to understand the peculiar morphological features we have performed a more detailed XRD study. In Figure 3a) we show the results of a texture analysis of the obtained non-polar ZnO films. We have selected an asymmetrical plane that contains both in-plane and out-of-plane components thus allowing the epitaxial relation between film and substrate to be determined. In order to get a angular reference between MgO substrate and ZnO film, within the same pole figure, we deliberately let the nearby peak from MgO (111) at $2\theta=37^{\circ}$ reach the detector so that one can detect the sharp MgO peaks at $\chi=54.7^{\circ}$ appearing at $\varphi\sim45^{\circ}$, as expected. The diagrams in Figures 3b) and 3c), together with the AFM image, allows the XRD pattern obtained to be interpreted. As shown schematically in Figure 3b), for single domain ZnO the only two spots at $\chi\sim28.4^{\circ}$ should appear (open opposite circles), while for diffraction spots at $\chi\sim63.9^{\circ}$ 4 spots per domain would be expected as indicated by filled circles.

The overall experimental pole figure can be explained considering the overlap of four different domains rotated in-plane by $26^{\circ}(+90)$, diffraction of each domain is represented by a different color, resulting in (4x2) 8 inner spots and (4x4) 16 outer spots. The in-plane rotation between each domain is 26°, which is in very good agreement between the angular separations between the stripped domains found at the surface (Fig.2). The schematic diagram in Figure 3c) shows the epitaxial relation deduced from the XRD measurements. We can see how the hexagonal lattice "sits on top" of the cubic MgO substrate lattice. The <00.1> direction from ZnO forms an in-plane angle of 13° with the <100> MgO direction. ZnO films grow in such way that the rectangular face of the hexagonal crystal lattice is rotated and the atomic position of the atoms along the diagonals nearly coincide! In this way the system minimizes the lattice mismatch, and thus the strain energy along this direction. Using the ZnO lattice constants, c=5.215 and a=3.253, and MgO lattice constant a=4.212 a mismatch of ~3% is deduced, with the hexagonal lattice compressed along the diagonal. The large strain anisotropy, with a good epitaxial match along the diagonals and high lattice lattice mismatch along other directions in the growth plane is the driving force for the highly directional surface corrugation. In our case this takes and extreme with the ZnO self organized NWs growth promoted along the 4 directions that allow a good in-plane epitaxial match between the MgO and non-polar ZnO film.

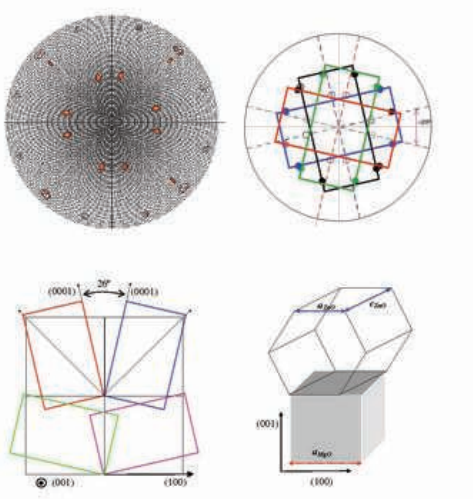

Figure 3. a) (top left) XRD pole figures obtained at $2\theta=36.21^{\circ}$, corresponding to the inter-planar spacing of the ZnO *{10.1}* planes. Pole densities are plotted in stereographic projection with polar and azimuthal angle χ and φ, respectively. The plane of the stereographic projection was chosen to be parallel to the sample surface, i.e. parallel to MgO *{001}* which in turn is also parallel to ZnO *{10.0}*. Note that within one circle there are two values of angular separation between *{10.0}* and *{10.1}* are expected: 28.4° and 63.9°. **b)** (top right) Schematic diagram showing the expected diffraction spots from each ZnO domain superimposed to match experimental pattern. **c)** (below) Schematic diagrams illustrating the epitaxial relation between the ZnO Film and the substrate.

[1] Department of Physics, CICECO, University of Aveiro, 3810-193 Aveiro, Portugal

SPEED DETERMINATION OF SINGLE Sr ADATOMS MOVING WITHIN Si(111)-7×7 HALF UNIT CELLS

Zhachuk R[1,2], Teys S[1], Olshanetsky B[1], Pereira S[2]

The diffusion and motion of adatoms on crystal surfaces are fundamental atomic processes which govern nanostructure formation and thin film growth. Thus, understanding the dynamics of such phenomena is of ultimate scientific and technological interest. Atomic motion and diffusion is influenced locally by surface reconstructions which determine the surface energy at a given site. An interesting and technologically relevant example of such local structural dependence is adatom diffusion above the Si(111)-7×7 reconstruction. High-frequency signal fluctuations in scanning tunneling microscopy (STM), which originate the appearance of fuzzy patches on the silicon surface images after the deposition of small amounts of Pb. These noisylike patches in the STM images

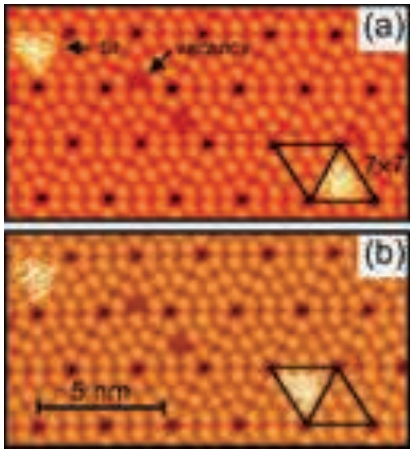

Figure 1. Two subsequent STM images of Sr atoms on Si(111) surface. The single Sr atom in the lower right corner in (a) "jumps" to the adjacent half of the 7×7 unit cell in (b).

can be ascribed to thermally activated motion of Pb adatoms, faster than the STM tip movement, among different adsorption sites within the 7×7 half unit cell (HUC). Si(111)-7×7 surface represents a model system to investigate the problem of adatoms wandering in a discrete and well-defined regular surface, whose elementary meshes are half cells of Si(111)-7×7. The signature of individual Sr adatoms on the Si surface can be recognized as fuzzy patches within Si(111)-7×7 HUCs in Figure 1. Sr diffusion on Si(111)-7×7 as atomic jumps between adjacent HUCs, is also observed.

A more quantitative description of such effects in the collected STM images can be obtained by performing a Monte Carlo simulation of a Sr atom moving randomly, with constant speed, within a surface area with the size of 7×7 HUC. One considers that the STM tip scans, line by line, a square area comprising the region with the moving Sr atom. For simplicity we assume that the brightness obtained in the STM images is proportional to exp(–r/*R*), where r is a distance from STM tip to Sr atom in *xy* scanning plane and *R* is the widening of an atom image due to the finite tip radius. Thus, the overall simulated image is governed by three parameters: scan range (*L*), speed of the Sr atom relatively to the STM tip (V_{tip}/V_{Sr}) and *R*-parameter. Figure 2 from (e) to (h) shows the results of the simulations described, in a representation similar to that of Figures 2a,2b,2c,2d. The evolution of the simulated noisylike patches as a function of the scanning tip velocity is in good agreement with the experimental results. When the tip is moving very slowly ($V_{tip}/V_{Sr} \sim 0.02$), Figures 2a,2e the signal spikes look isotropic, reflecting the fact that a Sr atom approaches the STM tip from all directions with equal probability. The spike size is therefore comparable to the pixel size. By increasing the scan speed the spikes become elongated, and turn into streaks along the fast scan direction. This occurs since the Sr atom, when moving in the same direction as the STM tip, is imaged for a longer period of time than when moving along the perpendicular direction. The image then becomes dominated by streaks; in this sense the STM becomes more sensible to atoms moving in the same direction as the tip. At a certain value of scan speed [$V_{tip}/V_{Sr} \sim 1.0$, Figs. 2d, 2h] the length of a streak almost doesn't change further, since this effect saturates. Such length is defined by the extension of 7×7 HUC and the *R*-parameter. With a further increase in the "scanning speed," considered in our simulation only, the long tracks of the adatom were observed ($V_{tip}/V_{Sr} \sim$ 10–100), which finally become an image of an atom at a given position when $V_{tip}/V_{Sr}>1000$ (not shown here).

In order to estimate the average speed of Sr atom within the 7×7 HUC, we compared the lengths of the observed streaks measured in the experimental and computer generated STM images. The correspondence between the sets of experimental and simulated STM images is established via the average streak's length. Since the average streak's length is a function of the absolute (V_{tip}) or relative speed (V_{tip}/V_{Sr}) for the experimental and simulated images, respectively, the established correspondence provides an estimate for the absolute value of the adatom speed. Accordingly, following the procedure detailed the average speed of the Sr atom moving within the Si (111) 7×7 HUC at RT could be estimated as 300 nm/s.

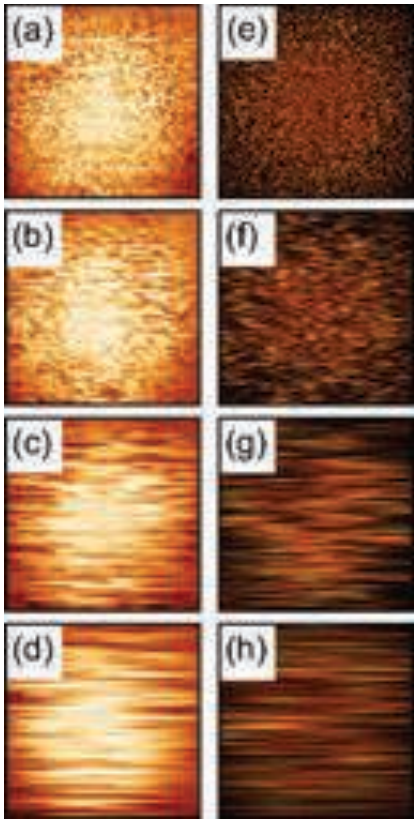

Figure 2. [(a)–(d)] Experimental STM images of a moving Sr atom within the limits of half of the 7×7 unit cell, taken with different scanning speeds. Scan range is 1.8×1.8 nm^2. (a) $V_{tip} = 7$ nm/s; (b) $V_{tip} = 28$ nm/s; (c) $V_{tip} = 125$ nm/s; (d) $V_{tip} = 292$ nm/s. [(e)–(h)] Results of a computer simulation implementing the model of independently moving Sr adatom and scanning tip. $L = 1.8$ nm, $R = 0.3$ nm. (e) $V_{tip}/V_{Sr} = 0.02$; (f) $V_{tip}/V_{Sr} = 0.1$; (g) $V_{tip}/V_{Sr} = 0.4$; (h) $V_{tip}/V_{Sr} = 1.0$.

[1] Institute of Semiconductor Physics, pr. Lavrentyeva 13, Novosibirsk 630090, Russia

[2] Department of Physics, CICECO, University of Aveiro, 3810-193 Aveiro, Portugal

Reference paper

Zhachuk R, Teys S, Olshanetsky B, Pereira S, *Appl. Phys. Lett.* **95**, 061901 (2009).

Computational Methods and Theory

HALOGEN BOND ANION TEMPLATED ASSEMBLY OF AN IMIDAZOLIUMPSEUDOROTAXANE

Serpell CJ[1], Kilah NL[1], Costa PJ[2], Félix V[2], Beer PD[3]

The term *halogen bonding*, R–X···B, describes the interaction of a halogen atom (X) in a molecule (R-X), with a negative site on another molecule (B). The halogen acts as electrophilic centre and the halogen bonding interaction can be explained by the existence of a positive region on the electrostatic potential surface at the halogen, named *σ-hole*. Among the many noncovalent interactions commonly utilized in solid-state and solution supramolecular assemblies, halogen bonding is arguably the least exploited.

In the frame of an extensive collaboration between our Molecular Modeling Group and the Beer's group at the University of Oxford, we explored this type of interaction as templating agent in the construction of new pseudorotoaxane architectures[1]. In particular, it was shown that the 2-bromo-functionalised imidazolium threading motifs interpenetrate an isophthalamide macrocycle *via* chloride anion templation assisted by cooperative halogen and hydrogen bonding interactions (Fig.1).

Our group performed molecular dynamics/molecular mechanic (MD/MM) simulations and Density Functional Theory (DFT) calculations in these systems, helping in the interpretation of the experimental data. The lowest energy co-conformation obtained by MD/MM was DFT-optimized (Fig 2) showing that the C–Br···Cl^- halogen-bond interaction is present with a distance of 2.92 Å and a bond angle of 174.9° which is compatible with the experimental data. The strength of the C-Br···Cl^- interaction was evaluated through a natural bond order (NBO) demonstrating the magnitude of the *σ–hole*. Calculation of the Wiberg Bond Indexes (WI), which are measures of bond strength, show that in the pseudorotaxane, the C–Br···Cl^- halogen bond (WI = 0.1335) is present and is strong enough to maintain the interpenetrated assembly.

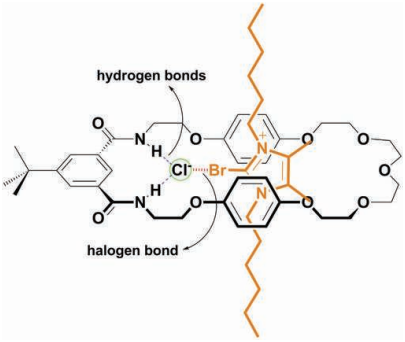

Figure 1. Assembly of a pseudorotoaxane structure using 2-bromo-functionalised imidazolium derivatives trough cooperative hydrogen and halogen bonds.

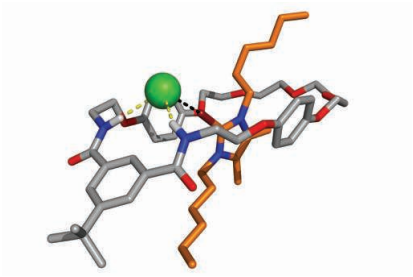

Figure 2. DFT-optimized structure of the pseudorotoaxane showing the linear C–Br···Cl– halogen bond (black dashed line) and the N–H···Cl– hydrogen bonds (yellow dashed lines). Br brown, C gray, N blue, O red.Imidazolium alkyl chains are shown in orange, and thechloride ion is shown as a green sphere.

[1]Chemistry Research Laboratory, Department of Chemistry, University of Oxford, Mansfield Road, Oxford, OX1 3TA (UK)

[2] Department of Chemistry, CICECO, University of Aveiro, 3810-193 Aveiro, Portugal

Referenc paper

[1] Serpell CJ, Kilah NL, Costa PJ, Félix V, Beer PD, "Halogen Bond Anion Templated Assembly of an Imidazolium Pseudorotaxane" Angew. Chem. Int. Ed. 2010, 49, 5322-5326

HIERARCHICALLY CONSTRAINED DYNAMICS AND EMERGENCE OF COMPLEX BEHAVIOR IN ORGANIC–INORGANIC NANOHYBRIDS

Carlos LD[1], Pacheco JM[2,3], Ferreira RAS[1], Videira ALL[3,4]

Similar to living organisms, highly structured materials may manifest an inherent complexity, deriving not only from the large number of their core constituent units, but also from the entanglement between the dynamics of the core components and their organization as a complex multi-agent system. As a result, such systems typically exhibit properties which cannot be anticipated from those of their constituents. This, in turn, has provided experimental guidelines in investigating the relationship between structural complexity and self-assembly mechanisms of nano-structured systems. Intriguingly, the potential role played by the complex organizing principles determining emergent physical phenomena has remained largely unexplored.

In the last three years, we provide experimental evidence[1] and theoretical insight[2] of the emergence of complex behaviour in the context of an extended multi-agent system: a self-assembled alkylene/siloxane hybrid monoamidosil nano-structure, henceforth named m-A(14), formed by highly ordered alkyl chains covalently cross-linked to siliceous nano-domains through amide bridges, Figure 1. A reversible order-disorder phase transition

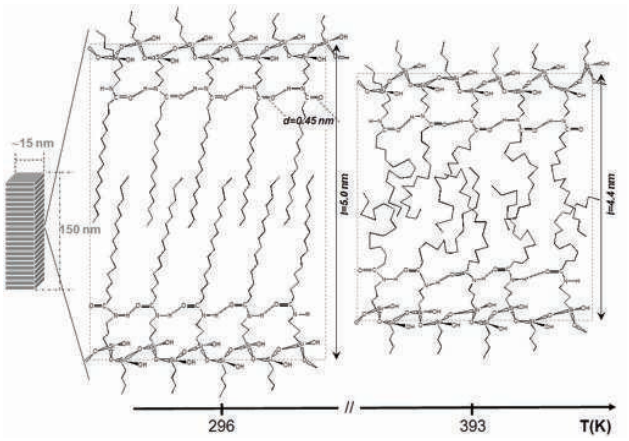

Figure 1. Structural illustration of the m-A(14) framework at 296 K and 393 K, illustrating the order-disorder phase transition.

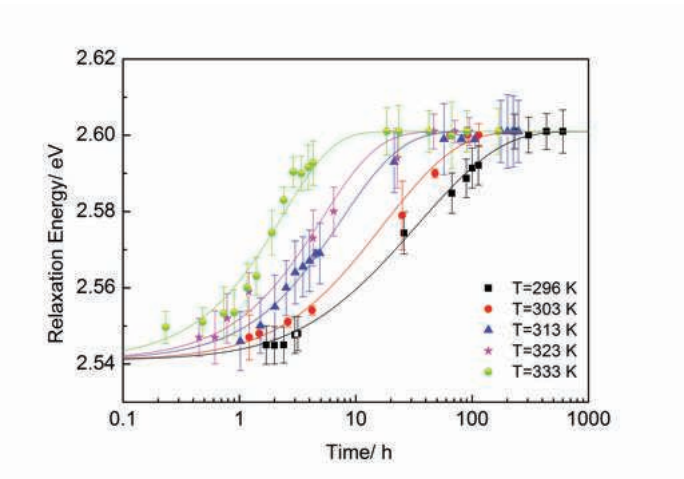

Figure 2. Emission relaxation of m-A(14). The solid coloured lines are fits (reduced- χ^2=0.372) to the experimental data using a minimal model which establishes a relation between individual dynamics in a multi-agent system and its hierarchical dependence on the collective dynamical pattern [2].

of the alkylene chains is observed via a series of heating/cooling cycles operating between 296-393 K (Fig.1). The emitted relaxation energy of the nano-hybrid upon repeated heating/cooling cycles exhibits a logarithmic time-dependence (Fig.2), thereby providing a conspicuous fingerprint of emergent complex behaviour; such logarithmic dependence has been associated with hierarchically constrained dynamics in many different multi-agent systems. We employ a simple model to relate the individual dynamics in the nano-hybrid with its hierarchical dependence on the system's collective dynamical features[2]. The model associates the nano-scale interactions between the amide cross-linkages connecting the organic and inorganic components with the entire hybrid organization at the mesoscopic scale. The strong correlations between adjacent cross-linkages establish a memory effect – stemming from the hierarchical organization of the hybrid – inducing light emission, governed by the system-wide dynamics. As the model's underlying rationale is insensitive to the particulars of the specific multi-agent analysed, we propose that the emergence of complexity may be the rule, rather than the exception, in what concerns the interplay between individual and collective behaviour.

[1] Department of Physics, University of Aveiro, 3810-193 Aveiro, Portugal

[2] ATP-group, CFTC & Departamento de Física da Faculdade de Ciências, P-1649-003 Lisboa Codex, Portugal

[3] GADGET, Apartado 1329, 1009-001 Lisboa, Portugal

[4] R. Sarmento de Beires, 31, 5 ESQ., 1900-411 Lisboa, Portugal

Funding

We thank Fundação para a Ciência e a Tecnologia, FEDER, and COMPETE (PTDC/CTM/72093/2006 and POCI/FIS/58418/04) for financial support.

Reference paper

[1] Carlos L D, de Zea Bermudez V, Amaral V S, Nunes S C, Silva N J O, Ferreira R A S, Rocha J, Santilli C V, Ostrovskii D, "Nanoscopic photoluminescence memory as a fingerprint of complexity in self-assembled alkyl/siloxane hybrids", *Adv. Mater.*, **2007**, 19, 341–348.

[2] Carlos L D, Pacheco J M, Ferreira R A S, Videira A L L, "Hierarchically constrained dynamics and emergence of complex behavior in nanohybrids", *Small*, **2010**, 6, 386–390.

PREDICTION OF THE CATALYTIC ACTIVITY OF METAL SURFACES FOR THE WATER GAS SHIFT REACTION BASED ON SIMPLE DESCRIPTORS

Fajín JLC[1], Cordeiro MNDS[1], Illas F[2], Gomes JRB[3]

The water gas shift (WGS) reaction, $CO + H_2O \rightleftharpoons CO_2 + H_2$, ΔH = -40.6 kJ·mol^{-1}, is a very important step in the industrial production of hydrogen, ammonia and other bulk chemicals utilizing synthesis gases. Furthermore, it is used to remove CO from gas streams used to run low temperature fuel cells or to reduce the CO contents in the reactants flow for the Fischer–Tropsch synthesis (FTS) process (i.e., converting CO and H_2 into hydrocarbons). WGS is a mildly exothermic, reversible reaction and, hence, favorable at low temperature. Elementary steps involved in WGS reaction are CO oxidation, H_2O dissociation and formate/formyl decomposition. Thus, the catalyst needs to be able to inhibit dissociative CO adsorption leading to methane formation without compromising shift activity.

In practice, the WGS reaction is carried out in industry using copper based catalysts and two mechanisms were proposed for this reaction, namely, the i) redox and the ii) associative routes, both starting with water dissociation on the catalytic surface, Scheme 1. Recently, we have calculated by means of density functional theory the reaction profiles for the possible reaction routes shown in Scheme 1 on a stepped Cu(321) surface

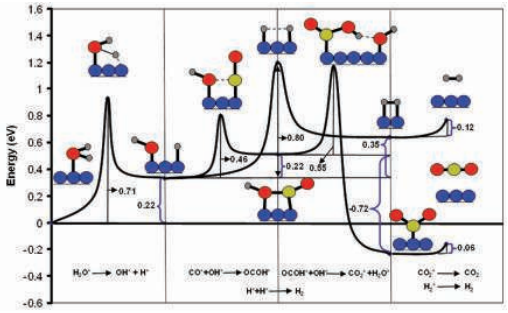

Figure 1. Reaction profile for the WGS reaction on a Cu(321) model surface following the associative mechanism calculated with density functional theory and a periodic slab approach.

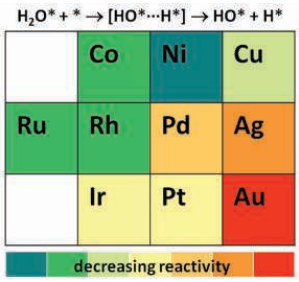

Figures 2. Scale for the reactivity of metal surfaces concerning the reaction of water dissociation which constitutes the rate determining step for the technologically important WGS reaction.

Redox mechanism through direct water dissociation

$$OH^* \rightarrow O^* + H^*$$

Redox mechanism through hydroxyl disproportionation

$$OH^* + OH^* \rightarrow O^* + H_2O^*$$

Associative mechanism through carboxyl intermediary with direct dehydrogenation

$$CO^* + OH^* \rightarrow OCOH$$

$$OCOH^* \rightarrow CO_2^* + H^*$$

Associative mechanism through carboxyl intermediary with assisted dehydrogenation

$$OCOH^* + OH^* \rightarrow CO_2^* + H_2O^*$$

Scheme 1. Redox and associative reaction routes proposed for the WGS reaction.

model and proposed that the associative mechanism, where an OCOH* intermediate appears and then reacts with surface OH* species, is the most probable[1]. Furthermore, the comparison of calculated results on stepped, Cu(321), and planar, Cu(111), surfaces showed that the presence of low-coordinated atoms on the catalytic surface was found to decrease significantly the calculated activation energy barriers, i.e., they are important catalytic centers with obvious implications on the calculated reaction rate constants. Importantly, both for the redox and associative routes, the first O-H bond dissociation in H_2O was found to be the rate-limiting step for the WGS reaction (*c.f.* leftmost panel in Fig.1). A striking result from our work that is rather encouraging for future studies was the proposal, for the first time, of a Brønsted-Evans-Polanyi (BEP) relationship between the calculated activation energy for the bottleneck reaction, i.e, $H_2O^* \rightarrow OH^* + H^*$, and the interaction energy of the products of reaction, i.e., $OH^* + H^*$, on planar and stepped copper and gold surfaces. This paved the way for a subsequent study where the aim was to find if the relationship was still valid for a larger number of Miller indices and of transition metals (TM). In fact, a clear BEP relationship was found between the activation energies for the cleavage of the first O-H bond in water and the energies of OH* and H* co-adsorbed on planar and/or stepped Rh, Ir, Ni, Pd, Pt, Cu, Ag and Au surfaces[2]. Importantly, new descriptors such as the reaction energy (a classic descriptor) and, surprisingly, the interaction energy of oxygen adatoms (a species that is not present in the WGS reaction) were also suggested and a reactivity scale was proposed (Fig.2). Finally, the BEP relationships were tested and found to work for TM surfaces that were not included in the elaboration of the relationships. In conclusion, it was shown that the adsorption energy of atomic oxygen on a given metallic surface provides an excellent descriptor of the activation energy for water dissociation on that surface thus allowing the screening of a large number of metallic (and bimetallic) systems in a simple way[2].

[1] REQUIMTE, Dept. of Chemistry, Faculty of Sciences, University of Porto (Portugal)

[2] IQTQUB, Dept. of Physical Chemistry, Faculty of Chemistry University of Barcelona (Spain)

[3] Department of Chemistry, CICECO, University of Aveiro, 3810-193 Aveiro, Portugal

Reference paper

[1] Fajín JLC, Cordeiro MNDS, Illas F, Gomes JRB, "Influence of step sites in the molecular mechanism of the water gas shift reaction catalyzed by copper", *Journal of Catalysis* **2009**, *268*, 131-141.

[2] Fajín JLC, Cordeiro MNDS, Illas F, Gomes JRB, "Descriptors controlling the catalytic activity of metallic surfaces towards water splitting", *Journal of Catalysis* **2010**, article in press, doi: 10.1016/j.jcat. 2010, *276*, 92-100.

THERMOLIB: A PORTABLE NUMERICAL LIBRARY FOR PERFORMING THERMODYNAMICS

Da Silva FA[1]

When was the last time you calculated a multicomponent vapor-liquid equilibrium? Did you remember how to compute a residual enthalpy using an EOS (equation of state)? Once in a while, the chemical engineering community, in their applied thermodynamic courses up-to the regular engineer, or in a minute to minute monitoring of a complex dynamic process, they are standing up their modeled units on well-established thermodynamic pillars, sometimes inadvertently. Nowadays, powerful commercial simulators

are available, resulting from systematic development in computing science, and of course, as result of much accurate thermodynamic models and experimental data available. However, these tools are often expensive, huge, or are restricted to specific operating systems. At the other extreme, a junior student, or young researcher when asked to do some of these "exotic" calculations, in common homework or in his/her research activity, armed with a bare command-driven computing software, soon realizes the daunting task to implement several routines, for performing a single thermodynamic calculation. Looking to these community requirement, Thermolib[1] was born to fulfill this gap, as a long term and continuous project, belonging to a more ambitious computing work located in a small in-house-made cluster flagged as *Quimera* (http://quimera.web.ua.pt) [2]. Thermolib is developed in Java, exploiting the object-oriented paradigm when implementing the thermodynamic blocks in simple concepts as pure component (single properties and database accessing), mixtures (aggregation of pure components) and streams (mixtures linked to vapor-liquid equilibrium calculations). Being built in Java, Thermolib has the advantage to be portable and easily to be embedded in those "command-driven computing systems" as Matlab® and/or Mathematica®, as shown in Figure 1. After loading the library, with simple common sense and following ordered steps sequence as: 1) create a list of pure components, loaded from local files or remote databases; 2) setting up an "object mixture" defining a target stream; 3) call a thermodynamic method; these steps allow us to carry out straightforward calculations as for example, mixture enthalpies, Gibbs free energies, fugacity, activity coefficients and LV calculations, to mention some. The user in less than ten lines of plain native code in Matlab® or Mathematica® can produce complete results accessing the Thermolib objects.

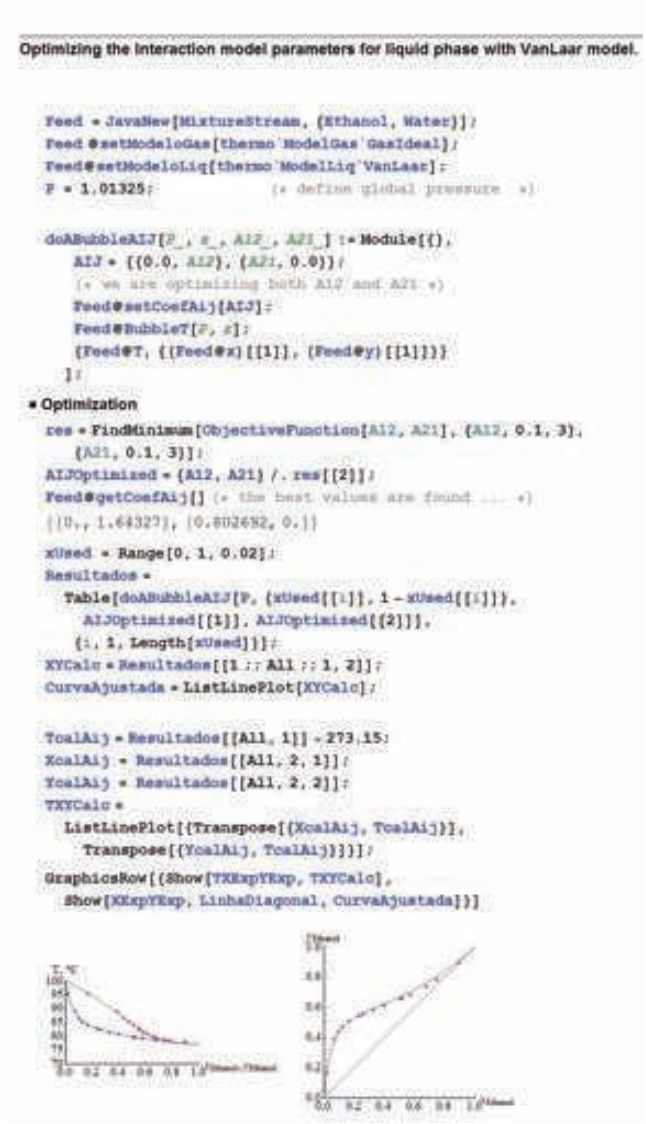

Figure 1. An example calculation, using Thermolib embedded in Mathematica®.

Thermolib has been used in annual Projects of Chemical Engineering Integrated Master [3,4] and is currently available to the students at the computer room of the new Technology Laboratory Complex at University of Aveiro.

[1] Department of Chemistry, CICECO, University of Aveiro, 3810-193 Aveiro, Portugal

Reference paper

[1] Da Silva, FA. "Thermolib: A middleware library for performing thermodynamic calculations", Thermodynamics 2009, book of abstracts, No. 65, page 77, September 23-25, Imperial College, London, 2009.

[2] Projecto FCT POCTI/EQU/46055/2002, "Simulação de processos cíclicos de separação usando computação em paralelo".

[3] Vieira, JM, "Desenvolvimento de uma Biblioteca para Cálculo de Propriedades Termodinâmicas", Teste de Mestrado Integrado em Engenharia Química, Universidade de Aveiro, 2007.

[4] Alves SA, "Coeficientes de Actividade de Aminoácidos em Solução Aquosa", Tese de Mestrado Integrado em Engenharia Química, Universidade de Aveiro, 2008.

AN UNIVERSAL CORRELATION FOR THE SOLUBILITY OF CO_2 IN IONIC LIQUIDS AND OTHER LOW VOLATILE SOLVENTS

Carvalho PJ[1], Coutinho JAP[1]

The solubility of CO_2 in solvents of low volatility or non volatile is highly relevant for many technological applications. Enhanced Oil Recovery (EOR) requires the knowledge of the CO_2 solubility in heavy hydrocarbons; purification of vegetable or animal oils, and the extraction of value added compounds from them using supercritical technologies, is related with the CO_2 solubility in these oils, and their fatty acids and esters; and the Selexol process uses a mixture of dimethyl ethers of polyethylene glycol for the removal of acid gases from feed gas streams. Recently there has been a great interest on the use of ionic liquids for CO_2 capture and gas separation purposes. In all these cases the understanding and description of the absorption of CO_2 in solvents of low volatility is of importance for the design and operation of processes or the design of new and enhanced sorbents for CO_2.

Our group has been actively engaged in understanding the solubility of CO_2 in non volatile solvents. On this study it was shown that the solubility of CO_2 in non volatile solvents is not driven, as previously admitted, by the favorable interactions between the gas and the solvent but instead is the result of a complex and delicate balance between the solute-solute, solute-solvent and solvent-solvent interactions and cannot be inferred from the strength of solute-solvent interactions alone. Moreover, in systems of non volatile solvents, these solvents presenting in general a large molar volume, the solute-solvent size and shape asymmetries will generate important entropic and free volume contributions that dominate the CO_2 solubility on these systems. Based on these considerations it was shown that the solubility of CO_2 on non volatile solvents is solvent independent, i. e. the solubility of CO_2 is identical in all solvents when expressed in the right units, and this solubility can be described by a universal correlation with the form:

$$p / MPa = m_i^0 / mol.kg^{-1}\, e(6.8591 - \frac{2004.3}{T/K})$$

1 Department of Chemistry, CICECO, University of Aveiro, 3810-193 Aveiro, Portugal

Funding

This work was financed by the FCT

Reference paper

Carvalho PJ, Coutinho JAP. "On the Nonideality of CO2 Solutions in Ionic Liquids and Other Low Volatile Solvents". *Journal of Physical Chemistry Letters*. **2010**. 1, 774-780.

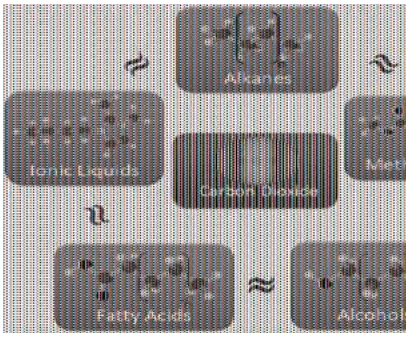

Scheme 1.

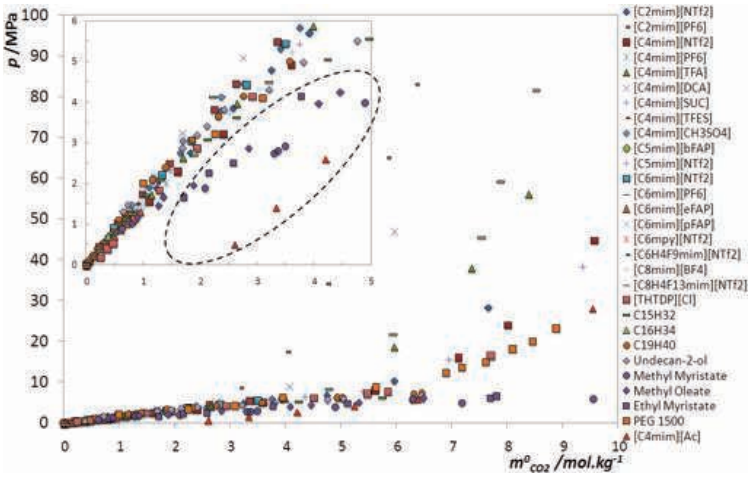

Figure 1. Pressure-molality diagram of CO_2 on nonvolatile solvents at 313 K.

Outreach Activities

RESEARCH WITH INDUSTRY: TOWARDS TECHNOLOGY VALORISATION AND FINANCIAL SUSTAINABILITY

Daniel AD[1], Pais PS[1], Fernandes V[1], Seabra MP[1,2]

A project developed by a CICECO's team in partnership with PortucelSoporcel Group and Cimianto companies related with fiber-cement production exemplifies one of the main goals of CICECO's Technology Transfer Interface (CDTM), the promotion of research projects with industry.
This project allowed solving two industrial problems: to avoid land filling solid wastes and to reduce production costs related with raw materials acquisition. By setting as goal the available waste valorisation, the researchers demonstrated the technical viability of producing fiber-cement roof sheets incorporating cellulose primary sludge generated on paper and pulp mills (Fig.1). Important benefits to the companies involved were originated, not only economic benefits (around 87.5k€/year to the fiber-cement factory), but also environmental, as the reduction of the waste landfill disposal for the paper and pulp company[1].
Similar important outputs were generated by other 14 R&DT contracts developed with the participation and co-promotion of CICECO since 2009 and exclusively financed by companies. Economically, they accounted for *ca.* 252 k€ of total income received by CICECO in 2009 to perform research with industry. Also relevant are the 6 co-promotion projects financed by QREN. These projects, with a total financing of more than 1.5 M€, represented a significant fraction of the total income received by UA in the so-called co-promotion projects.
Such figures represent CDTM's enduring efforts in several domains to enhance researchers' awareness regarding this type of collaboration, as well as to establish links with companies in order to identify potential industrial problems, which could be overcome by research. CDTM continuously screens additional sources of funding that may help to support the development of network connections among R&D institutions and industry. The European projects MNAA and ENERMAT are good examples of this line of action and provided CICECO with more than 1M€.
The promotion of working meetings with industrialists of about 60 companies and the participation in several technological events (Fig.2) contributed to advertise the scientific skills of CICECO and to attract further R&DT contracts with industry, promoting the technology valorisation of our knowledge and financial sustainability.

[1] CDTM, CICECO, University of Aveiro, 3810-193 Aveiro, Portugal
[2] Department of Ceramics and Glass Engineering, CICECO, University of Aveiro, 3810-193 Aveiro, Portugal

Reference paper
[1] Modolo R, Ferreira VM, Machado LM, Rodrigues M, Coelho I. "Construction materials as a waste management solution for cellulose sludge", Waste Management, accepted on 15th September 2010.

Figure 1. (top) Primary sludge ready to be processed (left) and to be incorporated in the disintegrator in big bags (right).
Figure 2. (bottom) CICECO booth at "Jornadas da Inovação 2009" (FIL, Lisbon).

"QUÍMICA POR TABELA" - A SERIES OF CHEMISTRY DEMONSTRATIONS PERFORMED AS A SHOW AT THE FÁBRICA CCVA SCIENCE CENTRE

Ribeiro-Claro P[1], Goodfellow BJ[1]

"Química por Tabela" is a chemistry-based show for the general public that is part of the permanent programme of the Fábrica CCVA Science Centre. Since January 2008 the show has been running three days a week and on the first Sunday each month at the "Fábrica de Ciência". Up until September 2010 the show has been performed 150 times and has been seen by approximately 10,000 people!
It all started back in 2005 when the authors found themselves showing a vid-

eo of some chemistry experiments to students during a Science and Technology Week at the UA to try and stimulate interest and enthusiasm for chemistry in young students. They decided then that actually watching experiments in real life would be much more exciting and stimulating than a video so they went away and conceived and developed experiments that would eventually become Química por Tabela.

Initially the show was performed by Paulo Ribeiro Claro and Brian Goodfellow intermittently during Science weeks, Summer Schools or by request at the UA. However, following a proposal from the director of the Fábrica, the show was adapted in order to allow the show to be performed regularly. This process included the selection of a group of visually exciting experiments, each chosen by considering the ease of execution, the availability of equipment, safety and cost. A script was written and two chemistry graduates were trained to present the show to the public. The show is devised in a way to convey a few basic notions of chemistry to the audience, to relate the experiments to the world around us (and also to the chemistry lessons at school) and finally to stimulate the inquiring scientist in all of us. Final touches, required for a performance in a Science Centre, were provided by the Fábrica team, at a highly professional level and include audio-visual aids, an appropriate stage and backdrop and lessons in presentation for the presenters.

Our audience consists mainly of students ranging from infants to secondary school but also inlcudes the general public. In addition to the regular Aveiro-based presentations, "Química por Tabela" has also been on the road (using a specially designed lab bench) and has appeared at international Science Fairs and has been presented at old peoples homes, at chemical companies, to local councils and at other science centers.

The actual chemical reactions used in the show include redox reactions, the formation of colourful complexes in solution, acid-base equilibria with indicators, chemioluminescence and of course some explosions. Our audience surveys show that four experiments are the most popular: chemical traffic light, burning money, chemioluminescence and fire from ice. The traffic light is also a favourite of ours and involves and redox reaction between an indictor and glucose in alkali. Glucose reduces the indicator which slowly turns from green through red to orange. By pouring the solution from one beaker to another the indicator is quickly oxidised by oxygen in the air back to green – the cycle can then be repeated a number of times.

The popularity of QpT has led to its successor "Química por Tabela 2.0". The new show includes an all new set of chemistry experiments developed over a period of 12 months with the help of a student with a grant from the Portuguese "Ciencia Viva" agency. Hopefully this new show will enjoy as much success as is predecessor and continue to excite, stimulate, intrigue and amaze people from all age groups in the future.

[1] Department of Chemistry, CICECO, University of Aveiro, 3810-193 Aveiro, Portugal

Reference paper

Ribeiro-Claro P, Goodfellow BJ, Trincão P, Valença, OM, Pereira T, Assis F, Mendes I, Marques C, Ferreira D, Rodrigues H and Cardoso M, "Química por Tabela – Espectáculo para comunicação de ciência", Química, 2008, 110, 5-9

Scheme 1.

Scheme 2.

Scheme 3.

TALKING AT HOME ABOUT SCIENCE

Pedrosa de Jesus J[1], Gil VMSS[2], Silva C[3]

Family involvement is recognized as an important factor in attenuating the effects of socioeconomic disadvantages and in promoting children school performance in reading[1], maths[2] and science[3]. In line with these findings, the reports of the Programme for International Students Assessment (PISA) present evidence for the influence of cultural and social communication at home on children school results. Portugal is recognized, in PISA reports, as a country in which family contexts play a major role in influencing children performance at school. That evidence led us to

Scheme 1.

Scheme 2.

design and implement a programme aiming at developing strategies, processes and materials to stimulate home conversation. *A Escola em Casa* is a project that involved the development of a strategy for schools (4th, 5th and 6th grades) in which schools' heads, teachers and parents were engaged in promoting communication at home on issues relevant for fostering children appreciation of learning at school. A pilot study[4] performed in 2004/5 showed that schools leaders, teachers and parents value the adoption of approaches that could facilitate communication at home about issues related with school science. The main study involved approximately 3000 children and their families, 150 teachers (class directors) and 35 schools, during the last five years. Ten booklets with guidelines for talking at home were developed focusing the following themes: *We and People Around us, Yesterday, Today and Tomorrow, We in Society, We and the Sun, We and the Technologies, We and the Environment; We and What we Eat, We and the Citizenship, We and the Health, We and Mathematics, Read with Me* (Scheme1). The results show that the materials selected, the topics proposed and the approaches used were effective in promoting conversation within families with distinct socio-economic backgrounds. In particular, the registered short reports of the conversations allowed the identification of family contexts, barriers and facilitators for the use, in home talking, of words with scientific meaning, learned at school[5]. It is hoped that, among other contributions, this work opens a way for schools to be more effective in stimulating communication at home, centred on science issues, in varied family environments.

[1] CICECO, University of Aveiro, 3810-193 Aveiro, Portugal

[2] Exploratório Infante D. Henrique, Centro Ciência Viva de Coimbra

[3] University of Aveiro, 3810-193 Aveiro, Portugal

Reference paper

[1] Senechal, M. and LeFreve, J. (2002). Child Development, 73: 445-460.

[2] Sheldon, S.; Epstein, J. (2005. The Journal of Educational Research, 98(4): 196-206.

[3] Van Voorhis, F. (2003). The Journal of Educational Research, 96(6): 323-338.

[4] Ramos, A. (2008). Conversas em casa sobre Ciência – um estudo piloto. Unpublished Master Dissertation. Universidade de Aveiro, Aveiro.

[5] Pedrosa de Jesus, Júlio; Gil, Victor; Pedrosa de Jesus, Helena; Miranda, António José; Vieira, João David; Tréz, Ticiana; and Silva, Celina, ESERA 2009, Istambul

Editorial coordination
João Rocha, Luís Dias Carlos, Joqauim Vieira e Dora dos Santos

Cover
Dora dos Santos e Sónia Pinto

Design and layout
GSADesign

Print process by
Gráfica Maia Douro

Number of Copies
1000 exemplares

This Publication was financially supported by

universidade de aveiro

FCT Fundação para a Ciência e a Tecnologia
MINISTÉRIO DA CIÊNCIA, TECNOLOGIA E ENSINO SUPERIOR

FAME nce

QREN QUADRO DE REFERÊNCIA ESTRATÉGICO NACIONAL

Com a participação da União Europeia
Projecto co-financiado pelo FEDER